Electronic Theses and Dissertations

2003

A parametric investigation into the effect of the dish depth and spoke angle on the crashworthiness characteristic of a four-spoke steering wheel armature.

Ophelia. Nabeta
University of Windsor

Follow this and additional works at: http://scholar.uwindsor.ca/etd

A Parametric Investigation into the Effect of the Dish Depth and Spoke Angle on the Crashworthiness Characteristic of a Four Spoke Steering Wheel Armature.

By

Ophelia Nabeta

A Thesis Submitted to the
Faculty of Graduate Studies and Research
through the
Department of Mechanical, Automotive, and Materials Engineering
in Partial Fulfillment of the requirements for the
Degree of Master of Applied Science
at the University of Windsor

Windsor, Ontario, Canada

2003

Canadä

989044

989044

ABSTRACT

This thesis investigates the effect of geometric variations on the crashworthiness performance of new steering wheels. Experimental tests were carried out on steering wheel armatures from popular 1996-2001 compact vehicles. The armatures were subjected to impact loading using a drop tower testing device in which a 57 kg rigid plate impacted a steering wheel with a velocity of 3.2 m/s. The purpose of the experimental tests was to investigate the crashworthiness characteristics of steering wheel armatures from a similar vehicle line in terms of peak loads, Crush Force Efficiency, elastic response, energy efficiency, specific energy absorption and the Energy Absorption Factor. In order to obtain comparable results a rigid plate was used to impact the steering wheel armatures.

Analysis of the experimental results indicated that the dish depth and fastening location of the spokes to the rim of the armature strongly influence the energy absorbed and the loading characteristics of the armature.

Based on these findings, a parametric study investigating the effects of dish depth and 3 o'clock and 9 o'clock spoke angle was conducted. Finite element simulations of the drop tower test were conducted for five spoke angles, and seven dish depths. For each spoke angle and dish depth configuration, three impact locations were analyzed. Although the models did not represent the exact geometries of the steering wheel armatures from the experimental tests, the range of magnitudes of the peak loads observed for the finite element simulations compared well with the magnitudes of the peak loads observed for the experimental tests.

A safety rating system for steering wheel armatures was developed and the armatures were ranked in descending order. The most favorable along with the least favorable armatures were then used to simulate a rigid barrier crash test with a Hybrid III dummy. Overall, the trends from impact with the rigid plate demonstrated consistency when impact occurred with the Hybrid III dummy. Observation on the of dish depth and 3 o'clock and 9 o'clock spoke angle fastening position versus crashworthiness variables are presented in this thesis.

The gods we worship write their names on our faces, be sure of that. And a person will worship something, have no doubt of that either.
One may think that tribute is paid in secret, in the dark recess of his or her heart, but it is not.
That which dominates imagination and thoughts will determine life and character. Therefore it behooves us to be careful what we are worshiping, for what we are worshiping we are becoming.

From GATES OF HEAVEN

To my father and mother,
With all my love.

ACKNOWLEDGEMENT

TABLE OF CONTENTS

LIST OF FIGURES

LIST OF FIGURES –CONTINUED

LIST OF TABLES

NOMENCLATURE

F_{peak}	Peak load
F_{avg}	Average load
e_e	Energy efficiency
L	Energy absorber length
$E_{initial}$	Available energy prior to impact
$E_{absorbed}$	Total energy absorbed
E_{max}	Maximum energy absorbed
L_{dish}	Steering wheel dish depth
$e_{specific}$	Specific energy
$m_{steering\ wheel}$	Mass of the steering wheel
m_{plate}	Mass of rigid plate
z	Position in the z-direction
t	Time
β	Wheel angle
θ	Spoke angle
α	Column angle
i	Index for the ith data point
Δt	Total time duration of the impact test
$\Delta E_{elastic}$	Elastic response
v_{impact}	Impact velocity of the rigid plate
Δ_{max}	Maximum displacement of the rigid plate
ρ	Density
μ	Poisson's ratio
$\sigma_{ultimate}$	Tensile Strength
σ_{yield}	Tensile Strength, Yield
E	Modulus of elasticity,

CONVERSION FACTORS

LENGTH

1.0 inch = 2.54 cm = 25.4 mm

1.0 inch = 3.208 ft =39.37 inch

MASS

1.0 kg = 2.204 lbm

1 slug = 14.59 kg = 32.174 lbm

SPEED

1.0 mph = 1.61 km/h = 1.476 ft/s

1.0 m/s = 3.28 ft/s = 2.24 mph

ACCELERATION

$1.0 \text{ g} = 9.81 \text{ m/s}^2 = 32.174 \text{ ft/s}^2$

FORCE

1.0 lbf = 4.448 N

ENERGY

1.0 lbf·in = 0.113 J = 0.113 N·m

STRESS/PRESSURE

1.0 psi = 1.0 lbf/in2 = 6.894 kPa

2.0 kpsi = 100 psi

GLOSSARY OF ABBREVIATIONS

C.F.E.	Crush Force Efficiency
EA	Energy Absorbed
E.A.F.	Energy Absorption Factor
FMVSS	Federal Motor Vehicle Safety Standards
CMVSS	Canada Motor Vehicle Safety Standards
HIC	Head Injury Criteria
CSI	Chest Severity Index
IC	Injury Criterion
IS	Injury Severity
TTI	Thoracic Trauma Index
AIS	Abbreviated Injury Scale
MAIS	Modified Abbreviated Injury Scale
ISS	Injury Severity Score
PM	Permanent Mold
SC	Sand Cast
DC	Die Cast

1. INTRODUCTION

Automobile manufacturers and their suppliers continue to face rapid changes in technology, increased regulations, and many formidable challenges as they address growing environmental concerns, tough global competition, and more demanding customers. It has become a major technological challenge to make cars not only strong and safe but also as lightweight and affordable as possible. As a result, research and development of lightweight, fuel-efficient and energy absorbing vehicles and vehicular components that can meet these standards has come to the forefront in the industry.

Controlled crash tests provide a means of assessing the protection offered by a vehicle during a crash event. They also provide necessary information for design engineers to develop and optimize a vehicle's safety features. As a result, there have been significant improvements in frontal crash protection including standard airbags, improved structural designs, and higher belt use rates. Full vehicle crash tests typically include full frontal impact tests, offset frontal impact tests and side impact tests. In addition to full vehicle crash tests, material, structural and component impact test are conducted to determine the performance of vehicular components like the seat, seatbelt, seat back, head restraints, airbags and the steering assembly.

Even with the airbag, seatbelt, and knee bolster as standard safety features in passenger cars, the steering assembly continues to be the leading cause of injury and fatalities among drivers in frontal collisions. As such, the safety and performance requirements of the steering assembly are subject to regulations issued by the government. Pursuant to the Motor Vehicle Safety act (1993) [1], the Canadian Federal Government created a number of motor vehicle safety regulations including Canadian Motor Vehicle Safety Standard (CMVSS) 203 (driver impact protection) [2] and CMVSS 208 (Occupant restraint systems in frontal impact) [3]. Most of these regulations are patterned after the Federal Motor Vehicle Safety Standards (FMVSS) developed in the United States by the National Highway Traffic and Safety Administration. FMVSS 203 (Impact Protection for the unrestrained Driver from the Steering Control System) [4] applies to the unrestrained driver

1

while FMVSS 208 (Occupant crash protection) [5] pertains to restrained driver and involves an entire vehicle crash test. The European equivalent, ECE regulation no. 12 [6], which was amended after the introduction of compulsory seatbelt wearing legislation to allow for the option on energy absorbing steering wheels, is similar to FMVSS 203. All these standards detail a testing procedure and acceptable outcome in terms of load developed during crash, chest compression, and head injury when a deformable body block impacts a steering wheel at a given velocity.

The continued advancement in both hardware and software for computer analysis and its potential cost and time advantages over laboratory experiments have made computational procedures an important tool in vehicle collision studies. Such simulations complement crash test results and are used to better evaluate injury mitigation techniques. Computational models involving a full vehicle, vehicular components or subsystems of a vehicle make it possible to predetermine the outcome mathematically through computer simulations, allowing engineers to create and investigate different design possibilities without having to physically construct the vehicle or vehicular component. A significant amount of research using computational models of crash events has been completed, demonstrating the accuracy of numerical simulations in predicting crash events. In addition, computer models offer the possibility of studying impact behavior at any location and at any time interval, providing information that would be unattainable experimentally.

Investigations in the past have been broad, encompassing the entire steering assembly and concentrating on the steering column and its components. Where research has included the steering wheel, geometrical variations have not been taken in to consideration. In addition, investigations on the steering wheel have involved impact between the steering wheel and a rigid or deformable body block. Because of its non-humanlike construction and a fundamental lack of biofidelity the body block does not accurately simulate the driver impacting the steering assembly in actual crash situations.

This investigation intends to address geometric and material concerns and their effect on the crashworthiness of a steering wheel armature. The Hybrid III crash test dummy available in LS-DYNA will be used to impact the steering wheel armature. Results from this investigation will be based upon an engineering analysis of the observations of both experimental and numerical crash tests. Results from this investigation will provide applicable information regarding favorable geometrical parameters aimed at maximizing energy absorption of steering wheel armatures and mitigating driver injury.

2. LITERATURE REVIEW

Early efforts to improve the safety of motor vehicles took place in an environment that made it necessary for safety engineers to investigate real-world crashes and work closely with physicians in order to understand how injuries occurred to real people. During this process, however, the focus of automotive safety engineers shifted to controlled laboratory experiments using crash test dummies and more recently to computer simulations. Experimental tests include full vehicle crash tests in addition to impact tests of automotive structures which the occupant may come in contact with during a crash event. Analysis of actual vehicle collisions, which involve interactions between the driver and the vehicle interior identify the steering assembly as the most common source of injury to the driver. Consequently, a significant amount of research investigating driver impact with the steering assembly has been completed.

2.1. Literature on Injuries sustained through impact with the steering assembly

Frontal damage in non-rollover car crashes is the most frequent type accounting for about 58% of all towed car crashes with the distribution pattern indicating 67.5% drivers [7]. An investigation by Morris et al [8] stated that although the post standard steering system reduced the incidence of column intrusion into the passenger compartment by 68%, the steering assembly is still responsible for 27% of all serious (AIS 3-6) injuries. Overall belt use is approximately 90% for passenger cars in Canada, 76% for passenger cars in the US, and 90% in the UK. Case studies on injuries sustained by drivers thrown against the steering wheel in an automobile accident [9, 10] demonstrate that the blunt impact force due to the steering wheel should not be disregarded even in cases in which the airbag has been successfully deployed. Even with the airbag to attenuate the load in frontal collision, studies show that an unbelted occupant continues to move after contacting the airbag and that the chest and abdomen of the occupant strike the lower portion of the steering wheel rim through the airbag experiencing a blunt impact force as a result, which in some rare cases has resulted in serious cardiovascular injuries. The steering wheel has also been

cited as a major source of head injury amongst restrained drivers in frontal collisions [11]. Of all restrained drivers 70% sustained their head injury from the steering wheel, 49% of those with an AIS 3+ head injury. A study by Petty confirms this finding, experimentally showing the difference in the mode of injury between the belted (head contact) and unbelted driver (chest contact)[12]. A summary of the injuries attributed to the steering wheel is illustrated in Figure 1 and Figure 2.

Harm source

Steering system 26%

Other sources 43%

Instrument panel 10%

Side pillars 8%

Windsheild 5%

Pillars/rails 8%
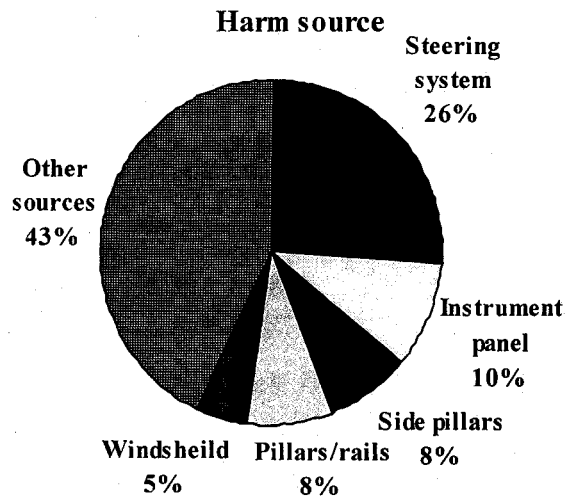
Figure 1.Distribution of crash injury by contact source [13].

Upper extremeties 5%

Face 12%

Chest 46%

Abdomen 37%
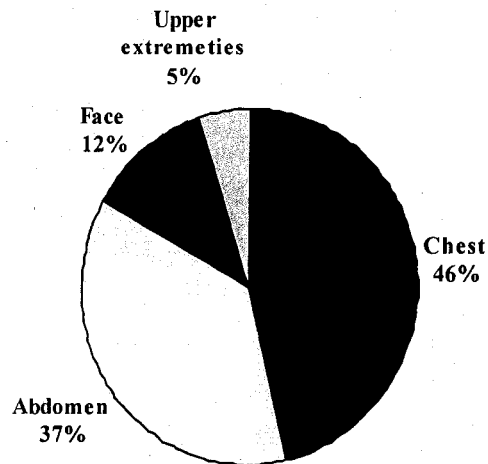
Figure 2. Distribution of injuries due to impact with the steering system by body region [13].

5

2.2. Standards testing procedures

Steering assembly testing is guided by FMVSS 203 (Impact Protection for the Unrestrained Driver from the Steering Control System) whose European equivalent is ECE No. 12, in order to safely absorb the energy to the upper torso of an unbelted occupant as defined by Society of Automotive Engineers-Steering Control System-Passenger Car- Laboratory Test Procedure SAE J944 recommended lab test procedure [14] using the body block test shown in Figure 3.
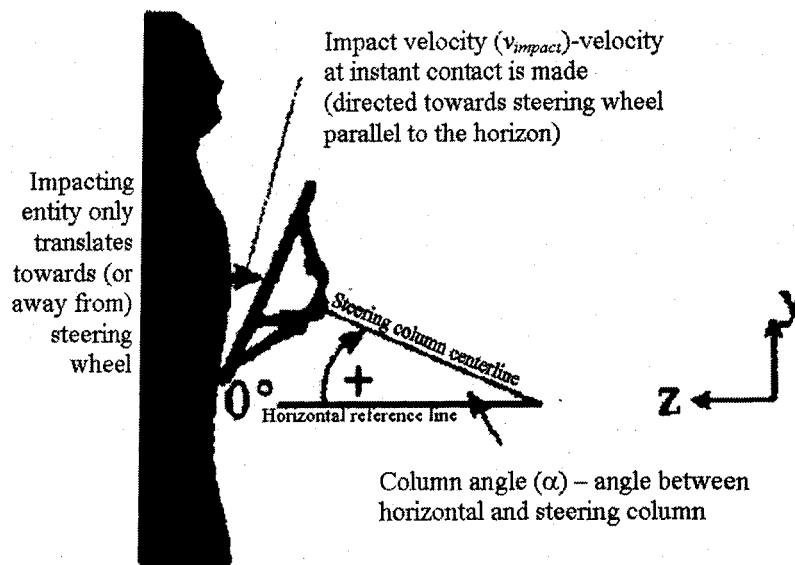
Figure 3. SAE J944 testing procedure

The standard is exempted for motor vehicles that conform to the frontal barrier crash test requirements of FMVSS 208 by means other than the seatbelt (passive restraints). However, should this crash protection system fail (airbag fails to deploy) or in a multiple crash situation in which the airbag deflates, then a steering assembly that complies with standard FMVSS 203 would ensure continued protection for the occupant. As well, a steering wheel tested under FMVSS 203 conditions experiences more severe and localized loading compared to that tested under FMVSS 208 conditions. This would suggest that a steering wheel that complies with FMVSS 203 would automatically comply with FMVSS 208. In addition, tests following FMVSS 203 do not require an entire vehicle test, rendering it a simpler and more economical test to perform.

Typically, steering assembly testing involves both laboratory experiments guided by FMVSS 208 and computer simulations to validate the computational models. Such simulations complement crash test results and are used to better evaluate injury mitigation techniques. Computer simulations are then further used to investigate new design changes and prototypes. This currently represents the technology used in steering wheel design. All the literature referenced here involves both experimental tests and numerical simulations guided by the SAE J944, FMVSS 203, or FMVSS 208. It should be noted that SAE J944 was cancelled and never replaced although the European equivalent ECE regulation no. 12 still exists and is being used.

2.2.1 Documentation regarding steering assembly modeling and testing

Steering assembly testing is guided by FMVSS 203 using the SAE J944 laboratory testing procedure which details the body block test in terms of geometry, material properties, test setup and mass of the body block in addition to acceptable results. Most of the studies the author has reviewed have used some part/variation of this testing procedure as a guide. Although SAE J944 was discontinued and has not yet been replaced, it still provides an acceptable indication of the performance of a steering wheel in terms of peak load.

Wang et al [15] developed a steering system impact model which was implemented in CAL3D. The drop tower test with a 44kg flat rigid impactor and a mini sled-test with the upper torso of a Hybrid III were used to validate the steering system impact model. The performance of the steering system was based on dummy acceleration, column load, stroke and displacement. Although his emphasis was on the steering column, using contact ellipsoid to model the wheel, the study shows the accuracy of numerical methods in predicting experimental results.

Lim et al [16], also completed a parametric study of an energy absorbing steering system using segments and contact ellipsoids to model the body block and the components of the steering system with an occupant analysis code, SAFE (safety analysis for occupant crash environment). His focus was mainly on the improving the performance of the steering column through stiffness variation of the energy absorbing parts to minimize the peak load indexed in FMVSS 203 on the body block. Similarly Young-Sun Park et al [17] also investigated optimum design of the steering column. His steering wheel model is very similar to that by Wang et al [15] although he used the body block test to validate the model. In the simulation, using the occupant analysis code ATB, the dummy was modeled by a segment of the chest which included characteristics of the head and shoulders and lower torso. In this study he used the unknown parameters, scale factors of the assumed force-deflection curves of the spring damper elements used to accommodate joint compliance, as design variables for the optimization process and the difference in the deceleration-time curves of the dummy between the tests and the simulation as the objective function. The steering assembly model, established by applying the obtained force-deflection curves to the steering system, compared favorably with test results obtained from the body block test. It should be noted that these force-deflection curves can be obtained by carrying out component test. Both studies [16, 17] were able to improve on existing designs with the performance of the latter based on peak load while that of the former was based on chest acceleration (g's).

Naab et al [18] completed a study in an attempt to isolate the contributions of single parameters and combinations of parameters to the performance of an energy absorbing steering system based on the HIC, sternal deflection, chest acceleration and abdominal deflection of a Hybrid III dummy. The parameters investigated include rim stiffness, wheel/column mass, hub recession, hub area and steering column angle. He used the PADS (Passenger And Driver Simulation) computer model to simulate the unrestrained deriver in a frontal

barrier test as well as experimental tests to verify his results. Naab found that in addition to other parameters, low mass of the assembly was beneficial to reduce inertia effects. Steering assemblies with a variation of parametric modifications were tested and results showed that deep dished, stiff rim armatures performed better than the baseline systems (existing designs) he tested.

Shyu et al [19] developed a steering wheel design using finite element software PAMCRASH. In the study, he simulated the body block test using a magnesium steering wheel and a rigid body block. He was able to improve the performance of an existing wheel design, in terms of peak load and energy absorption, through material and geometrical modifications. Petty et al [12] also carried out impact tests on a number of steering wheels to try to investigate the possibility of reducing the aggressiveness of steering wheels for facial injuries. The steering wheel design is not presented and it is not mentioned as to what parameters were modified. The investigation was purely experimental with the wheel rigidly mounted on the steering column and a cylindrical impactor whose impacting face is a disc of aluminum honeycomb with a crushing force of 13.8 MN/m^2. Performance was based on crush of the impactor face and the deceleration.

Altenhof et al [20] conducted experimental testing and numerical simulations using LS-DYNA to investigate the energy absorbing properties of a 3-spoke steering wheel armature during impact following SAE recommended practice J944. Simulation results were in good agreement with experimental tests. The study provided significant information regarding percentage energy absorption of specific regions of the steering wheel armature (rim, spokes and hub) which wouldn't have been possible experimentally. Altenhof et al. [21] also conducted a similar study on a 4-spoke steering wheel and in addition to results pertaining to 'region specific' energy absorption, he developed a least squares estimation of the total energy absorbed by the entire armature as

function of column angle and wheel angle. A good correlation coefficient between numerical simulation results and the least squares estimation indicated good prediction potential of the estimation. It should be noted that this estimation is only valid for test carried out at 6.7 m/s.

2.3. Investigations involving finite element modeling of the human body and crash test dummies

Mathematical models of the human body require a high level of detail and knowledge of the physical specimen. Although these models are quite effective for investigating injury mechanisms which would not be possible with experimental tests, they are difficult and computationally intensive. More commonly developed are models of various dummies and individual components of the human body, thorax models [22, 23], human neck models [24], head models [25,26], and the human pelvis [27].

The Hybrid III is the most advanced development in anthropomorphic crash test dummies and its use is federally mandated for certifying the crashworthiness in frontal impact of all passenger cars sold in the North America. Developed by General Motors in 1976 [28], it exhibits better biomechanical response especially in frontal impact than previous dummies. The 50th percentile male Hybrid III is the most widely used frontal crash test dummy, but the Hybrid III family also includes dummies representing different sizes, ages, and genders. The 95th percentile or large male is bigger than 95 percent of the adult male population with a standing height of 1.89 meters and weight of 101.2 kg. The 5th percentile or small female Hybrid III is smaller than 95 percent of the adult female population with a standing height of 1.52 meters and weight of 50 kg. In addition, there are two child-size Hybrid III dummies including a 21.32 kg, 6 year-old, and a 15 kg, 3 year-old.

Hybrid III dummies are designed for use in frontal crash tests. For tests representing crashes in which a vehicle is struck in the side, side-impact dummies have been created to measure injury risk to the ribs, spine, and internal organs such as the liver

and spleen. SID was the first side-impact dummy. It was developed in the late 1970s by the U.S. National Highway Traffic Safety Administration and is used in U.S. government-required side-impact testing of new cars. EuroSID was developed by the European Experimental Vehicles Committee and is used to assess compliance with the European side-impact requirements. BioSID is based on a General Motors design. It is more advanced than SID and EuroSID, but it is not specified as a test dummy to be used in regulatory tests.

SID, EuroSID, and BioSID are designed to represent the 50th percentile or average-size man 1.55 meters tall and 77.11 kg. SID II(s) was created by a research partnership of U.S. automakers. It is the first in a proposed family of technologically advanced side-impact dummies. SID II(s) represents a 5th percentile small female who is 1.52 meters tall and 50 kg.

The 50th percentile male Hybrid III has been successively used by several researchers to investigate thorax tolerance in high velocity frontal impacts and is specified as a test dummy to be used in regulatory tests [29]. A study by John D. Horsch, and Dennis Schneider [30] in which a comparison of cadaver and Hybrid III response was made, indicates that although the Hybrid III has a comparable energy to compress the chest with cadaver results, it returns more energy to the steering system than the cadaver subjects, meaning the cadaver absorbs more energy than does the Hybrid III dummy. Also, the Hybrid III is designed to simulate a tensed occupant resulting in higher peak loads and lower maximum chest compressions than human cadavers.

A number of researchers have carried out studies on human body models. Hapee et al. [31] using MADYMO, presented a human body model aiming at omni-directional biofidelity. Noureddine et al [32] integrated a thorax model with a Hybrid III dummy model in order to measure chest deformation at desired locations to investigate chest injury criteria using LS-DYNA. The thorax model was validated against a standard impactor test. The model response was generally similar to experimental tests. Lizee

et al. [33], using the explicit Radioss code, developed a very detailed finite element model of the human body, including soft tissue, which was modeled using brick elements. The neck, shoulders, thorax, abdomen and pelvis were modeled with deformable elements while the rest of the parts were modeled as rigid bodies. The model was validated against over 100 biomechanical corridors including frontal, lateral and rear impact conditions. Comparison of the model results to the Hybrid III and the Eurosid I (European equivalent of Hybrid III) showed that the flexibility of the model spine greatly influenced results. Similarly in a study by Demetropoulos et al. [34] comparing the Hybrid III and cadaveric lumbar spine, he noted that the Hybrid III spine is much stiffer than the cadaveric lumbar spine. Ruan et al. [35] developed a detailed finite element model of the human head coupled with a Hybrid III dummy representing a 50th percentile male using PAMCVS which couples PAMCRASH with MADYMO. The main intention was to examine brain injuries sustained in various frontal crashes with the dummy restrained by a seat belt and airbag. An excellent agreement of results between simulation and experimental results for the frontal barrier impact test was obtained. This study along with those previously mentioned [31-35] further validate the kinematics of the Hybrid III finite element model and illustrate the ability to investigate injuries and loads at specific regions of the human body when coupled with the Hybrid III dummy model using finite element analysis. Marzougui et al [36] completed a study of a New Car Assessment Program (NCAP) full scale crash test using LS-DYNA for the simulations. The test consists of the vehicle in a frontal impact with a Hybrid III dummy and driver side airbag. For this study he modeled the thorax and neck with flexible parts while the rest of the dummy parts were modeled with rigid parts. Joints were modeled using spherical or cylindrical rigid body joints. The thorax was validated against a standard impactor test and showed good correlation with experimental tests in terms of chest accelerations and deflections.

The Hybrid III dummy model available in LS-DYNA allows for the user to choose between rigid and deformable body parts and to input joint characteristics although the default characteristics give reasonable results [37].

2.4. Summary of literature reviewed

The steering assembly model presented by Wang et al. was merely developed for implementation in CAL3D. The drop tower and sled tests were carried out for the purposes of validating the steering assembly model. The investigation conducted by Lim et al.'s concentrated on the stiffness characteristics of the steering column on impact with the body block. Young-Sun Park et al. also only considered stiffness characteristics of the steering column to reduce driver injury. The investigation conducted by Naab et al., although fairly extensive, also concentrated on stiffness properties of the steering wheel in addition to column stroke, wheel/column weight, column angle and dish depth. The investigation conducted by Shyu et al. involved improving on an existing design through material and geometric modifications. However, the geometric modifications only involved the hub. Perhaps the most pertinent contribution were the investigations conducted by Altenhof et al. which concentrated on the steering wheel as opposed to the entire steering assembly. These investigations considered wheel angle, column angle, and impact velocity on already existing steering wheel designs.

From the literature reviewed, several observations can be made regarding the research of steering wheel armatures under impact conditions.

- The torso plays an important role in the injuries and fatalities resulting from automobile accidents and should be high on the priority list of body areas to be protected by safety devices.

- Previous research involving the steering assembly has been primarily directed towards steering wheel orientation and steering assembly stiffness characteristics. More importantly, previous investigations have only dealt with already existing steering assembly designs.

- The need to fully understand how the steering wheel geometry affects its crashworthiness performance very much exists. There is no guarantee that

the steering column will compress, that the occupant will be restrained or that the airbag will deploy. Even with airbag deployment, documentation on steering wheel induced trauma through the airbag exists.

These observations indicate that an investigation into the effect of steering wheel geometry on the crashworthiness performance of a steering wheel armature is necessary. A parametric study of the steering wheel armature's geometry will provide information that will enable engineers to properly design steering wheel armatures for maximum energy absorption and acceptable load management capabilities. In addition, this information may also be used by design engineers to enhance the performance of already existing steering wheel armatures during crash events.

3. FOCUS OF RESEARCH

Previous investigations have focused mainly on the steering assembly as a whole. In addition, investigations pertaining to the steering wheel in the past have focused on already existing steering wheel designs with emphasis on steering wheel orientation.

This work will address geometric and material concerns on new steering wheel geometry as follows:

- Select a number of steering wheel armatures with variations in armature geometry and material composition.
  - Carry out experimental testing under identical test conditions on all steering wheel armatures. The purpose of the experimental testing is to examine how the variations in armature geometry affect the performance of steering wheels in terms of;
    - Peak Load, F_{peak}
    - Crush Force Efficiency, $C.F.E$
    - Elastic Response, $\Delta E_{elastic}$
    - Energy Efficiency, e_e
    - Specific Energy, $e_{specific}$
    - Energy Absorption Factor, $E.A.F$
- Conduct an analysis of the results from the experimental test to determine which geometrical parameters to investigate.
- Develop a highly detailed parametric model of a steering wheel armature.
  - Carry out simulations with variations in predetermined design parameters which strongly influence crash performance.
  - Conduct an analysis based on the performance criteria given above with the aim of optimizing steering wheel geometry for impact loading.
  - Develop a rating score as a function of both dummy and steering wheel performance criteria.
  - Evaluate the performance of the steering wheels on impact with a Hybrid III.

4. DEFINITIONS AND INJURY CRITERIA ASSOCIATED WITH STEERING WHEEL TESTING AND PERFORMANCE

This investigation deals extensively with impact testing of the steering wheel and requires definition of some common terms associated with the steering wheel geometry and crash testing performance measures.

4.1. Definitions

4.1.1. Steering wheel armature

The steering wheel armature refers to the skeleton of the steering wheel which supports the majority of devices attached to the steering wheel as shown in Figure 4.

4.1.2. Rim

The rim refers to the quasi-toriodal outer ring usually griped by the driver's hands during driving as illustrated in Figure 4.

4.1.3. Spokes

The spokes refer to the entities connecting the rim to the hub as shown in Figure 4.

4.1.4. Hub

The hub refers to the region in the center of the steering wheel that joins the spokes to the steering shaft.
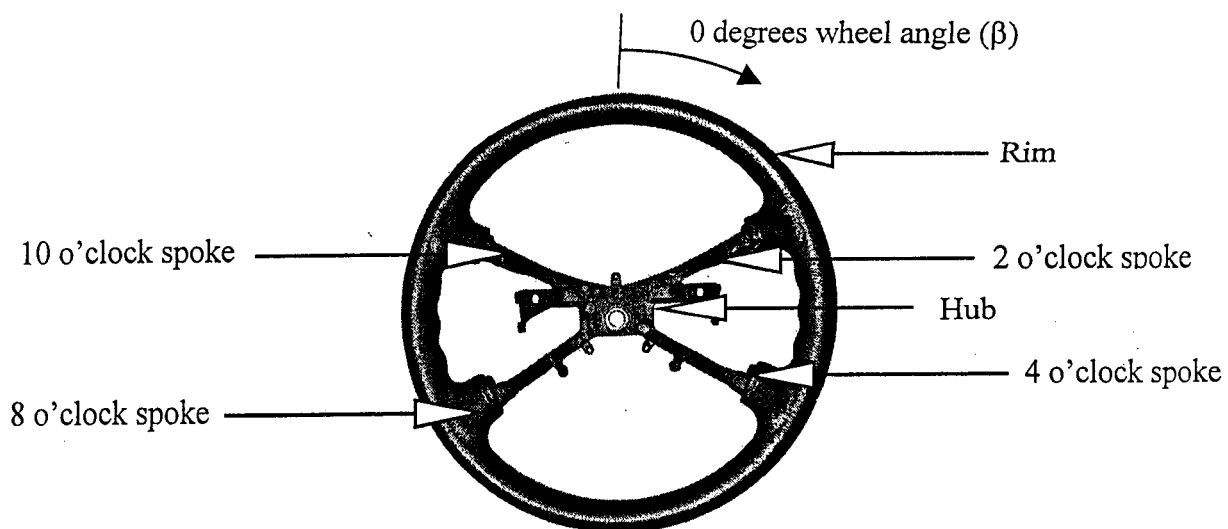
Figure 4. Definitions associated with steering wheel geometry and orientation.

4.1.5. Wheel angle

The wheel angle refers to the rotational orientation through which the steering wheel is being turned. The wheel angle is commonly measured using an identical approach to that of an analog clock, or in degrees as illustrated in Figure 4.

4.1.6. Dish depth

The dish depth refers to the perpendicular distance from a plane through the top of the rim to the top of the hub as illustrated in Figure 5.
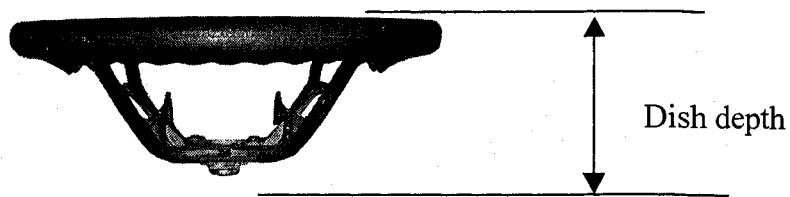
Figure 5. Definition of the dish depth.

4.1.7. Column angle

The column angle refers to angular displacement from a horizontal reference line to the centerline of the steering column. In measuring the column angle, positive values are taken in a clockwise sense from the horizontal reference line as illustrated in Figure 6.
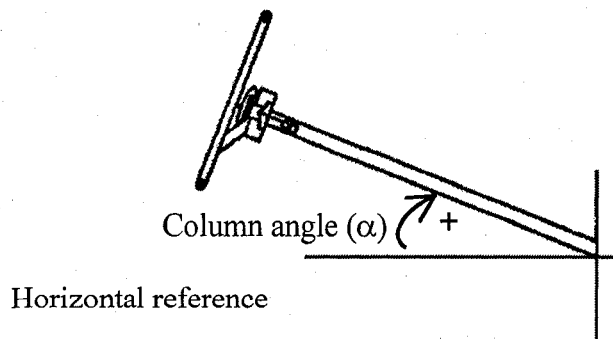
Figure 6. Definition of the Column angle.

4.2. Performance measures used to quantify crashworthiness

Federal Motor Vehicle Safety Standards, detailed in references [1 and 2], specify motor vehicle crash tests that ensure occupant safety and stipulate acceptable performance requirements in terms of occupant injury and load levels developed on both the occupant and vehicular structure when a vehicle traveling at specified velocity impacts a fixed rigid barrier. A description of the occupant based criteria and the structural based criteria is given in the following section.

4.2.1. Occupant based criteria

The development of the occupant injury criteria stems from laboratory experiments in which drop tests and pendulum tests where carried out on different parts of embalmed cadavers [38]. The acceleration (and deceleration) associated with various types of impact obtained from these tests demonstrated the influence of pulse length on the severity of the injuries sustained by the cadavers.

4.2.1.1. Injury criteria

The Wayne state tolerance curve illustrated in Figure 7 was developed for head injuries caused when the front of the head strikes a hard object or when the head is loaded through the neck by a decelerating body.
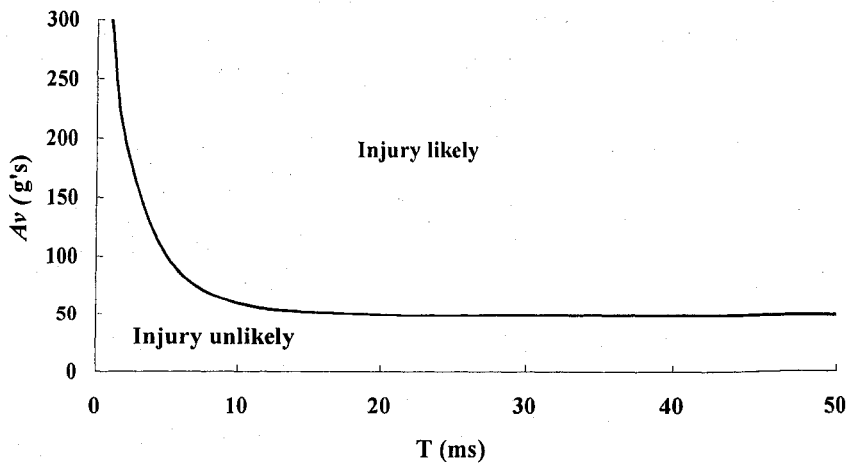
Figure 7. Wayne State tolerance curve for head impact [38].

18

Gadd [38] introduced the severity index (SI)

$$SI = \int_0^T A_v^{2.5} dt \qquad (1)$$

Where $A_v = a_v/g$, a_v is the average head acceleration (or deceleration) which may vary throughout the loading pulse having a duration of T(s) with 2.5 ms < T < 5 ms. Gadd suggested that $SI = 1000$ marks the threshold between non-fatal and fatal injuries. The Head Injury Criterion (HIC) was then developed by replacing the dimensionless acceleration A_v by an average value and is calculated as;

$$HIC = \left[\left\{ \frac{1}{t_2 - t_1} \int_{t_1}^{t_2} a(t) dt \right\}^{2.5} \cdot (t_2 - t_1) \right] \qquad (2)$$

Where $a(t)$ is the resultant acceleration magnitude (in g's) at the center of gravity of the head, t_2 and t_1 are the time instants (in seconds) during the impact that maximize the *HIC*. The time interval, t_1 to t_2, may not be greater than 36 ms. A value of $HIC = 1000$ is considered life threatening.

Neathery [39] developed thoracic response corridors for crash tests dummies when impacted under part 572 [29]. Use of these corridors is required in FMVSS 208 to evaluate the deflection and acceleration of the thorax. The resultant acceleration at the center of gravity of the upper thorax of the crash test dummy must not exceed 60 g's except for intervals whose cumulative duration is not more than 3 milliseconds and the chest deflection developed on the crash test dummy must not exceed 75 mm.

In order to evaluate the injury of the occupant with a quantitative analysis the Injury Criterion (IC) is defined as follows;

$$IC = 0.6 \cdot HIC + 0.4 \cdot CSI \qquad (3)$$

The CSI is the Chest Severity Index and is calculated by applying the chest acceleration into the acceleration term of the SI in equation (1) and is given by;

$$CSI = \int_{t_{begin}}^{t_{end}} a(t)^{2.5} dt \qquad (4)$$

Where $a(t)$ is the acceleration magnitude and t is time. The limit of integration, t_{begin} and t_{end} are the times at the beginning and end of the impact respectively.

The Thoracic Trauma Index (TTI) [40] was developed to assess the performance of restraint systems because of the significant difference in loading pattern on the thorax of the occupant when contact occurs with a seatbelt, airbag or steering wheel. The TTI is given by the following expression:

$$TTI = \frac{1}{2}\left[T_{12} + \max(a_{lu}, a_{ll})\right] \qquad (5)$$

Where T_{12} is the peak lateral acceleration of the T_{12} spinal segment in g's, a_{lu} is the peak left upper rib Y acceleration in g's, and a_{ll} is the peak left lower rib Y acceleration in g's.

Table 1 summarizes the injury criteria specified by government regulations for the head and chest deflections and accelerations measured on a Hybrid III dummy in test crashes.

Table 1- Summary of Injury measures. [41]

Measurement	Good	Acceptable	Marginal	Poor
HIC	<750	750-899	900-999	1000 or more
Chest Compression	<50mm	50-59mm	60-74mm	75mm or more
Chest Acceleration	<60g	60-74g	75-89g	90g or more

4.2.1.2. Injury severity

The Abbreviated Injury Scale (AIS) is an anatomical scoring system which provides a method of ranking the severity of an injury. It is the foundation for methods assessing multiple injuries or for assessing cumulative effects of more than one injury. Injuries are ranked on a scale of 0 to 6 as shown in Table 2.

Table 2-AIS scoring system. [41]

Injury	AIS Score
0	No injury
1	Minor injury
2	Moderate injury
3	Serious injury
4	Severe injury
5	Critical injury
6	Fatal (Unsurvivable) injury

The Maximum Abbreviated Injury Score (MAIS) is derived from the AIS and is used to represent the overall injury severity. For cases with multiple injuries, the MAIS is the single highest AIS score. For cases involving single injuries, the AIS is also the MAIS.

The Injury Severity Score (ISS) is an anatomical scoring system that provides an overall score for patients with multiple injuries. Each injury is assigned an AIS score and is allocated to one of six body regions. (Head, face, chest, abdomen, extremities and external). The three most severely injured body regions have their score squared and summed to produce the ISS score. The score takes values from 0 to 75.

4.2.2. Structural based criteria

An ideal energy absorber would have a square force versus deflection curve where the uniform crush force is determined by the safe maximum load (peak

load tolerance) to be transmitted and the available crush distance (displacement). Peak load tolerances for the frontal thorax and upper torso derived from the response corridors recommended by Neathery [39] are shown in Figure 8.
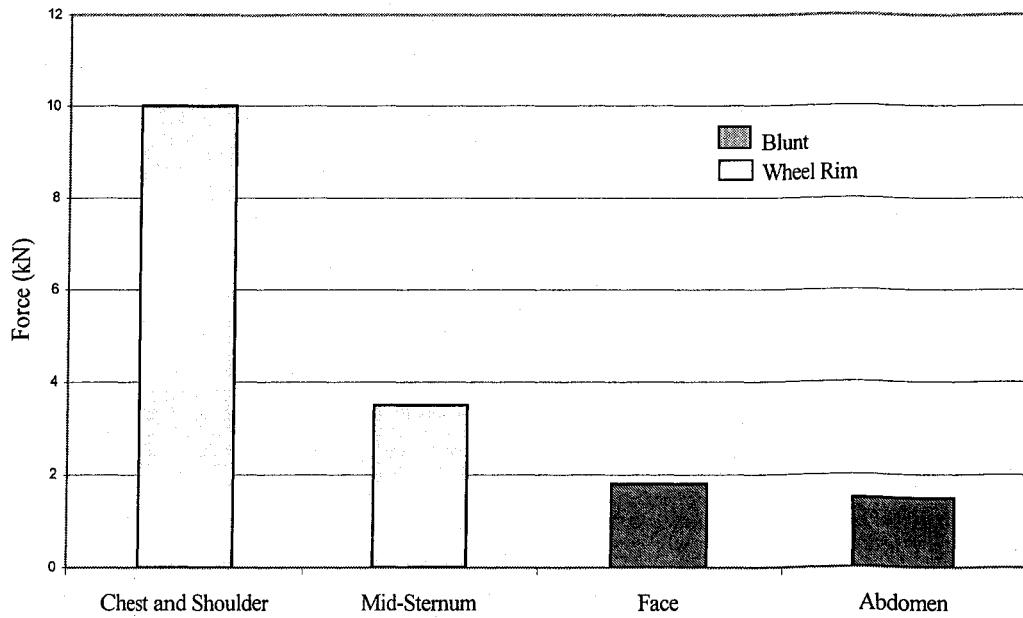
Figure 8. Peak load tolerances for the chest, shoulders, face and abdomen [18].

A stiff rim will offer protection to the chest at the expense of the abdomen and face (restrained occupant), which have lower load tolerances. In order to maintain a balance between the two, a recommended limit [18] as to how stiff/soft the rim should be is illustrated in Figure 9 in terms of radial and tangential loads.
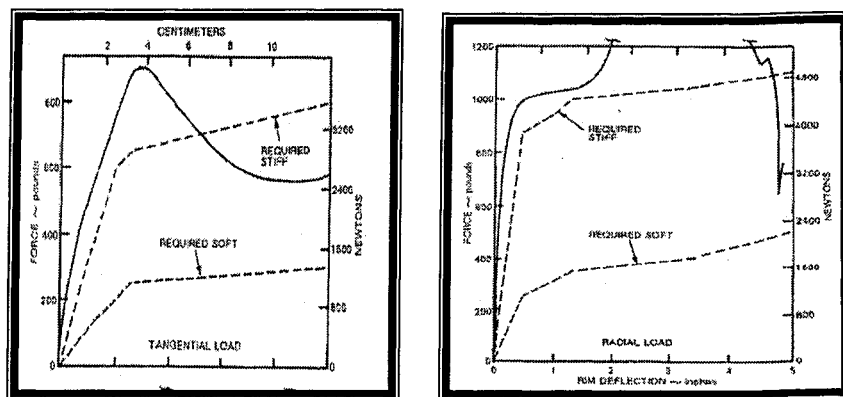
Figure 9. Radial and tangential loading specification curves [18].

5. EXPERIMENTAL IMPACT TESTING OF ARMATURES OF DIFFERENT GEOMETRY AND MATERIAL COMPOSITION

Samples of steering wheel armatures from popular 1996-2001 compact vehicles were selected according to the current percentages sales of motor vehicles [Appendix A] in order to provide meaningful results pertinent to the performance of on road vehicles involved in real life vehicle collisions. All the steering wheel armatures are four spoke steering wheels from a similar vehicle line.

All the steering wheel armatures tested in this investigation were acquired from an automobile recycler. No damage or deformation was visible in any of the test specimens. The steering wheel was removed from the vehicle and the armature was then extracted from the steering wheel by removing any attached switches or back covers. The polyurethane covering was not removed from the armatures as this material has little or no influence on the structural strength of the armature. Table 3 summarizes the geometrical, material, and production characteristics of each steering wheel armature considered in the investigation.

Table 3-Summary of steering wheel armatures investigated.

Company	Year	Model	# of Spokes	Rim Diameter (mm)	L_{dish} (mm)	$m_{steering\ wheel}$ (kg)	Material Composition	Production Method	Urethane Application
Daimler Chrysler	2000	Neon	4	368.3	139.7	1.345	Magnesium alloy	Cast	Rim
Daimler Chrysler	2001	Neon	4	368.3	139.7	1.357	Magnesium alloy	Cast	Rim
General Motors	1996	Cavalier	4	355.6	120.65	1.923	Alloy Steel	Welded	Rim
General Motors	2000	Cavalier	4	355.6	120.65	1.929	Alloy Steel	Welded	Rim
Ford Motor Company	2000	Focus	4	342.9	95.25	1.216	Magnesium Alloy	Cast	Rim, hub & spokes
Ford Motor Company	2001	Focus	4	342.9	95.25	1.174	Magnesium alloy	Cast	Rim, hub & spokes

5.1. Experimental testing procedure

A custom designed drop-tower testing device developed by Altenhof [42] was used for impact testing of the steering wheels. An illustration of the testing device is shown in Figure 10. Two guideposts allow translation of a crosshead in the vertical direction (z axis direction). A 57.3 kg rigid plate is attached to the translating crosshead. A pin joint allows for variation in the steering assembly column angle and variation of the steering wheel angle is achieved through a rotary joint, which permits rotation about the column axis if a hydraulic power supply is energized to unlock the joints. De-energizing a hydraulic power supply locks the wheel angle and column angle joints. A 44.5kN triaxial load cell mounted directly below the rotary joint is used to determine the impact force acting between the rigid plate and the steering wheel. An accelerometer mounted on top of the rigid plate is used to determine the acceleration of the rigid plate in an impact test. Figure 10 and Figure 11 illustrate the experimental testing apparatus and setup and the accelerometer mounted on top of the rigid plate respectively. A linear variable differential transformer (LVDT) with a 400 mm range is rigidly attached to the translating crosshead to determine displacements of the crosshead during the impact.

Rigid plate

Neon steering wheel armature

Triaxial Load cell
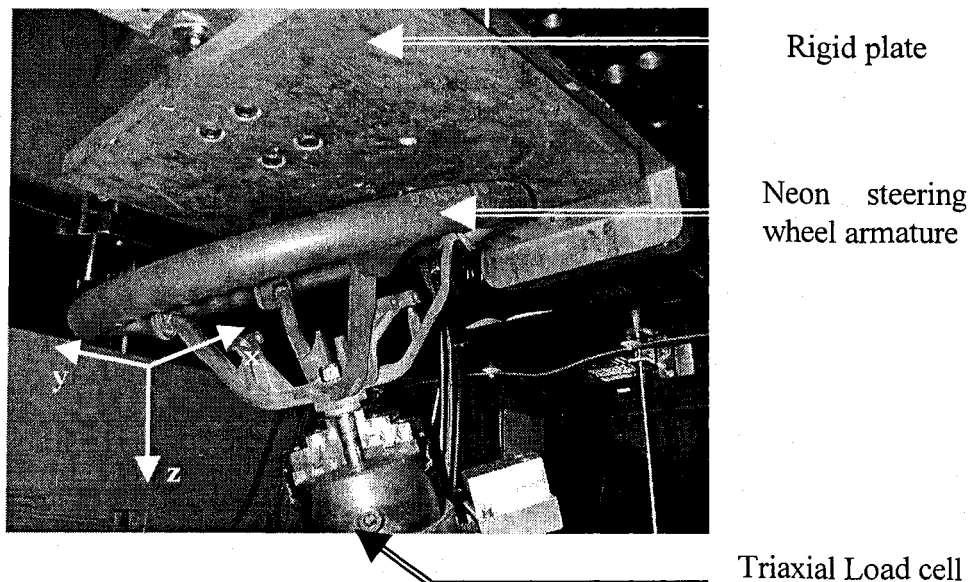
Figure 10. Experimental testing apparatus and setup.
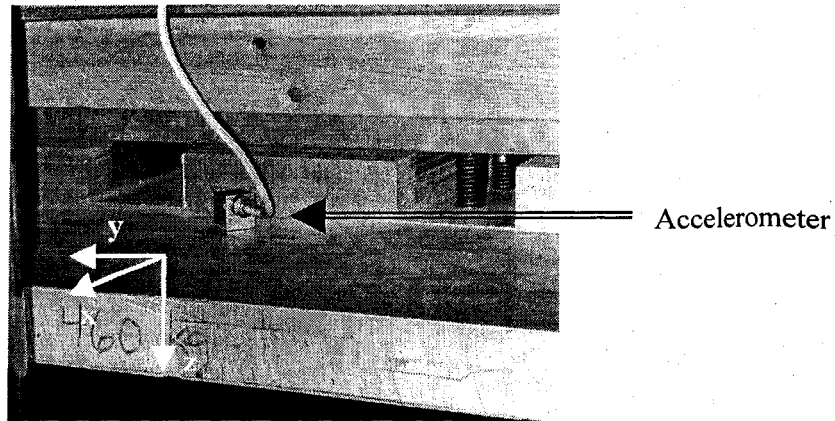
Figure 11. Accelerometer mounted on top of the rigid plate.

All the steering wheels were impacted at the 6 o'clock position with a 24-degree column angle. For each test a new steering wheel was bolted to the mounting device. The triaxial load cell, LVDT, and accelerometer were zeroed (placed into reference position). The rigid plate was then raised to a specific height such that when released it would develop an impact speed of 3.2 m/s.

Measurements from all the transducers were taken using high speed data acquisition in which observations were recorded every 0.16 ms.

5.2. Methods used in this investigation to quantify the crashworthiness performance of steering wheels

Crashworthiness performance measures have been developed by a number of researchers. Altenhof [42] developed the Energy Absorption Factor, Baumeister et al [43] developed the Energy Absorption Capacity, Krauss and Laananen [44] developed the Crush Force Efficiency, Magee and Thorton [45] developed the Energy efficiency, and Maiti et al. [46] developed the energy absorption diagrams. All these methods help to better understand how structures perform during impact.

A description of the performance measures considered in this study is presented in the following paragraphs.

5.2.1. Energy absorbed

Data from the load cell or the accelerometer and the LVDT is used to develop the load versus displacement curves. From the load versus displacement data the energy absorbed during the impact is equated to the work done by the impacting force and is determined by integration of the load versus displacement profile represented by equation (6). It is experimentally difficult to measure displacements in the x and y directions, therefore the energy absorbed by the steering wheel armature is an approximated by equation (7). The integration in equation (7) is replaced with a summation as presented in equation (8). For a finite number of data points, a number of integration schemes can be employed. Equation (8) represents the rectangular rule for integration of a series of data points which provides similar results when the trapezoidal rule is employed [21].

$$E_{absorbed} = \int \vec{F} \cdot d\vec{r} = \int F_x \cdot dx + \int F_y \cdot dy + \int F_z \cdot dz \qquad (6)$$

$$E_{absorbed} = \int F_z \cdot dz \qquad (7)$$

$$E_{absorbed} = \sum_{i=2}^{N-2} F_{z_i} \cdot \left(\frac{z_{i+1} + z_{i-1}}{2} \right) \qquad (8)$$

5.2.2. Peak Load

The peak load is the square root of the sum of squares of the loads in the x, y, and z direction and is given by equation (9).

$$F_{peak_i} = \max\left(\sqrt{F_{x_i}^2 + F_{y_i}^2 + F_{z_i}^2} \right) \qquad (9)$$

5.2.3. Crush Force Efficiency (C.F.E.)

The C.F.E. is the ratio of the average crushing force in the z-axis direction to the peak force in the z-axis direction and is given by equation (10). Equation (11) is used to determine the average crushing force where Δt is the total time during impact.

$$C.F.E. = \frac{F_{avg}}{\max(F_{peak_z})} \quad (10)$$

$$F_{avg} = \frac{1}{\Delta t} \int F_z(t) \cdot dt \quad (11)$$

The most desirable situation would be a value of unity, where the magnitude of the initial peak force is equal to the average crush force, represented by a square load-displacement curve. Thus, for a given maximum load, energy absorption is maximized throughout.

5.2.4. Elastic response

The difference between the maximum energy absorbed and the total energy absorbed represents the elastic response of the system and is given by equation (12).

$$\Delta E_{elastic} = E_{max} - E_{absorbed} \quad (12)$$

A value of zero, representing a completely plastic impact situation, would be most desirable.

5.2.5. Energy efficiency

The energy efficiency is a measure of crush effectiveness developed by Magee and Thorton [45] for crushing tubes and is given by equation (13).

$$e_e = \frac{E_{absorbed}}{F_{max} L} \quad (13)$$

For the purpose of quantifying steering wheel performance, taking into account the steering wheel column angle, this measure was adapted and modified to equation (14).

$$e_e = \frac{E_{absorbed} \cdot \cos\alpha}{F_{avg} L_{dish}} \quad (14)$$

5.2.6. Specific energy

The specific energy is defined as the energy absorbed per unit mass and is calculated using equation (15).

27

$$e_{specific} = \frac{E_{absorbed}}{m_{steering\ wheel}}$$ (15)

The specific energy presents a method to quantitatively compare the energy absorption characteristics of structures with different masses.

5.2.7. Energy Absorption Factor (*E.A.F.*)

The *E.A.F.* normalizes the absorbed energy by the armature to the available energy before the impact as presented in equation (16).

$$E.A.F. = \frac{E_{absorbed}}{E_{initial}}$$ (16)

The initial energy is the sum of the kinetic and potential energy of the rigid plate before impact which can be mathematically represented as;

$$E_{initial} = \frac{1}{2} \cdot m_{plate} \cdot v_{impact}^2 + m_{plate} \cdot g \cdot \Delta_{max}$$ (17)

The impact velocity is obtained through differentiation of the displacement-time data. Equations (8), (16) and (17) are then combined to determine the *E.A.F.* as shown in equation (18).

$$E.A.F = \frac{\sum_{i=2}^{N-2} F_{z_i} \cdot \left(\frac{z_{i+1} + z_{i-1}}{2} \right)}{\frac{1}{2} \cdot m_{plate} \cdot v_{impact}^2 + m_{plate} \cdot g \cdot \Delta_{max}}$$ (18)

5.3. Experimental testing results

The force versus displacement profiles for all steering wheel armatures are presented in Figures 12 though 18. An SAE Class 600 [47] filter was used to reduce the high frequency noise from the observation obtained from the accelerometer. Loading results calculated from the observations obtained from the accelerometer are compared with results obtained from the load cell. In addition, Figure 18 illustrates the energy absorbed for all steering wheel armatures as a function of crosshead displacement during testing. Table 4 summarizes the results obtained for the F_{peak}, *C.F.E.*, $\Delta E_{elastic}$, e_e, *E.A.F.*, and the $e_{specific}$.
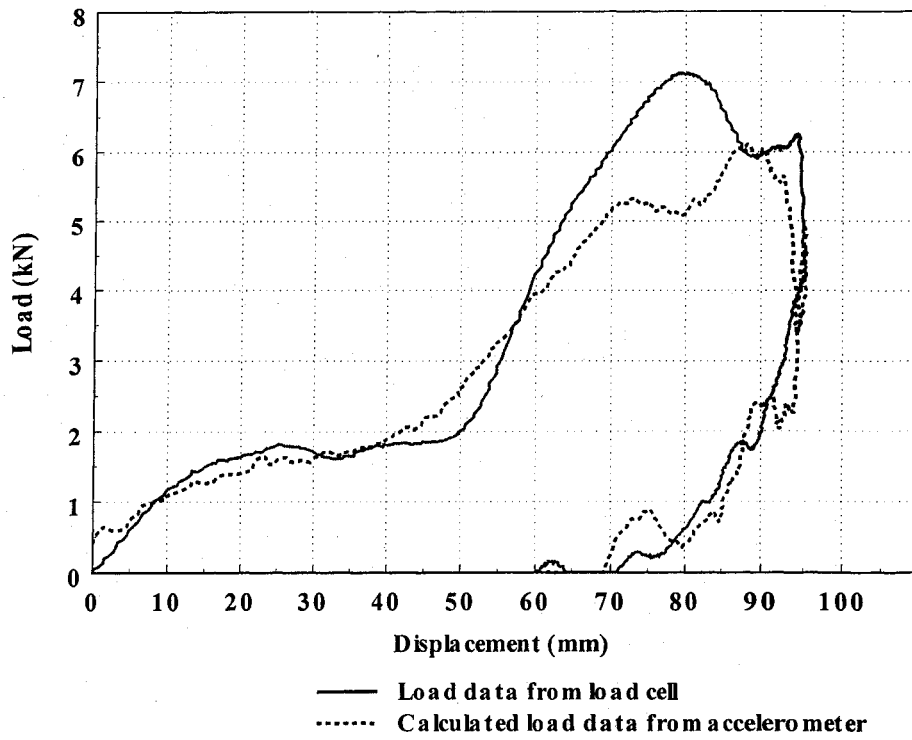
Figure 12. Load versus Displacement profile for the Neon 2000.
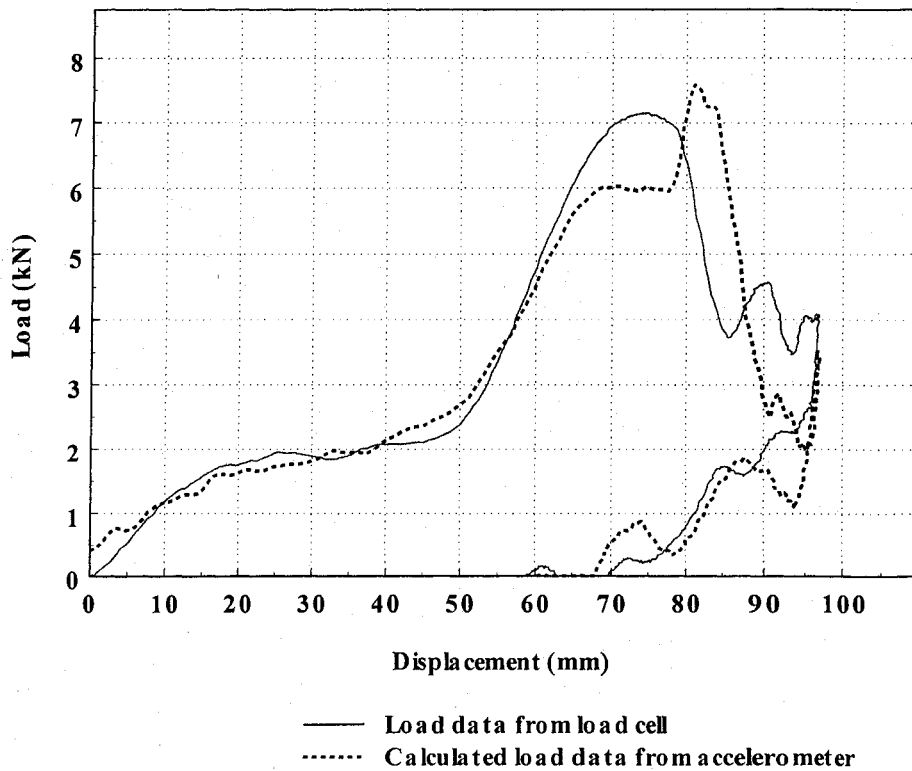
Figure 13. Load Versus Displacement profile for the Neon 2001.
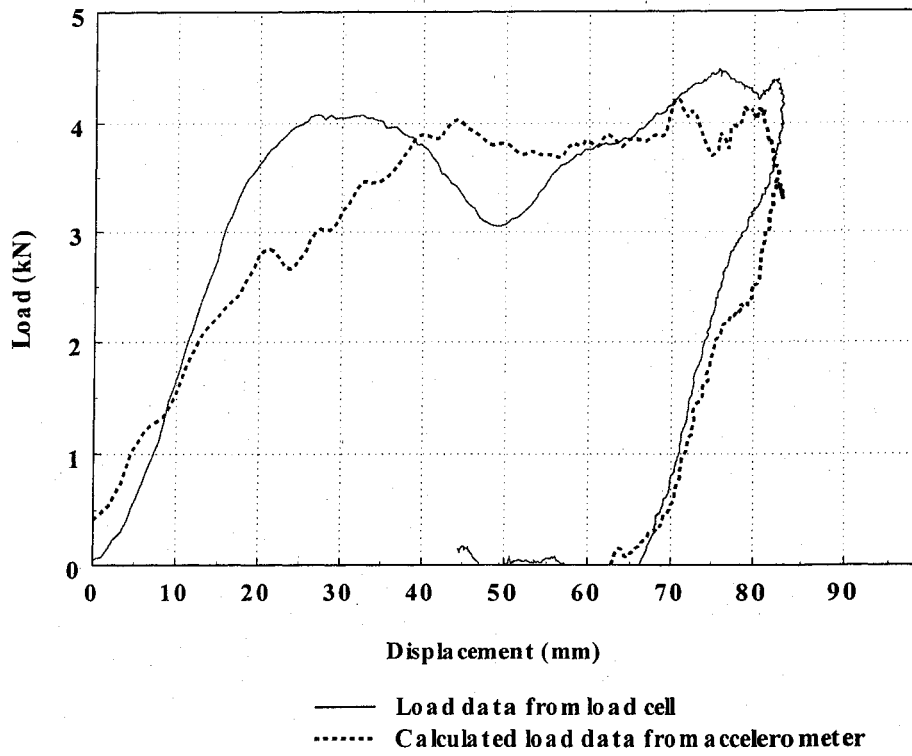
Figure 14. Load Versus Displacement profile for the Cavalier 1996.
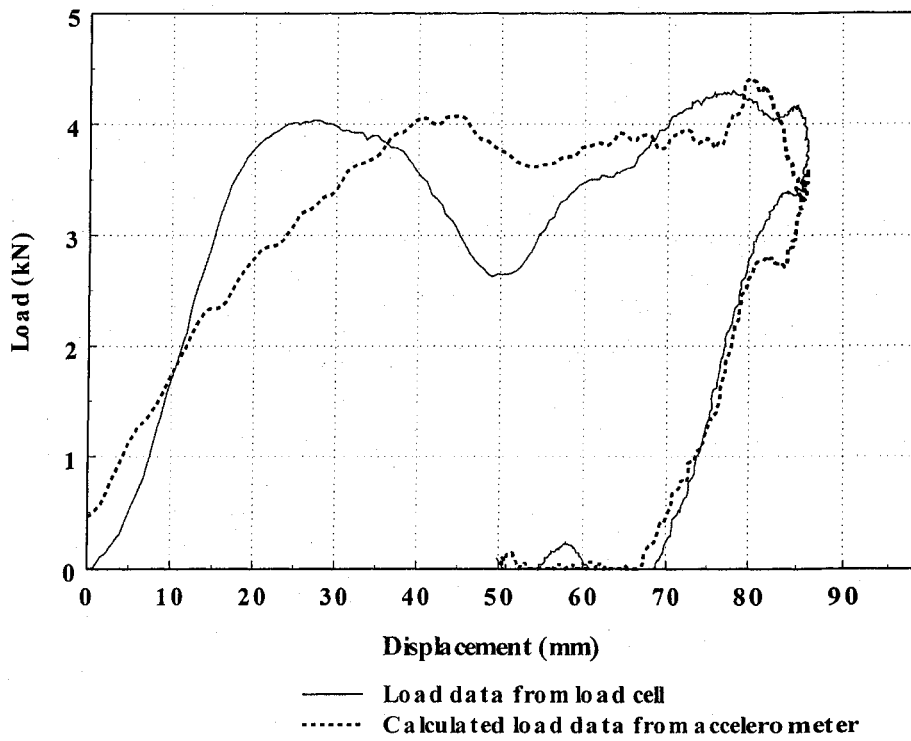
Figure 15. Load Versus Displacement profile for the Cavalier 2000.
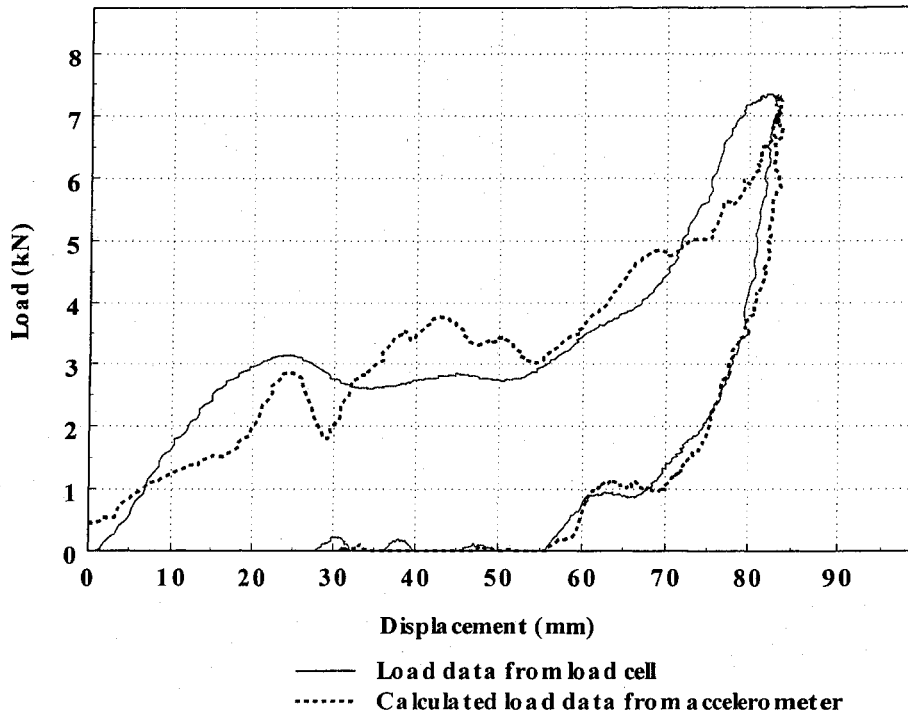
Figure 16. Load Versus Displacement profile for the Focus 2000.
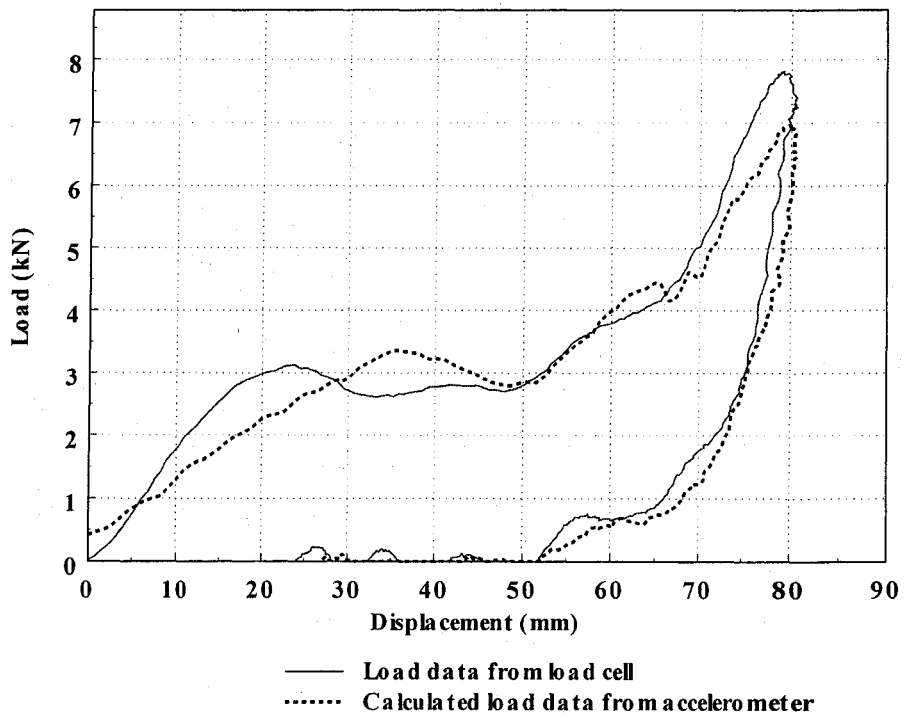
Figure 17. Load Versus Displacement profile for the Focus 2001.
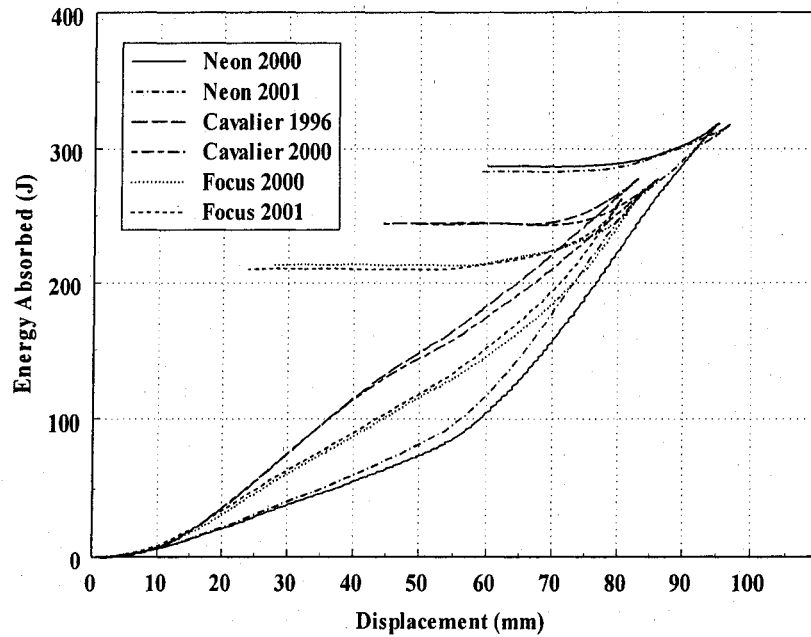
Figure 18. Energy Absorption versus crosshead displacement profiles for all steering wheel armatures.

The difference between the load cell and accelerometer data in Figure 12 through Figure 18 is attributed to the inertia properties of the steering in the z-axis direction as illustrated by the free body diagram in Figure 19.
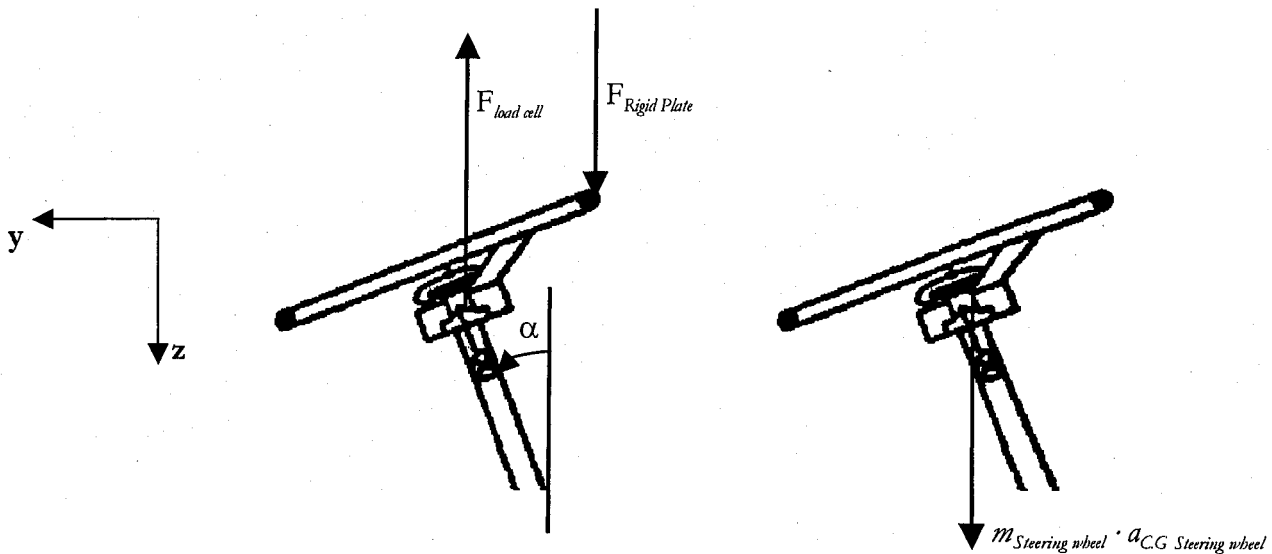
Figure 19. Free body diagram illustrating the loads acting on the steering wheel during impact with the rigid plate.

$$+ \downarrow \sum \vec{F} = m_{Steering\ wheel} \cdot a_{C.G\ Steering\ wheel} \qquad (19)$$

$$F_{rigid\ Plate} - F_{load\ cell} = m_{Steering\ wheel} \cdot a_{C.G\ Steering\ wheel} \qquad (20)$$

$$a_{C.G\ Steering\ wheel} = (F_{rigid\ Plate} - F_{load\ cell}) / m_{Steering\ wheel} \qquad (21)$$

Where $F_{load\ cell}$ is the z component of the support reaction at the hub mounting measured by the load cell and $F_{rigid\ Plate}$ is the contact force on impact with the rigid plate developed from the accelerometer data. Using equation (21), the acceleration at the mass center of the steering wheel armature is calculated and presented in Figure 20 Through Figure 22.
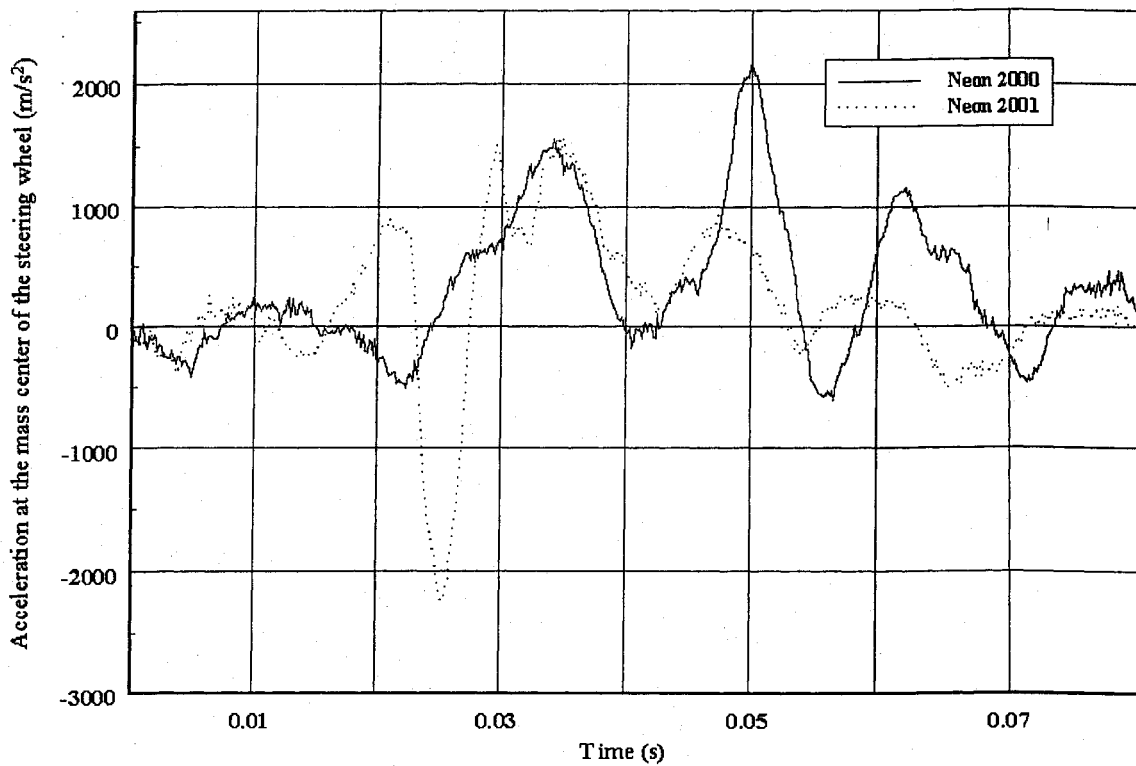
Figure 20. Difference between load cell and accelerometer data for the
Neon 2000 and Neon 2001 versus time
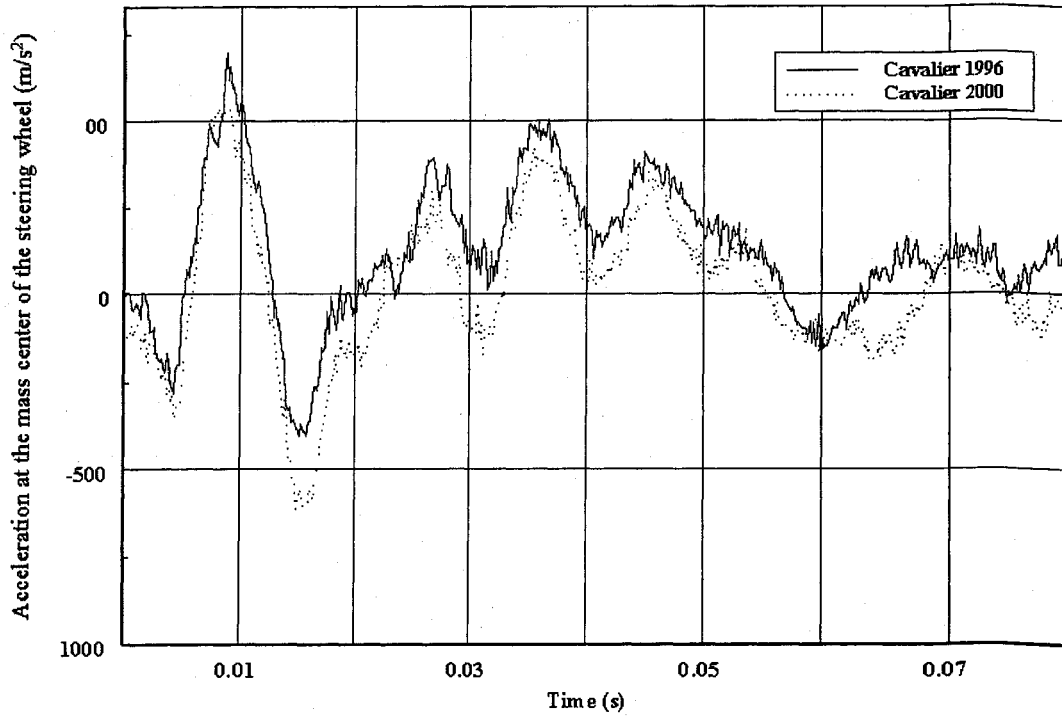
Figure 21. Difference between load cell and accelerometer data for the
Cavalier 1996 and Cavalier 2000 versus time
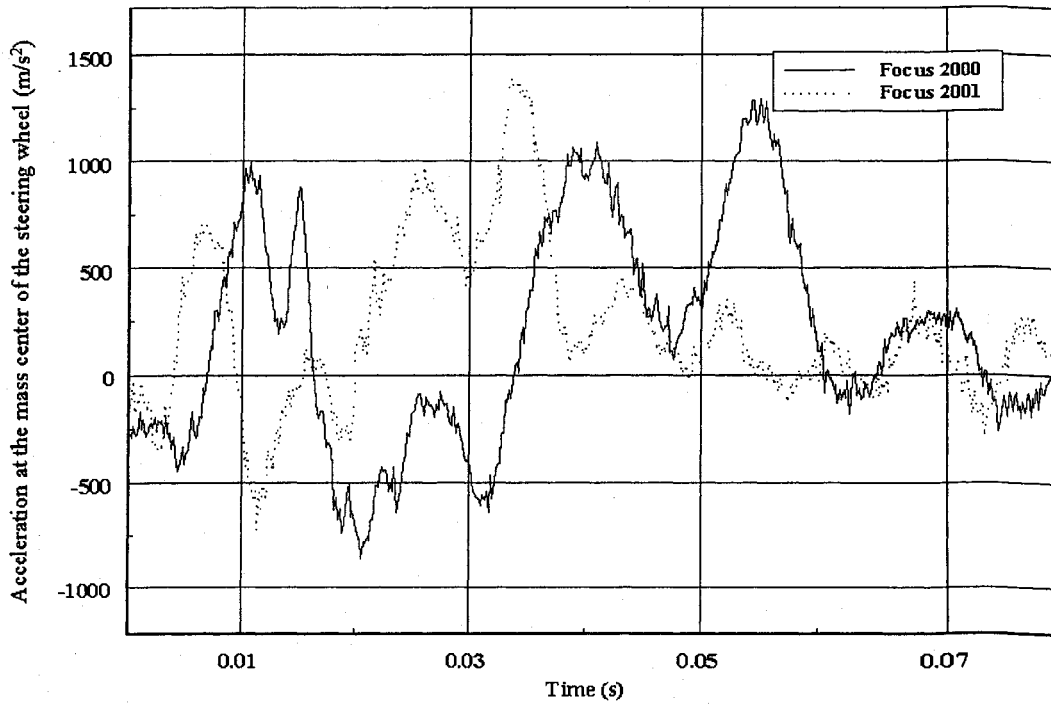
Figure 22. Difference between load cell and accelerometer data for the
Focus 2000 and Focus 2001 versus time

Table 4- Summary of Test Results.

Armature	F_{peak} (kN)	C.F.E	$E_{absorbed}$ (J)	$\Delta E_{elastic}$ (J)	e_e	$e_{specific}$ (J/kg)	E.A.F
Neon 2000	7.25	0.41	286.81	32.20	0.63	213.24	0.90
Neon 2001	7.27	0.34	283.09	35.05	0.75	208.62	0.94
Cavalier 1996	4.62	0.51	244.31	33.31	0.78	127.06	0.66
Cavalier 2000	4.43	0.53	244.06	33.18	0.79	126.52	0.82
Focus 2000	7.47	0.38	213.47	56.57	0.73	175.55	0.73
Focus 2001	7.94	0.31	210.16	53.21	0.82	179.01	0.73

5.4. Observations on the crashworthiness performance of the steering wheel armatures

Based upon the graphical illustrations in Figures 12 through 18, some general observations can be made regarding the crash performance of the armatures under consideration.

Similar shapes for the force versus displacement profiles were observed for both the Neon and the Focus steering wheel armatures. Curves from both armatures illustrated an initial plateau followed by a sharp increase in load as the 2 o'clock and the 10 o'clock spokes came into contact with the rigid plate resulting in an increase in the overall stiffness of the entire armature. The similarity in these results could be attributed to the similarity in the spoke connections to the rim for both the Neon and Focus armatures.

Failure was observed for both models of the Neon armatures. Failure of the 2000 model occurred at the change in cross sectional shape of the 8 o'clock spoke. This geometry variation, which develops stress concentrations, is most likely the cause of the failure as no voids within the die-cast part were observed below the armature surface. Failure of the 2001 model occurred at the hub/spoke joint of the 8 o'clock spoke. This failure was most likely caused by the stress riser developing due to the close proximity of the puller hole of the armature near the failure location.

The closest approximation to the square force versus displacement profile exists for the Cavalier steering wheel armatures as demonstrated in Figure 14 and Figure 15. Due to the geometry of the spokes and the joining method at the 4 o'clock and 8 o'clock rim positions, all four spokes come into contact with the rigid plate at approximately the same instant, resulting in a fairly uniform load distribution for the duration of the crash. Furthermore, the spoke geometry for the Cavalier armatures results in a significant bending loading condition for all the spokes.

Although all six steering wheel armatures exhibit similar average loads the Neon and Focus armature have lower *C.F.E* as a result of higher peak loads. This, once again, emphasizes the need for steering wheel designs that minimize peak loads.

From Figure 18 it is observed that for all the armatures tested, the energy absorption increases with displacement up to a maximum value of energy which coincides with the peak crosshead displacement. At this position the steering wheel armature transfers its elastic energy back to the rigid plate causing it to rebound. The value of the total energy absorbed represents the amount of energy used to plastically deform the steering wheel. This value is very important in designing steering wheel armatures for crashworthiness. The Neon armatures demonstrated the highest energy absorption followed by the Cavalier and Focus armatures respectively. These results indicate a direct relationship between the dish depth and energy absorption. The Neon armature has the largest dish depth resulting in larger deformations and higher energy absorption. The Cavalier armature has a moderate dish depth while the Focus armature has a much smaller dish depth. Accordingly, the Focus armature demonstrated the least amount of energy absorption. In addition, the Focus armatures exhibited the largest elastic response while similar elastic responses were observed for the Neon and Cavalier armatures.

The Neon steering wheel armatures exhibited the highest specific energy and *E.A.F* followed by the Focus and Cavalier steering wheel armatures respectively. Although the Cavalier armatures minimize peak loads and demonstrate the most favorable *C.F.E,*

the approximate weight savings of 500 grams for the Focus and Neon steering armatures emphasize the need for not only geometrical considerations for crashworthiness optimization but also for proper material selection.

Results from this experimental investigation provided essential information pertaining to geometrical characteristics and material selection that can be used in designing steering wheel armatures for crashworthiness. The dish depth has been shown to directly influence the energy absorption, although the energy efficiency may suffer somewhat if too large a dish depth is selected. In addition, the spokes may experience large bending stresses. The joining of the spokes to the rim of the steering wheel armature affects the profile and the magnitude of the loads developed on the armature under impact loading. Ideally, one would want a large dish depth to maximize energy absorption and continuous spokes along the rim of the armature to negate a sharp increase in load versus displacement profile. But consideration must be given to the effect of the dish depth on the energy efficiency of the entire armature.

An additional analysis of the data obtained from [21] was carried out to investigate the behavior of the 4-spoke steering wheel armature for impacts occurring at the midpoint of the longest unsupported part of the rim (0 degrees) and the midpoint of the shortest unsupported part of the rim (180 degrees). This analysis was done in order to observe the effect of the length of unsupported rim on the energy absorption of the rim. For all column and wheel angles, the 4-spoke rim absorbed more energy for impacts occurring at the 0 degree position and minimum for impacts occurring at the 180 degrees position. In addition, rim energy absorption decreased for impacts from 0 degrees to 180 degrees. This would suggest that the length of unsupported rim directly influences the energy absorbed by the rim and that a longer unsupported rim region is more favorable.

The experimental observations obtained from this research as well as from references [18-21] provide a basis for the parametric investigation of the influence of armature geometry on steering wheel crashworthiness.

6.0 PARAMETRIC STEERING WHEEL FINITE ELEMENT MODEL AND IMPACT INVESTIGATION

Finite element simulation of crash events is a computationally intensive process, with the amount of computational time depending on the degree of discretization generated for a specific geometry. The large deformations encountered in crash events necessitate a quality hexahedral mesh in order to accurately capture the dynamic event [48].

The explicit non-linear finite element software used for all numerical simulations is LS-DYNA. This software is often used for automotive-type crash simulations. The duration of automotive crashes is usually less than 200 milliseconds with the calculation time steps in the order of microseconds. The calculation time step depends on the material characteristics and model discretization. The numerical analysis involved a pre-processor to create and mesh the steering wheel model, a finite element analysis code to analyze the problem, and a post-processor to investigate the results.

6.1. Parameterization of the steering wheel geometry

A parametric model of the steering wheel armature was developed for preprocessing with TrueGrid [49]. TrueGrid is a powerful pre-processor with extensive parameterization capabilities which simplify mesh modifications and regeneration.

The exact surface geometry of the part under investigation is defined separately. A meshed block, which is an approximation of the model, is then defined. Excess volumes of the mesh are removed to match the general shape of the part. The meshed block is then projected on to the exact surface geometry of the part. Both the meshed block and the surface geometry are parametric allowing extensive flexibility in model development. Holes, fillets, surface definitions for contact, and node definitions for boundary conditions are also included in the part definition which follows new parametric changes. This projection method removes much of the manual work associated with mesh generation.

38

Several papers with finite element models of the steering wheel armatures were reviewed for qualitative information on dimensions, form, and orientation of the steering wheel [18-21, 50, 51]. In addition, measurements were taken over a wide range of vehicle models [Appendix B]. A total of 23 parameters were required in order to complete the model and produce an accurate geometric description of the steering wheel armature. The parameters used to describe the rim, the spokes, and the hub are illustrated in Figure 23 through Figure 28.

As illustrated in Figure 23 the rim consists of a celery section typical of the more recent models of steering wheel armatures observed. The radius of the arc, rimr1, controls the width and depth of the section while the location of the spoke on the rim is controlled by the angle rimt2. Also illustrated in Figure 24 and Figure 25 is the dish depth and rim radius respectively.
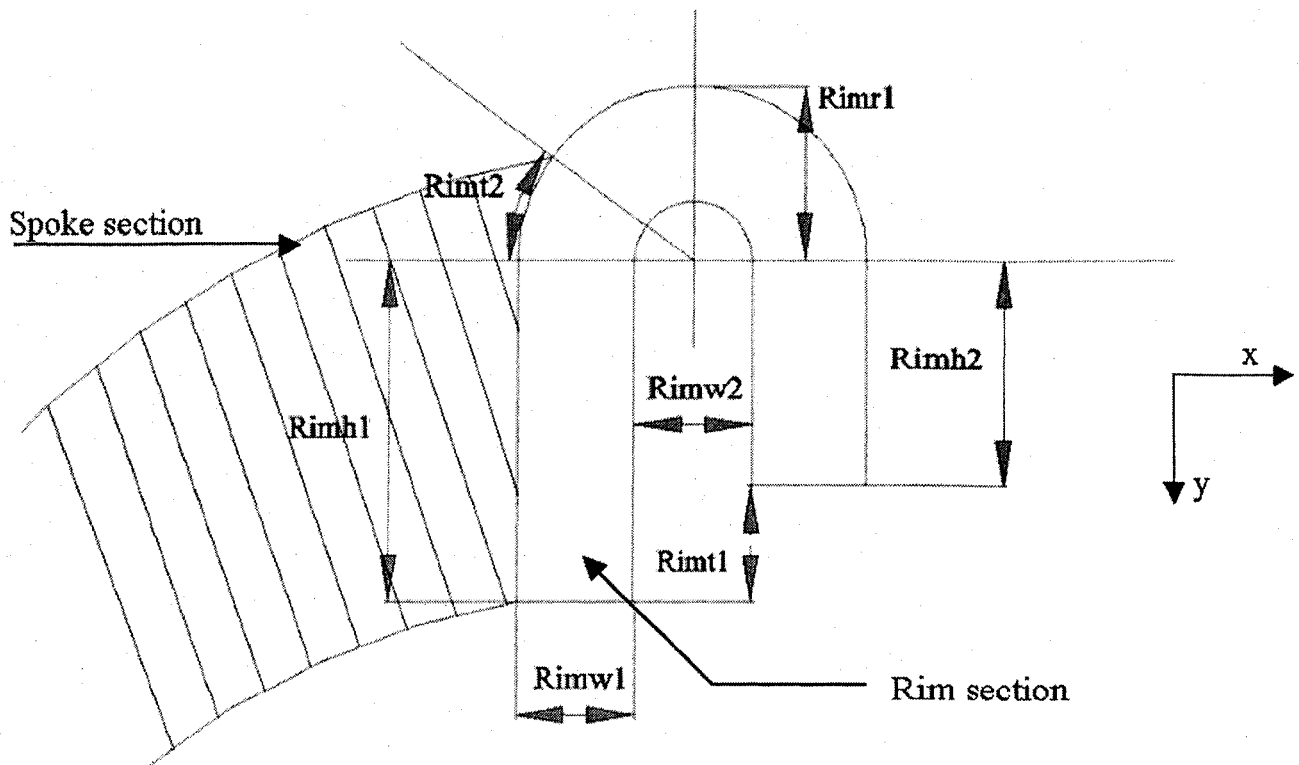
Figure 23. Parameters associated with the rim's local Geometry

39
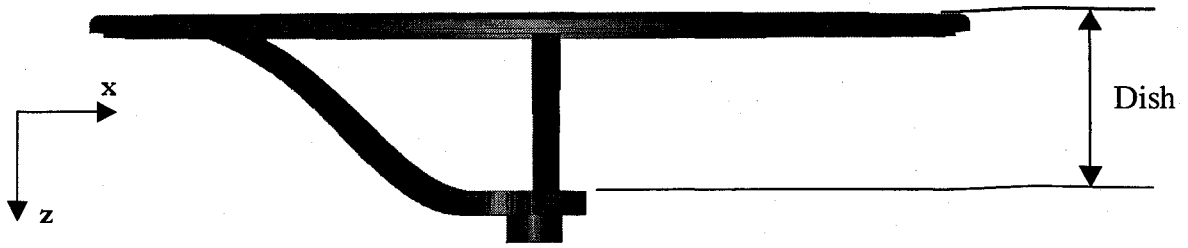
Figure 24. Dish Depth
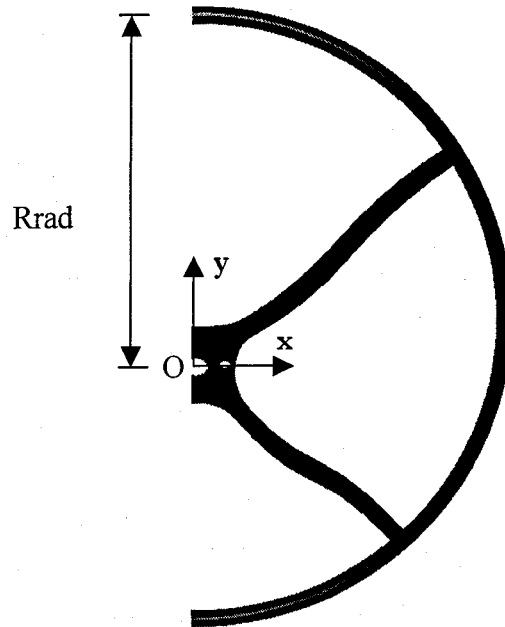
Figure 25. Rim Radius

The geometry of the hub, illustrated in Figure 26, is controlled by the orientation of the spokes along the rim of the armature through angles spk3theta1 and spk5theta1. The origin (O) is also the center of the hub. It is important to note that the center of the hub is not the center of steering wheel. The center of the steering wheel is located 3-6 mm above the hub center. The depth of the hub, Hdepth, illustrated in Figure 27, also

controls the depth of the spokes which influence the cross sectional geometry of the rim. For this reason, the parametric hub model was developed first.
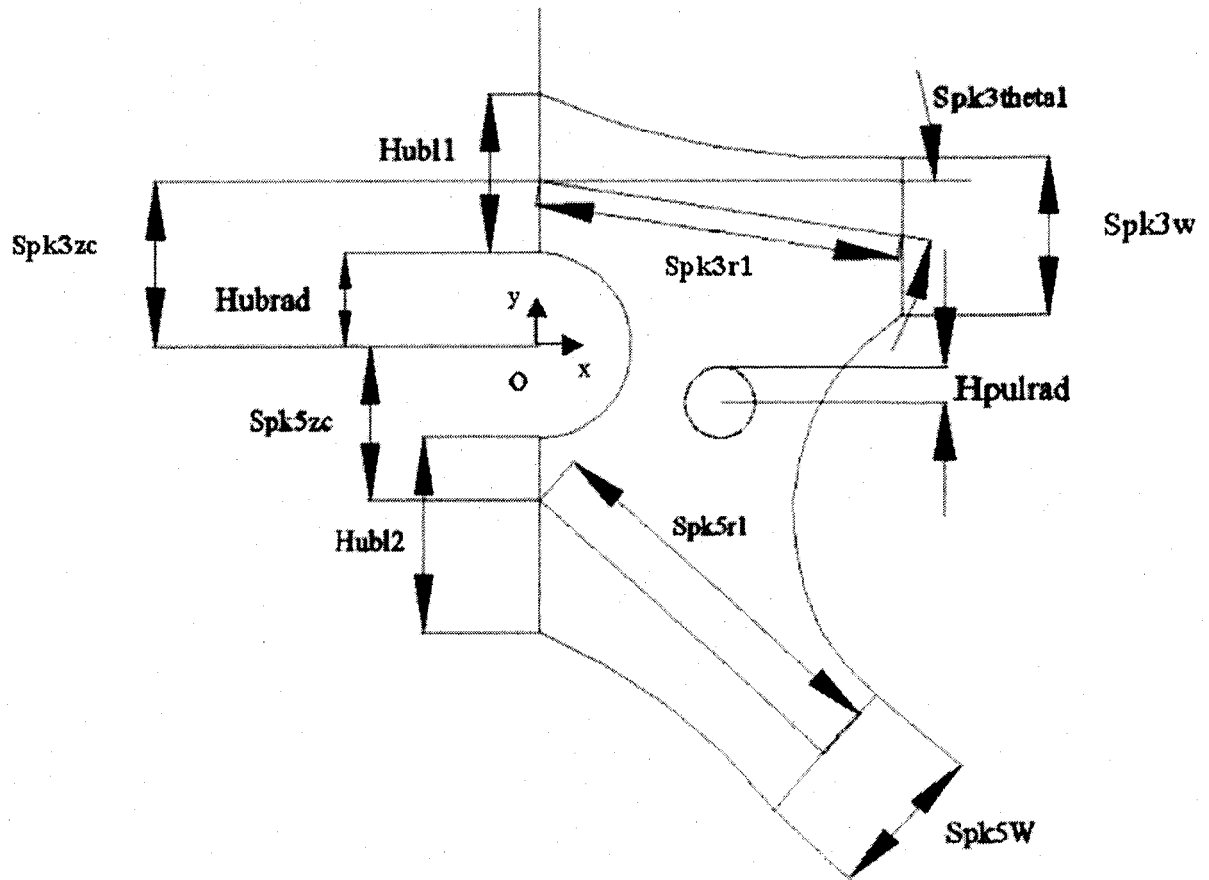
Figure 26. Parameters associated with the hub's local geometry (Top view).
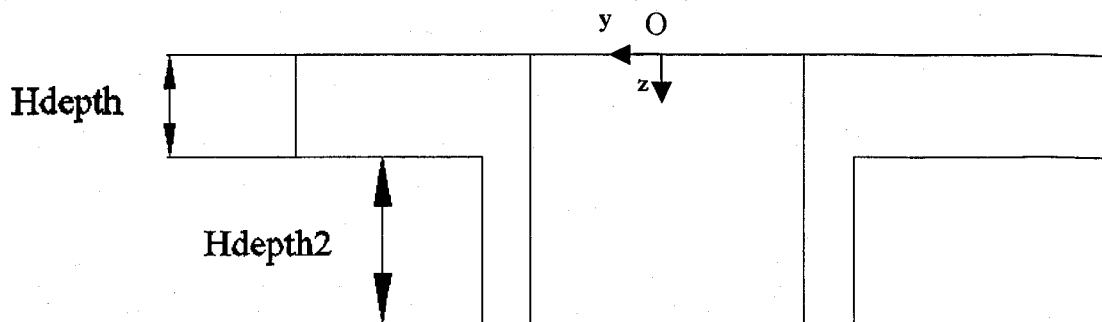
Figure 27. Parameters associated with the hub's local geometry (Side view).

41
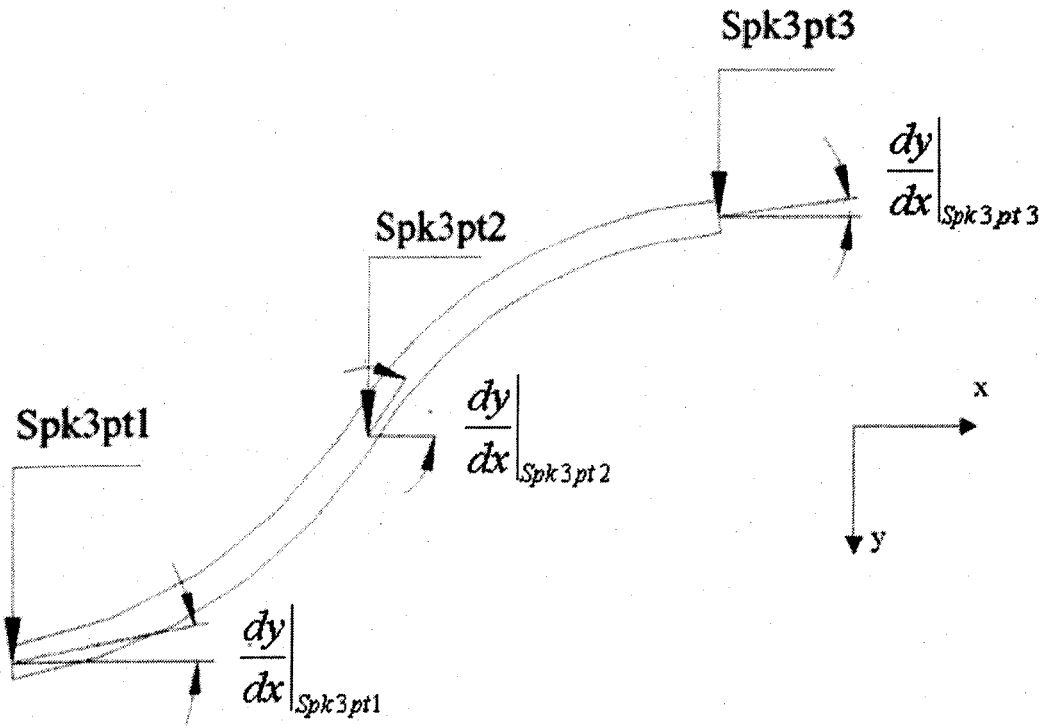
Figure 28. Parameters associated with the spokes' local geometry.

As illustrated in Figure 28, each spoke consists of a spline with three control points along a straight line joining the hub to the rim. The radius and curvature of each spline is determined by the position of the control points along the line and their derivatives at these points. Points 1 and 3 are fixed and controlled by the hub and rim local geometries respectively while point 2 is variable. The depth of the spokes depends on the depth of the hub and may vary along the spoke. In this model, spoke depth was kept constant along the spoke as it results in better deformation characteristics and casting quality [50].

A summary of the parameters required to define the steering wheel geometry is presented in table 5.

Table 5-Summary of all the parameters used to define the steering wheel armature's geometry.

Description	Lower Limit	Variable	Upper Limit	Baseline
HUB				
Upper width	10 mm	Hubl1	47 mm	14 mm
Lower width	10 mm	Hubl2	47 mm	17 mm
Center hole radius	10 mm	Hubrad	20 mm	16 mm
Puller hole radius	0 mm	Hpulrad	10 mm	4 mm
Hub depth	10 mm	Hdepth	15 mm	10 mm
Boss depth	10 mm	Hdepth2	17 mm	22 mm
3 O'CLOCK SPOKE				
Distance to hub center line	40 mm	Spk3rl	50 mm	45 mm
Width	10 mm	Spk3w	20 mm	14 mm
Width to hub center	2 mm	Spk3zc	6 mm	5 mm
Spoke angle	-10 deg	Spk3theta1	30 deg	0 deg
5 O'CLOCK SPOKE				
Distance to hub center line	40	Spk5rl	60	50
Width	10 mm	Spk5w	20 mm	10 mm
Width to hub center	0 mm	Spk5zc	5 mm	3 mm
Spoke angle	-60 deg	Spk5theta1	-45 deg	45 deg
RIM				
Flange width	3 mm	Rimw1	5 mm	3 mm
Web width	3 mm	Rimw2	7 mm	3 mm
Difference in flange heights	0 mm	Rimt1	2 mm	0 mm
Angular spoke position	0 deg	Rimt2	20 deg	15 deg
Inner flange height	5 mm	Rimh1	10 mm	5 mm
Outer flange height	3 mm	Rimh2	10 mm	3 mm
Section radius	5 mm	Rimrl	10 mm	5 mm
GLOBAL				
Rim radius	140 mm	Rrad	190 mm	177 mm
Dish depth	57 mm	Dish	140 mm	140 mm

The parameters summarized in Table 5 provide a complete description of the steering wheel armature's geometry. Since steering wheel geometries vary greatly from one model to the next, and there is no specific standard detailing the dimensional requirements of steering wheel armatures [52], measurements of the parameters given in Table 5 were taken over a wide range of steering wheels including after market steering wheel armatures to provide the baseline dimensions, Appendix B.

6.2. Design variables

6.2.1. Dish depth

In any impact situation where deformation is observed, the available crush distance will limit the energy absorbed through plastic deformation. In the case of a steering wheel armature, the available crush distance is the dish depth. Through the experimental testing, the dish depth demonstrated a direct influence on the total energy absorbed by the steering wheel armature. The Neon armatures demonstrated the highest energy absorption followed by the Cavalier and Focus armatures respectively. These results indicate a direct relationship between the dish depth and energy absorption. The Neon armatures had the largest dish depth resulting in larger deformations and higher energy absorption. The Cavalier armatures had a moderate dish depth while the Focus armatures had a much smaller dish depth. Accordingly, the Focus armature demonstrated the least amount of energy absorption. The baseline dimension of 140mm was selected from the Neon armature because it resulted in maximum energy absorption among all the armatures impacted in the experimental test.

6.2.2. Spoke/rim joint location

Through analysis of the results obtained from experimental testing and numerical simulation, it was observed that the length of the unsupported portion of the rim has a direct influence on the magnitude of the peak load and the total energy absorbed by the steering wheel armature. The closest approximation to the square force versus displacement profile existed for the Cavalier steering wheel armatures as previously demonstrated in Figure 14 and Figure 15. Due to the geometry of the spokes and the joining method at the 4 o'clock and 8 o'clock rim positions, all four spokes came into contact with the rigid plate at approximately the same instant, resulting in a fairly uniform load distribution for the duration of the crash.

The length of the unsupported portion of the rim is dictated by the angular orientation of the spokes along the rim as illustrated in Figure 29. For this

44

reason the 3 o'clock and 9 o'clock spokes' orientation along the rim were selected as the second parameter to investigate. A baseline dimension of 0 degrees, also illustrated in Figure 29, was used as it was the most frequently observed spoke angle in both literature and motor vehicle measurements. Table 6 provides a summary of all the different geometries considered in this investigation.
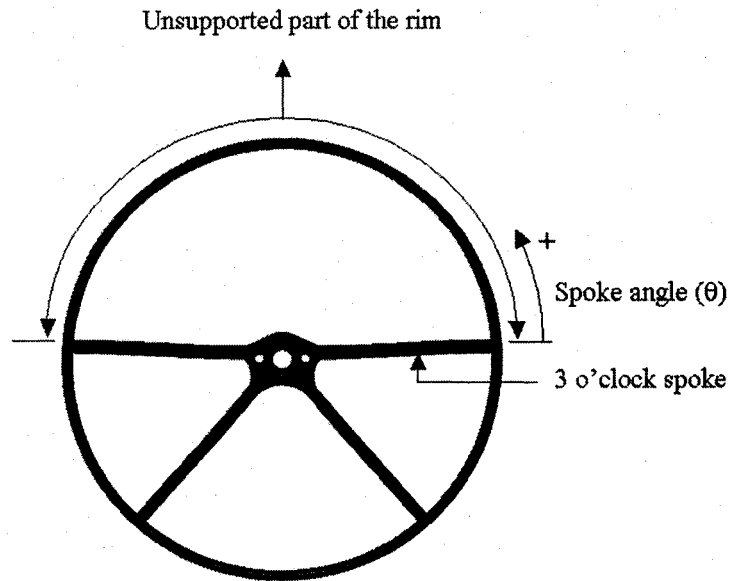
Figure 29. Illustrating the 0 degree spoke angle

Table 6-Summary of all the different geometries investigated

Test No	Impacting Entity	Parameters		Dimensions	
		Dish depth	Spk3theta1	Dish depth mm	Spk3theta1 degrees
1	Rigid plate	Baseline	Baseline	108.00	0
2	Rigid plate	10% increase	Baseline	118.67	0
3	Rigid plate	20% increase	Baseline	129.33	0
4	Rigid plate	30% increase	Baseline	140.00	0
5	Rigid plate	10% decrease	Baseline	97.33	0
6	Rigid plate	20% decrease	Baseline	86.67	0
7	Rigid plate	30% decrease	Baseline	76.00	0
8	Rigid plate	Baseline	plus 10 degrees	108.00	10
9	Rigid plate	10% increase	plus 10 degrees	118.67	10

45

Test No	Impacting Entity	Parameters		Dimensions	
		Dish depth	Spk3theta1	Dish depth mm	Spk3theta1 degrees
10	Rigid plate	20% increase	plus 10 degrees	129.33	10
11	Rigid plate	30% increase	plus 10 degrees	140.00	10
12	Rigid plate	10% decrease	plus 10 degrees	97.33	10
13	Rigid plate	20% decrease	plus 10 degrees	86.67	10
14	Rigid plate	30% decrease	plus 10 degrees	76.00	10
15	Rigid plate	Baseline	Plus 20 degrees	108.00	20
16	Rigid plate	10% increase	Plus 20 degrees	118.67	20
17	Rigid plate	20% increase	Plus 20 degrees	129.33	20
18	Rigid plate	30% increase	Plus 20 degrees	140.00	20
19	Rigid plate	10% decrease	Plus 20 degrees	97.33	20
20	Rigid plate	20% decrease	Plus 20 degrees	86.67	20
21	Rigid plate	30% decrease	Plus 20 degrees	76.00	20
22	Rigid plate	Baseline	plus 30 degrees	108.00	30
23	Rigid plate	10% increase	plus 30 degrees	118.67	30
24	Rigid plate	20% increase	plus 30 degrees	129.33	30
25	Rigid plate	30% increase	plus 30 degrees	140.00	30
26	Rigid plate	10% decrease	plus 30 degrees	97.33	30
27	Rigid plate	20% decrease	plus 30 degrees	86.67	30
28	Rigid plate	30% decrease	plus 30 degrees	76.00	30
29	Rigid plate	Baseline	minus 10 degrees	108.00	-10
30	Rigid plate	10% increase	minus 10 degrees	118.67	-10
31	Rigid plate	20% increase	minus 10 degrees	129.33	-10
32	Rigid plate	30% increase	minus 10 degrees	140.00	-10
33	Rigid plate	10% decrease	minus 10 degrees	97.33	-10
34	Rigid plate	20% decrease	minus 10 degrees	86.67	-10
35	Rigid plate	30% decrease	minus 10 degrees	76.00	-10

6.3 Finite element models used in the parametric study

In order to simulate the impact between the steering wheel armature and the rigid plate, finite element models were developed for both the steering wheel armature and the rigid plate. A description of details and development of these models is presented in the following section.

6.3.1 Development of the steering wheel armature finite element model

The steering wheel armature model was developed using the parametric model developed in TRUEGRID. The parametric model was imported into FEMB as a LS-DYNA file. The steering wheel armature was then meshed using 27614 constant stress solid elements. All boundary constraints were placed on the nodes located at the center of the hub using the *BOUNDARY_SPC_NODE card in an effort to model the actual experimental test setup with the hub rigidly bolted onto the mounting device.

6.3.1.1 Material selection

Weight reduction of the steering wheel armature is important for the development of the airbag system because the bag and inflator add undesirable weight to the steering wheel assembly. On the other hand, the steering wheel armature needs proper stiffness, strength and energy absorption characteristics to meet safety requirements. A review of literature [19 – 21, 50, 51] revealed that although magnesium alloys offer significant potential weight saving advantages over the traditional steel steering wheel armatures, aluminum alloys provide additional ductility characteristics necessary for energy absorption. The mechanical properties of aluminum casting alloys with various compositions are shown in Table 7.

Table 7-Mechanical properties of various Aluminum casting alloys [53].

	Alloy	ρ (g/cc)	$\sigma_{ultimate}$ (MPa)	σ_{yield} (MPa)	Elongation @ break, %	E (GPa)	μ	$\sigma_{ultimate}/\sigma_{yield}$
1	204.0-T4, PM	2.8	331	200	8	71	0.33	1.66
2	296.0-T4, General	2.796	255	130	9	69	0.33	1.96
3	C443.0-F, DC	2.69	228	97	9	71	0.33	2.35
4	850.0-T5 PM	2.88	160	75	8	71	0.33	2.13
5	851.0-T6, PM	2.83	124		8	71	0.33	
6	*514.0-f, SC*	*2.65*	*170*	*85*	*9*	*71*	*0.33*	*2.00*
7	206.0-T7, General	2.80	436	350	11.7	70	0.33	1.25
8	A535.0-F, General	2.62	275	140	13	71	0.33	1.96
9	A444.0-T4, PM	2.68	138		20			
10	705.0-T5, PM	2.76	225	117	10	71	0.33	2.18
11	520.0-T4, SC	2.57	330	180	16	66	0.33	1.83
12	201.0-T4, SC	2.8	365	215	20	71	0.33	1.70

The aluminum alloy 514.0-F (alloy 6) was chosen because of its favorable strength (170 MPa) and elongation (9%) properties. Tensile test specimens were then obtained from the Materials Technology Lab at Natural Resources Canada [54] in order to obtain the stress versus strain curve needed for the numerical analysis.

The material model of steering wheel armature employs the *MAT_PIECEWISE_LINEAR_PLASTICITY material model. This material model requires input for

1. The density of the material
2. Young's modulus of the material
3. Poisson's ratio of the material
4. The yield stress of the material
5. Strain rates
6. A stress versus effective plastic strain curve of the material

Tensile tests were conducted on an Instron Servo Hydraulic Testing Machine according to ASTM B557M [55] at a strain rate of 1 mm/min. The Young's modulus (72 GPa) and the yield stress (67 MPa) required for this material model were then calculated from this stress-strain data.

Strain rates are accounted for in LS-DYNA using the Cowper and Symonds constitutive relation which scales the yield stress as shown in equation (22).

$$\frac{\sigma_0'}{\sigma_0} = 1 + \left(\frac{\dot{\varepsilon}}{D}\right)^{\frac{1}{q}}$$ (22)

Where σ_0' is the stress at the strain rate $\dot{\varepsilon}$, σ_0 is the stress based upon a quasi static tensile test, D and q are the strain rate material parameters. The strain rate constants for aluminum alloys recommended by Bodner

and Symonds for the values of D and q in equation (22) are 6500/s and 4 respectively.

Alternatively, strain rate effects may be accounted for by defining a table of stress versus strain curves with each curve corresponding to a strain rate. Effective plastic strain versus yield stress must be provided.

The stress versus effective plastic strain curve is derived from the engineering stress versus strain curve using equations (23) and (24).

$$\sigma_{true} = \sigma_{eng}(1 + \varepsilon_{eng}) \tag{23}$$

$$\varepsilon_{true} = \ln(1 + \varepsilon_{eng}) \tag{24}$$

The effective plastic strain is calculated from equation (25).

$$\varepsilon_{effective\ plastic} = \varepsilon_{true} - \frac{\sigma_{true}}{E} \tag{25}$$

The stress versus effective plastic strain curve used in the material model for the steering wheel armature is illustrated in Figure 30.
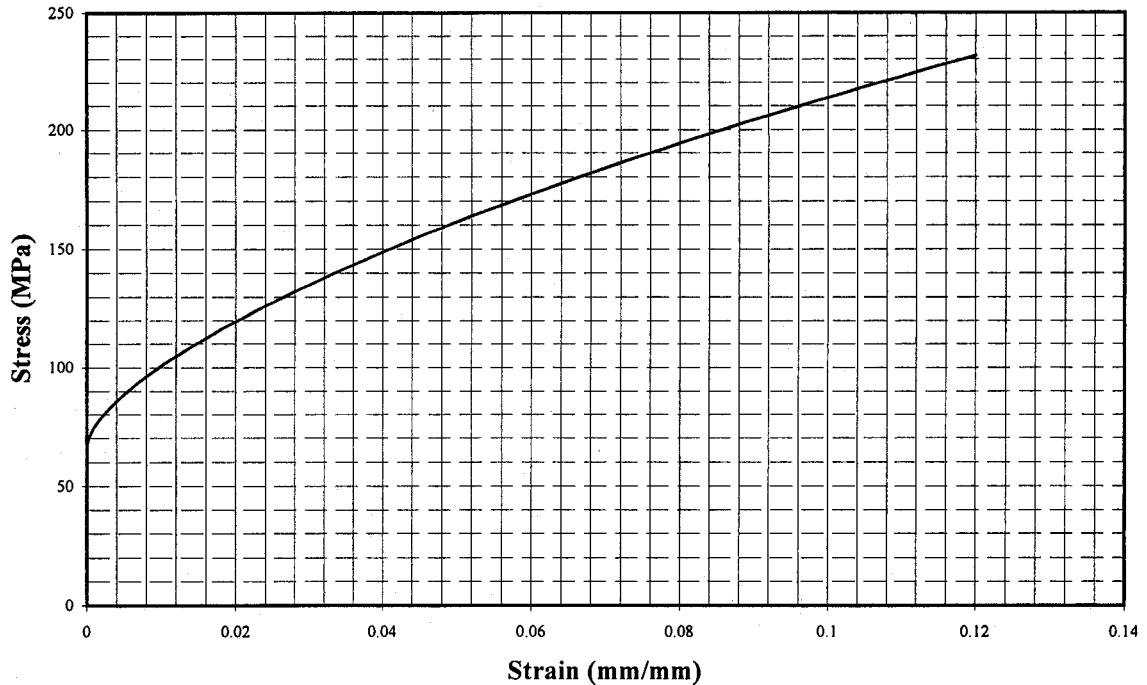
Figure 30. Stress Versus Effective Plastic Strain for the Aluminum alloy of the
Four-Spoke Steering Wheel Armature.

6.3.2 Development of the rigid plate finite element model

From the experimental tests, it was observed that the majority of deformation occurs in the steering wheel armatures. Although, deformation of the rigid plate was occurring, it was negligible with respect to the magnitude of deformation observed in the steering wheel armatures. For this reason, the rigid plate was modeled using a rigid material model with 2500 Belytschko-Tsay shell elements and the *MAT_RIGID material model. This material model requires input for

1. The density of the material
2. Young's modulus of the material
3. Poisson's ratio of the material

The density of the rigid plate material was selected so that the mass of the rigid plate model was identical to the mass of the actual rigid plate (57.2 kg) used in the experimental setup. All the nodes on the plate were constrained to translate in the vertical direction (z-axis direction), no nodal rotations were permitted.

6.3.3 Modeling contact

Treatment of sliding and impact along interfaces is very critical in simulating the correct load transfer between components in any analysis. Contact forces generated influence the acceleration of a body. The contact algorithms employed in LS-DYNA divide the nodes of bodies involved in contact into slave nodes and master surfaces. After the initial division, each slave node is checked for penetration against master surfaces. A variety of contact algorithms are available in LS-DYNA. The penalty method was employed for all simulations carried out in this investigation. This method consists of placing normal interface springs between all penetrating nodes and contact surfaces.

All the contact interfaces in this investigation were modeled using the *CONTACT_AUTOMATIC_SURFACE_TO_SURFACE algorithm. Modification of the penalty scale factors was required based upon preliminary numerical observations illustrating excessive penetration from contacting surfaces. In addition, the *CONTACT_AIRBAG_SINGLE_SURFACE algorithm specifically designed to treat the contact between airbag folds, was employed to model contact associated with airbag.

The algorithms employed between all contacting surfaces may be found in Appendix C.

6.4. Numerical setup and procedure

The steering wheel armature model was combined with the rigid plate model as illustrated in Figure 31. A single contact algorithm, CONTACT_AUTOMATIC_SURFACE TO SURFACE, was implemented for impact between the rigid plate and the steering wheel. The rigid plate was prescribed an initial velocity of 3.2 m/s using the keyword command INITIAL_VELOCITY_GENERATION.
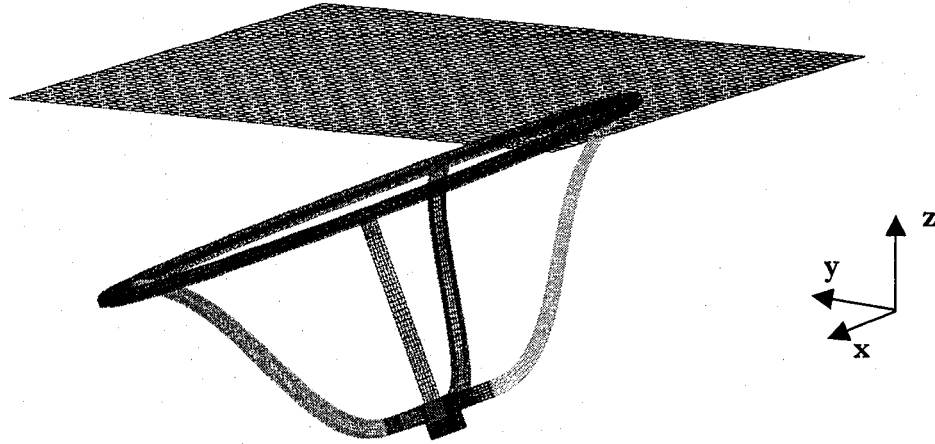
Figure 31.Illustration of the rigid plate and steering wheel armature finite element models

A total of 105 simulations (35 steering wheel geometries at 3 impact locations) were run on a personal computer with two 1.6 GHz AMD-Athlon processors with 384 Megabytes of RAM. Time steps in the simulation ranged from 0.0386 to 0.109 microseconds. Mass scaling was utilized for only the steering wheel armature model which effectively added mass to the smaller finite elements to increase the maximum allowable time step for those elements. In no case did the mass of the steering wheel model increase by more than 300%. Typical simulations required 100 ms analysis time, although some simulation required from 60 ms to 140 ms. Processing times ranged from 7 to 12 hours for a 110 ms crash event.

Impacts at different wheel angle positions were considered in this investigation. Although the column angle was maintained at 24°, three different wheel angles were investigated for each armature geometry. Impacts at the 6 o'clock, 3 o'clock position and 12 o'clock were completed as illustrated in Figure 32.
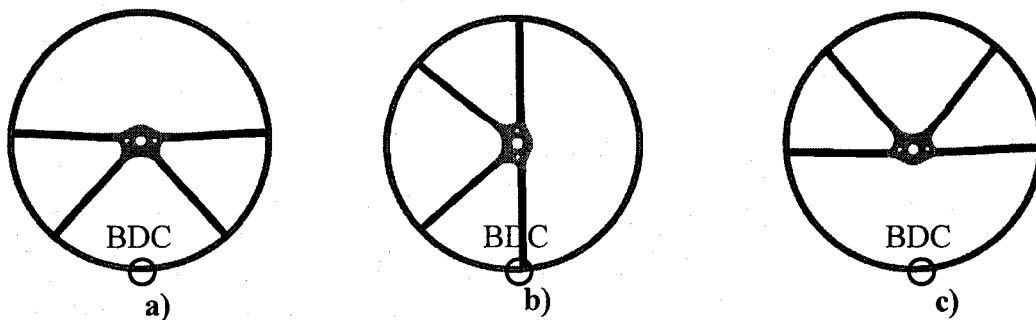
Figure 32. Impact at different wheel angle positions. a) 6 o'clock impact,
b) 3 o'clock impact, c) 12 o'clock impact

52

The bottom dead center (BDC) of the steering wheel is the 180 degree position which is the 6 o'clock position when driving straight ahead. It should be noted that any impact between the rigid plate and the steering wheel armatures always occurred at the bottom dead center (BDC) of the steering wheel. However depending on how the steering wheel is turned this may not represent the 6 o'clock position.

6.5. Discussion of results

The peak load, *C.F.E.*, elastic response, energy efficiency, and the *E.A.F.* versus spoke angle and dish depths are presented as 3D surface plots to provide an illustration of the influence of the spoke angle and dish depth on the crashworthiness performance of the steering wheel armatures investigated. These plots are presented in Figure 33 through Figure 38.

6.5.1 Discussion on the energy absorbed

For impact at the 6 o'clock position the energy absorption is generally higher for armatures with a dish depth above 108mm for all spoke angles investigated as illustrated in Figure 33. a). Since a larger dish depth presents a larger crush space, it is expected that steering wheel armatures with larger dish depths will generally absorb more energy. This was also observed with the experimentally tested steering wheel armatures. For impact at the 3 o'clock position, illustrated in Figure 33. b), the armatures demonstrated higher energy absorption for large dish depths, similar to impact at the 6 o'clock position. With peak energy absorption at 140 mm dish depth and −10 degrees of spoke angle. Lower spoke angles and dish depths demonstrated the largest energy absorption for impact at the 12 o'clock position. This mode of energy absorption is undesirable in these cases (12 o'clock impact), because the armature bottoms and gives rise to the excessive peak loads observed in Figure 33. c). As previously discussed these large loads are undesirable because they are concentrated over a small area (the hub) and pose a significant threat to the ribs and soft tissue of the torso.
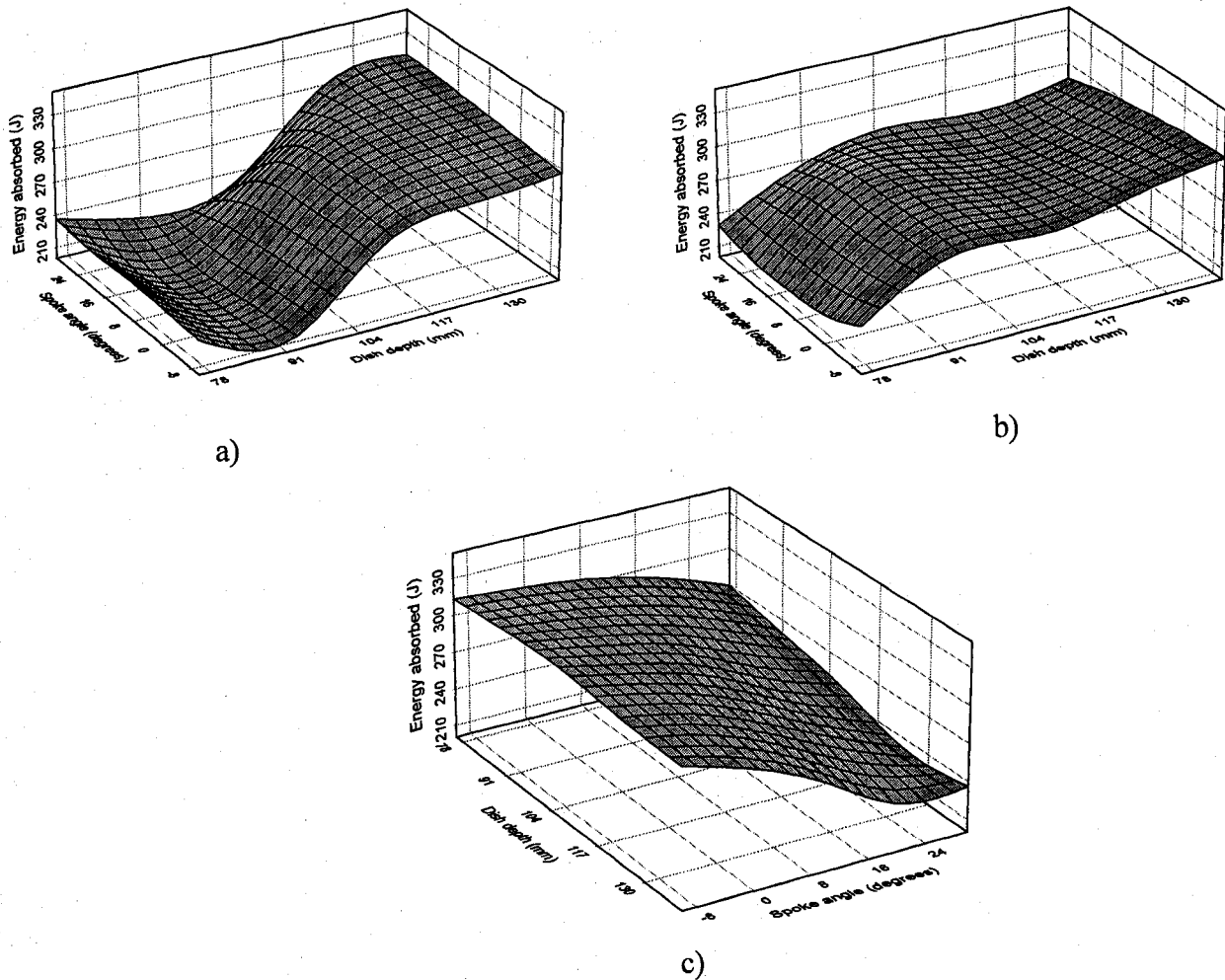
Figure 33. Energy absorbed versus dish depth and spoke angle for impact at the different wheel angle positions. a) 6 o'clock position, b) 3 o'clock position, c) 12 o'clock position.

6.5.2 Discussion on the peak load

For impact at the 6 o'clock position, the peak load is significantly lower for larger dish depths for all spoke angles investigated as illustrated in Figure 34. a). Similarly for impact at the 3 o'clock position, illustrated in Figure 34. b), peak loads are lower for larger dish depths. The large peak loads observed for the lower dish depths for impact at both the 3 and 6 o'clock positions are due to bottoming out of the steering wheel. For impact at the 12 o'clock position, the peak load increases with both dish depth and spoke angle as illustrated in Figure 34. c). In all these cases the armatures bottomed out. Although all observed peak

loads are unacceptably large for impact at the 12 o'clock position, the difference in magnitude may be attributed to the difference in dish depth, with larger dish depths and higher spoke angles resulting in a stiffer response and lower peak loads.
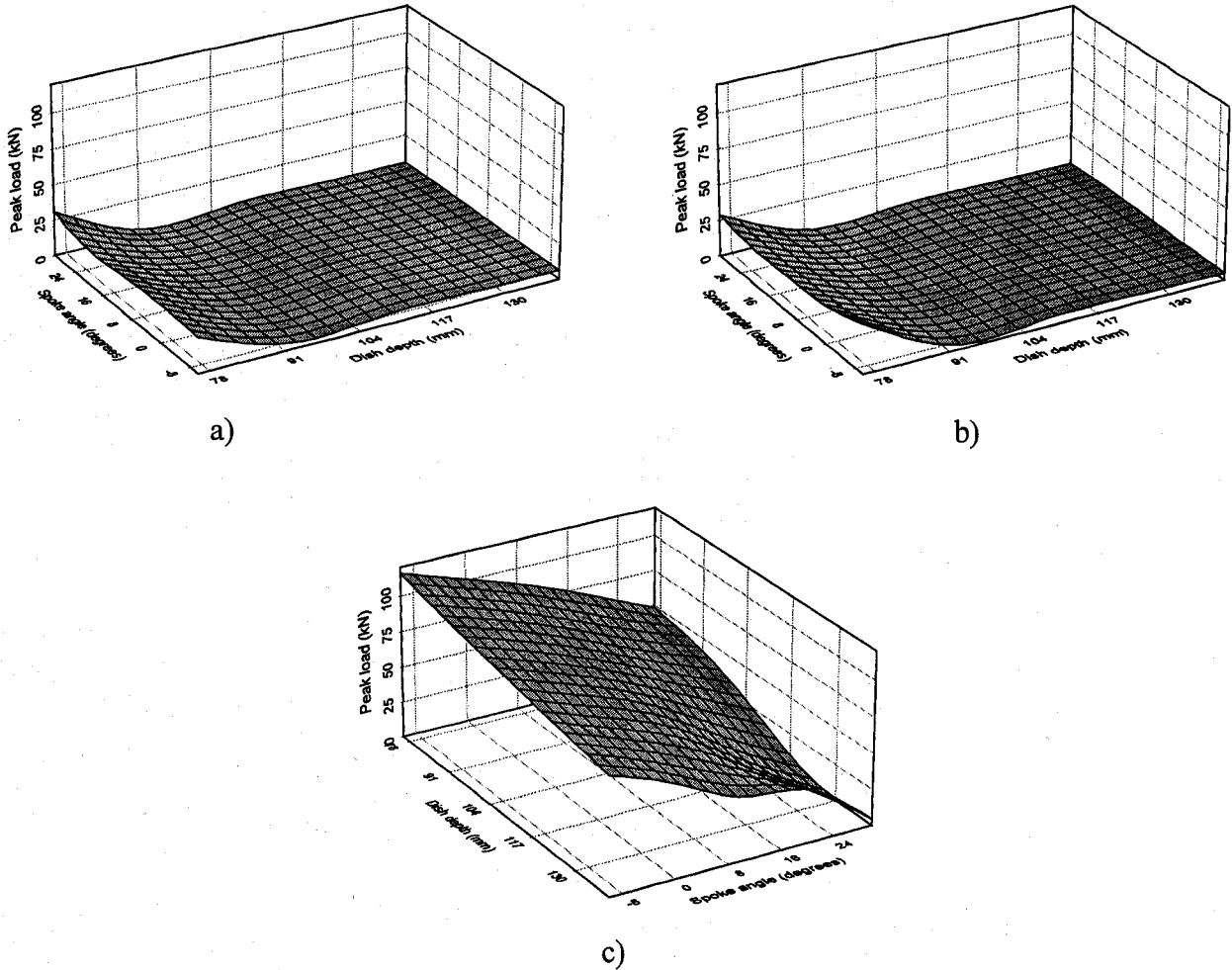
Figure 34. Peak load versus dish depth and spoke angle for impact at the different wheel angle positions. a) 6 o'clock position, b) 3 o'clock position, c) 12 o'clock position.

6.5.3 Discussion on the crush force efficiency

For impact at the 6 o'clock position, it is observed that larger dish depths are more favorable demonstrating higher efficiencies as illustrated in Figure 35. a). Impact at the 3 o'clock position results in a similar response in terms of *C.F.E.*,

with larger dish depths resulting in higher efficiencies as illustrated in Figure 35. b). For impact at the 12 o'clock position, illustrated in Figure 35. c), the spoke angle significantly influences the efficiency of the armatures with the highest efficiencies observed for larger dish depths and spoke angles. The lower efficiencies observed for the lower dish depths and spoke angles can be attributed to the considerably larger peak loads experienced when the armature bottoms out.

a)

b)

c)
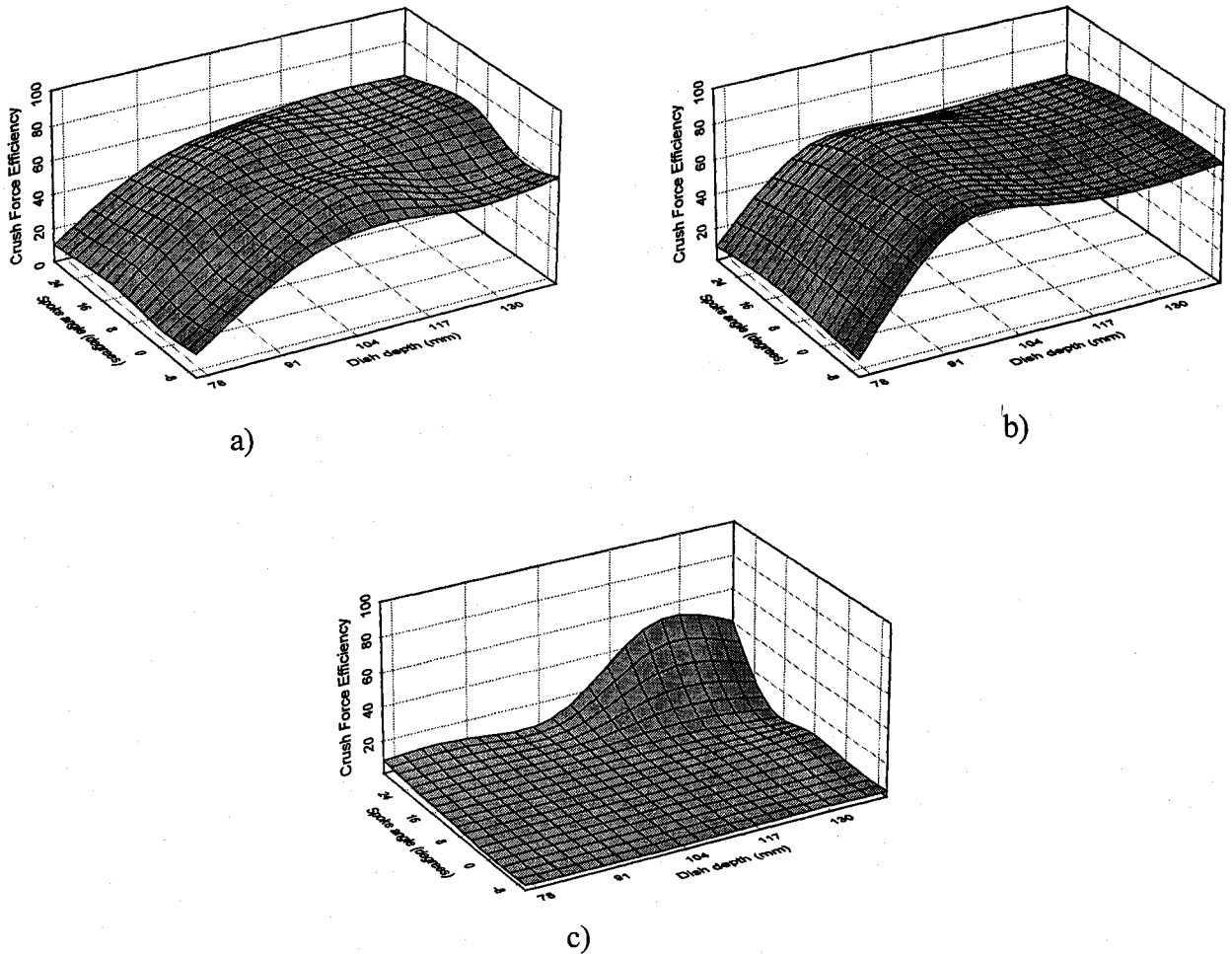
Figure 35. Crush Force Efficiency versus dish depth and spoke angle for impact at the different wheel angle positions. a) 6 o'clock position, b) 3 o'clock position, c) 12 o'clock position.

6.5.4 Discussion on the energy efficiency

The performance of the steering wheel armatures in terms of energy efficiency is similar to the crush force efficiency. This should be expected since both performance measures are normalized using the average force. For impact at both

the 6 and 3 o'clock positions illustrated in Figure 36. a). and Figure 36. b), the energy efficiency increases with dish depth for all spoke angles investigated, reaching a maximum at 86 mm dish depth. The efficiency then decreases slightly and plateaus as the dish depth increases. The illustrations suggest that past the 86 mm dish depth, increase in the dish depth has no significant effect on the energy efficiency of the steering wheel armature. For impact at the 12 o'clock position illustrated in Figure 36. c), the energy efficiency is considerably low. Increase in both spoke angle and dish depth results in an increase in the energy efficiency. Once again, this may be attributed to the increase in overall stiffness of the armature as the dish depth and spoke angle increase.

a)

b)

c)
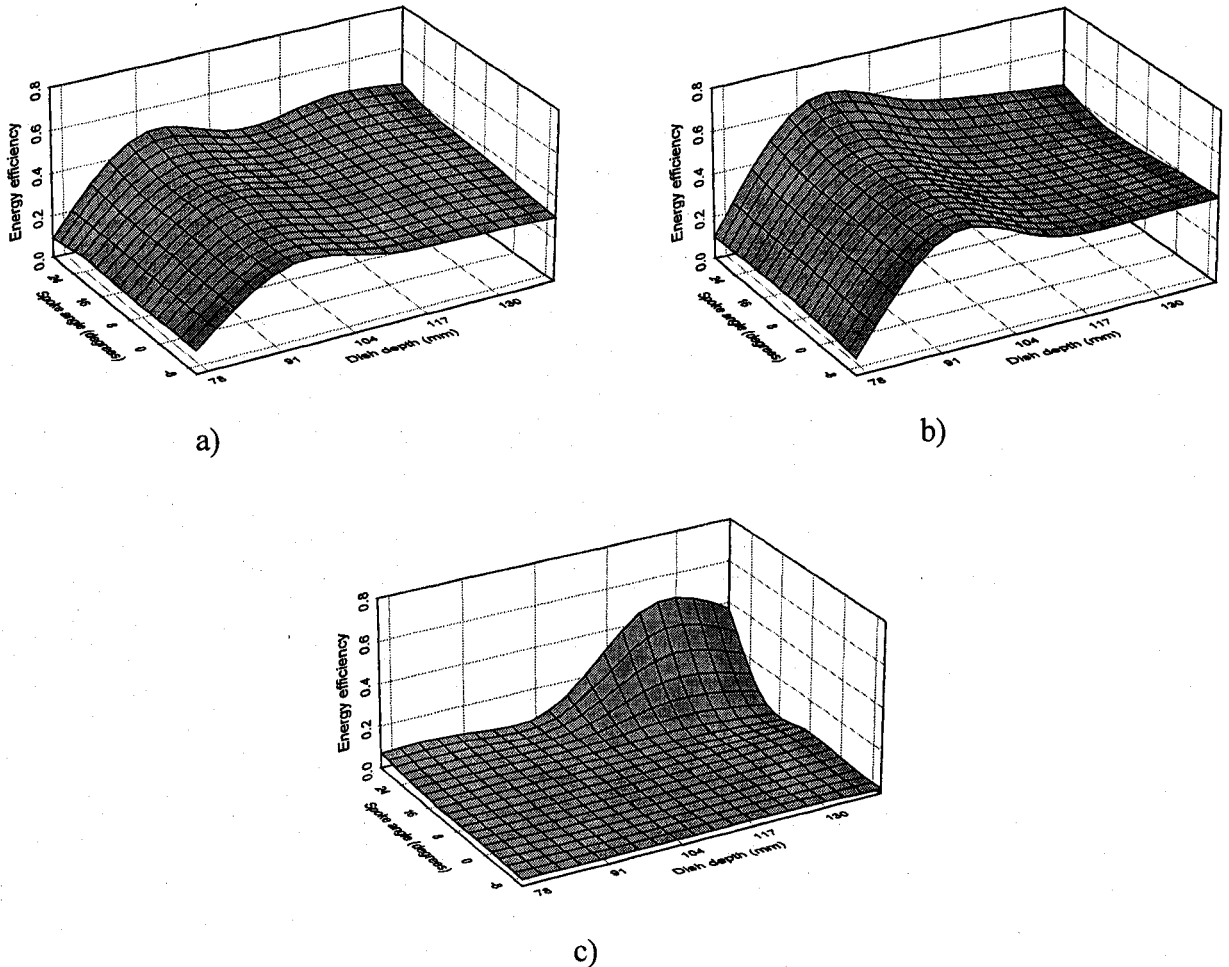
Figure 36. Energy Efficiency versus dish depth and spoke angle for impact at the different wheel angle positions. a) 6 o'clock position, b) 3 o'clock position, c) 12 o'clock position.

6.5.4 Discussion on the elastic response

The elastic response for all steering wheel armatures investigated for all impact positions illustrated in Figure 37 is minor, no greater than 3% of the total energy absorbed by the entire armature.

a)

b)

c)
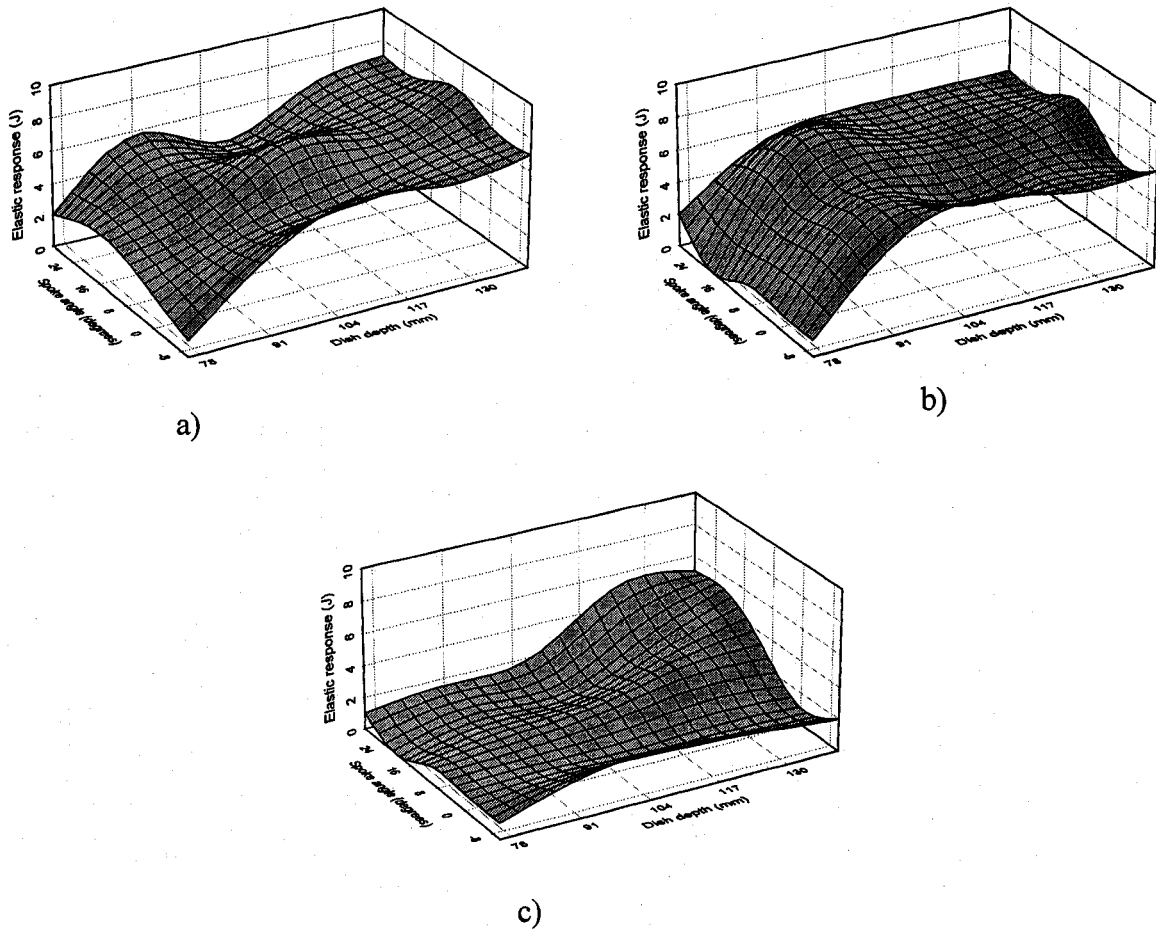
Figure 37. Elastic response versus dish depth and spoke angle for impact at the different wheel angle positions. a) 6 o'clock position, b) 3 o'clock position, c) 12 o'clock position.

6.5.5 Discussion on the Energy Absorption Factor.

For impact at the 6 o'clock position illustrated in Figure 38. a), the armatures with the larger dish depths exhibited the highest E.A.F. Given that a larger dish depth presents a larger deformation space, it follows that armatures with larger dish depths should absorb more energy on impact. For impact at the 3 o'clock

position, larger dish depth and lower spoke angles resulted in higher *E.A.F* as illustrated in Figure 38. b). The lower spoke angles result in a drop of the overall stiffness of the armature resulting in larger deformations and hence higher energy absorption. For impact at the 12 o'clock position illustrated in Figure 38. c), lower spoke angles and dish depths result in higher *E.A.F.*, once again due to the reduction in the overall stiffness of the armatures.
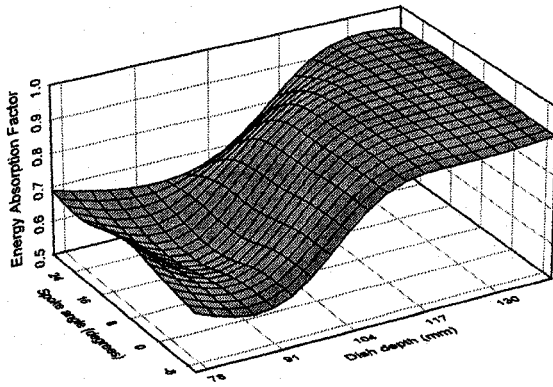
a)
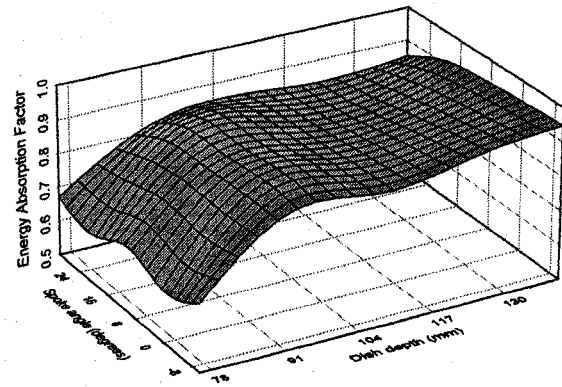
b)
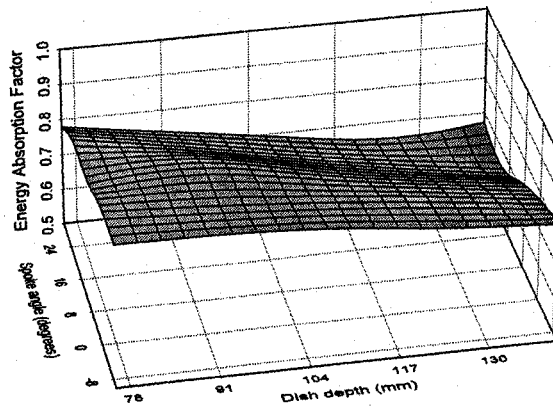
c)

Figure 38. Energy Absorption Factor versus dish depth and spoke angle for impact at the different wheel angle positions. a) 6 o'clock position, b) 3 o'clock position, c) 12 o'clock position.

6.6 Optimization based upon the armature variables considered in this investigation

The design variables selected for the optimization problem are the dish depth and the spoke angle based upon the peak impact load, energy absorbed, *C.F.E*, energy efficiency, and the *E.A.F* of each steering wheel armature. The objective is to minimize the peak load while maximizing energy absorption. Performance requirements for steering wheel armatures are not readily available in the public domain due to the proprietary nature of cash testing performance. A review of existing literature yielded one reference [18] providing load-deflection specifications similar to those used in automotive companies. For this reason, the constraints placed on each criterion were derived from the load-deflection specifications presented in [18] and illustrated in Figure 39.
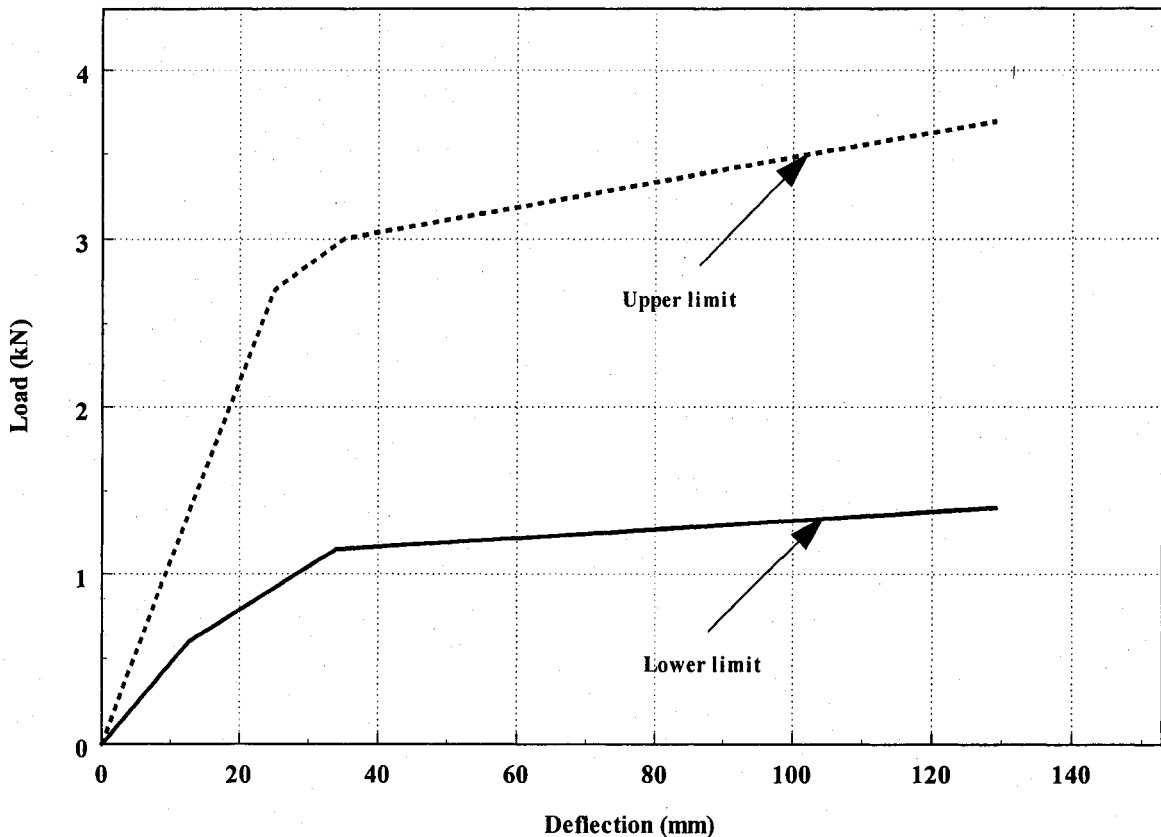
Figure 39. Load versus deflection specification curve as presented in [18].

6.6.1 Development of the constraints.

Descriptions of the limits developed for the peak impact load, $C.F.E$, energy efficiency, and the $E.A.F$ for the optimization problem derived from the load-deflection specifications presented in [18] are presented in the following paragraphs.

6.6.1.1 Peak load

The maximum allowable peak load is the maximum load given in the Figure 39. The specification curve has an upper limit (UL) curve and a lower limit (LL) curve. The peak maximum force for the upper limit curve represents the maximum allowable peak load, $F_{peak_s}(UL)$. A value for the peak load is also indexed in FMVSS 203, which indicates that the force developed on the steering wheel armature on impact may not exceed 11kN. Since the objective is to minimize the peak load, the formulation for the peak load becomes:

$$F_{peak_s}(LL) < F_{peak} < F_{peak\,203}$$

(26)

Where the subscript s refers to the specification curve data.

6.6.1.2 Crush Force Efficiency

The crush force efficiency is calculated using equation 10. From the specification curve in Figure 39, the average force is calculated using equation 11. The average force was calculated for both the upper limit, $F_{avg_s}(UL)$, and the lower limit, $F_{avg_s}(LL)$, curves. These two values represent the maximum and minimum allowable average loads respectively. The $C.F.E$ was then calculated using the average force for the lower limit and the peak force for upper limit as shown in equation (27), which represents the minimum allowable $C.F.E$.

$$C.F.E_s = \frac{F_{avg_s}(LL)}{F_{peak_s}(UL)}$$

(27)

The formulation for the C.F.E then becomes:

$$C.F.E_s < C.F.E$$

(28)

6.6.1.3 Energy absorbed

The area under the curves presented in Figure 39 represent the energy absorbed by the steering wheel armatures. For each curve the energy absorbed was calculated using equation 8. The energy absorbed, calculated for the lower limit, $E_{absorbed_s}(LL)$, represents the minimum allowable energy absorption requirements. The formulation for the energy absorption becomes:

$$E_{absorbed_s}(LL) < E_{absorbed} \qquad (29)$$

6.6.1.4 Energy efficiency

The energy efficiency is dependent on the dish depth of the steering wheel armature, the column angle and the energy absorbed. In [18] the dish depth, L_{dish_s}, used to develop the specification curves is 117 mm, the column angle is zero and the energy absorbed is calculated using equation 8. The energy efficiency was calculated for both the upper limit and the lower limit curves. The energy absorbed by the lower limit represents the minimum allowable energy absorption requirements. From the upper limit curve, the maximum allowable average force can be calculated. Using the energy absorption based on the lower limit and the average force based on upper limit, the minimum allowable energy efficiency from the specification curves is then calculated using equation (30).

$$e_{e_s} = \frac{E_{absorbed_s}(LL)}{F_{avg_s}(UL) \cdot L_{dish_s}} \qquad (30)$$

The formulation for the energy efficiency requirement becomes:

$$e_{e_s} < e_e \qquad (31)$$

6.6.1.5 Energy Absorption Factor

The *E.A.F* is dependant on the energy supplied to the system. The energy supplied to the system was not specified in reference [18] therefore the

constraints placed on the energy absorption requirements were derived from past experience and data from [18-22].

Table 8 summarizes the constraints derived from the force-deflection specification curves.

Table 8-Summary of constraints for the optimization problem

Criterion	Constraint
F_{peak}	< 3.9kN
C.F.E	> 0.303
$E_{absorbed}$	> 143J
e_e	>0.416
E.A.F	>0.70

These specifications for the load-deflection requirements apply to quasi-static loading however, aluminum alloys exhibit very little strain rate sensitivity. For this reason, the load-deflection specification curves were deemed suitable for the optimization problem.

6.7. Rating system

A safety rating system based on the constraints described in the previous section was developed. This rating system was developed in order to isolate the effects of the parametric variations on each performance measure.

From the load versus deflection specification curve, Figure 49, the minimum and maximum allowable values for each performance measure were determined. From these values, an acceptable response window was obtained. A rating value was then assigned to each region of the response for each performance measure. A value of zero was assigned for response falling below the acceptable window, a value of one was assigned for response falling within the acceptable window, and a value of two was assigned for response falling above the acceptable response window. The rating system ranges from 0 to 10, with 10 being the maximum score. Table 9 summarizes the rating system for each performance measure.

Table 9-Summary of the rating values for each performance measure

Rating value	0	1	2
F_{peak}	$F_{peak} > 11$ kN	$3.7 < F_{peak} < 11$ kN	$1.4 < F_{peak} < 3.7$ kN
C.F.E	C.F.E < 30 %	$30 < $ C.F.E < 80 %	C.F.E > 80 %
$E_{absorbed}$	$E_{absorbed} < 143$ J	$143 < E_{absorbed} < 375$ J	$E_{absorbed} > 375$ J
e_e	$e_e < 0.41$ %	$0.41 < e_e < 0.88$ %	$e_e > 0.88$ %
E.A.F	E.A.F < 0.7	$0.7 < $ E.A.F > 0.9	E.A.F > 0.9

A summary of the rating score for all steering wheel armatures investigated may be found in Appendix F.

6.8. Optimum design based upon considered variables and discussion

Test no. 24 with a dish depth of 129mm and a spoke angle of 30 degrees demonstrated the most favorable response. The peak load was slightly above optimum however all the constraints were satisfied. The overall rating score, averaged over the three impact positions was 5, with a rating of 6, the highest score among all the armature designs investigated, for impact at the 6 o'clock position. Test no. 35 with a dish depth of 76mm and a spoke angle of –10 degrees demonstrated the least favorable response with a peak load five times the desired optimum peak load and an overall rating score, averaged over the three impact positions, of 1. A summary of the results obtained for the optimization problem is shown in Table 10.

Table 10-Results of optimization

Test no.	F_{peak}	C.F.E	$E_{absorbed}$	e_e	E.A.F
Optimum	< 3.9kN	> 0.303%	> 143J	> 0.416	> 0.70
24 (Most Favorable)	4.9	58.7	304	0.44	0.95
35 (Least Favorable)	25.1	13.7	230	0.11	0.67

These results underline the significance of the spoke angle in the load distribution and overall stiffness of the steering wheel armature. At very low spoke angles, the upper rim region is virtually without support and impact at this location would result in severe

bending stresses and considerable loads to the head and chest of the occupant. In order to overcome this, the dish depth must be large thus increasing the effective length of the spokes and providing a more adequate load path, which would reduce the risk of bottoming out.

Illustrated in Figure 40 is the resulting load-deflection response for test no. 24 with a dish depth of 129 mm and a spoke angle of 30 degrees. It displayed the closest approximation to the load-deflection requirements as seen here. Also illustrated in Figure 41 is the resulting load-deflection response for test no. 35 with a dish depth of 76 mm and a spoke angle of –10 degrees. This armature demonstrated least desirable response resulting in peak loads well above 50kN.
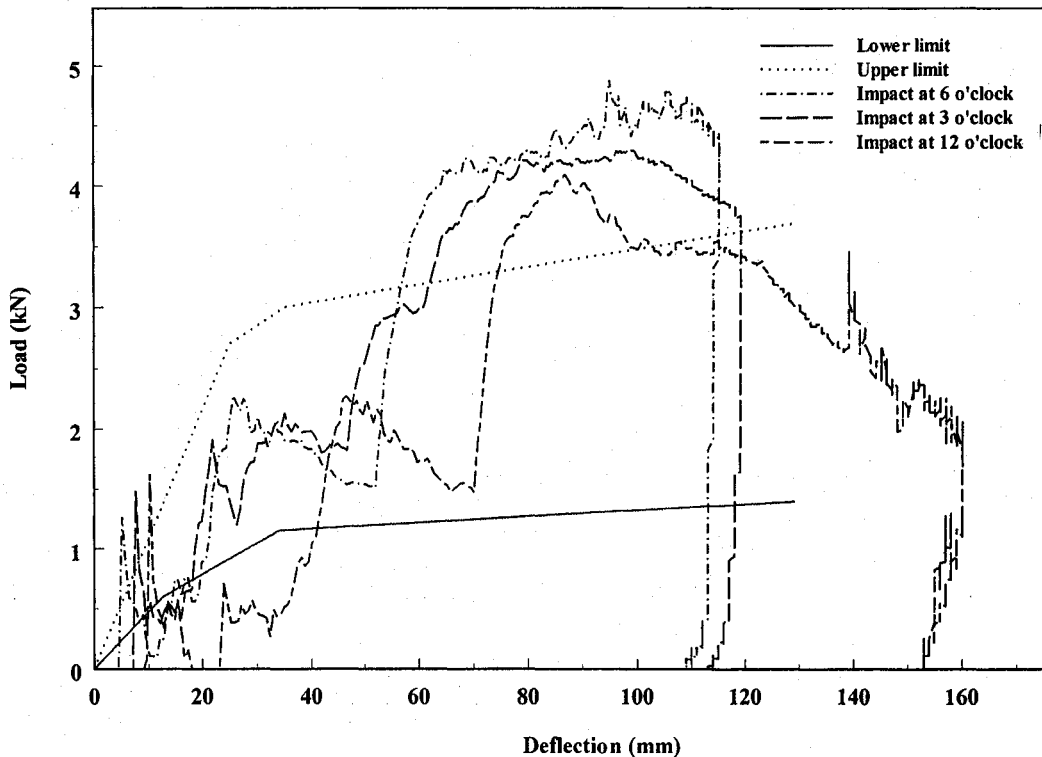
Figure 40. Load versus deflection response of test no. 24 for impact at the 6 o'clock, 3 o'clock, and 12 'clock position.

As illustrated in Figure 40 the load versus deflection profile exhibited two peaks for impact at both the 6 and 12 o'clock positions while impact at the 3 o'clock position showed a gradual increase in load with deflection. For both the 6 and 12 o'clock

positions the impact is symmetrical so the lower spokes come into contact with the rigid plate at the same instant resulting in the first peak as seen in Figure 40. The second peak is considerably larger than the first peak because of the increase in overall stiffness of the armature due to the presence of the 4 o'clock and 8 o'clock spokes, for impact at the 6 o'clock position and the presence of the 2 o'clock and 10 o'clock spokes for impact at the 12 o'clock position. These load versus displacement profiles characterize the response of four spoke armatures because of the position of the four spokes along the rim of the armature. In order to eliminate the two peaks observed here, the armature design would require continuous spokes positions along the rim resulting in a gradual increase in load with deflection as required by the load versus deflection specification curves.
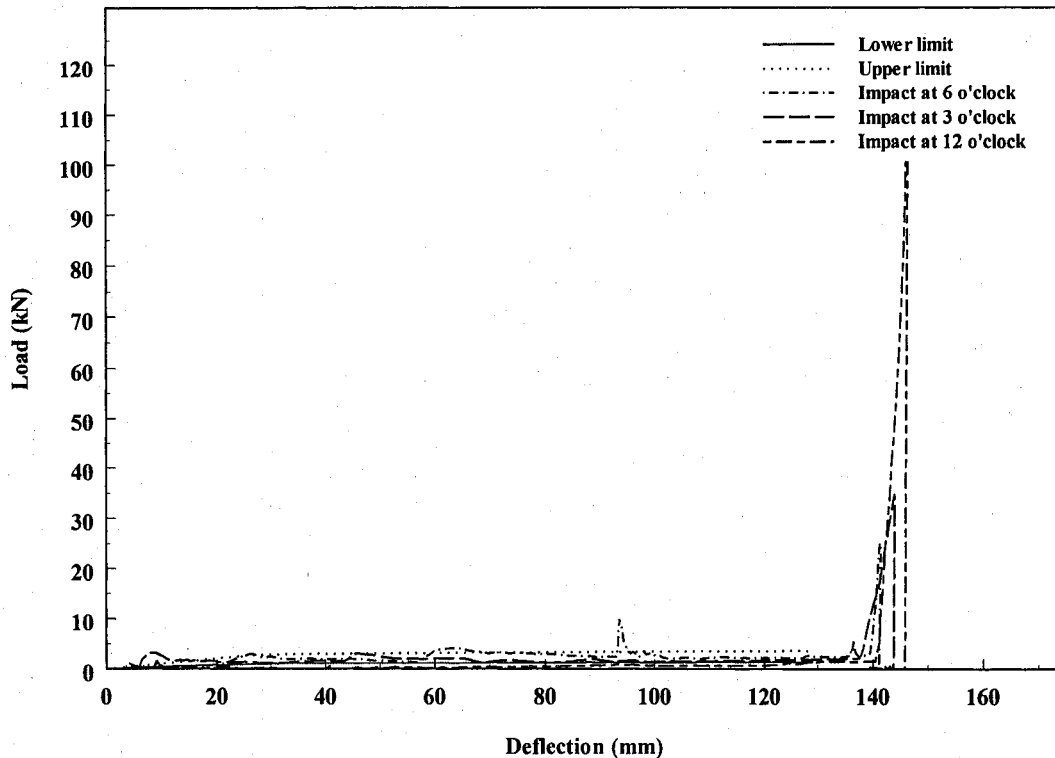
Figure 41. Load versus deflection response of test no. 35 for impact at the
6 o'clock, 3 o'clock, and 12 'clock position.

For test no. 35 illustrated in Figure 41 there is a gradual increase in load followed by a plateau which is followed by a sudden increase in load with deflection. This sudden

increase in load occurs when the armature bottoms out. Figure 42 provides a clear illustration of the armature's response prior to bottoming out.
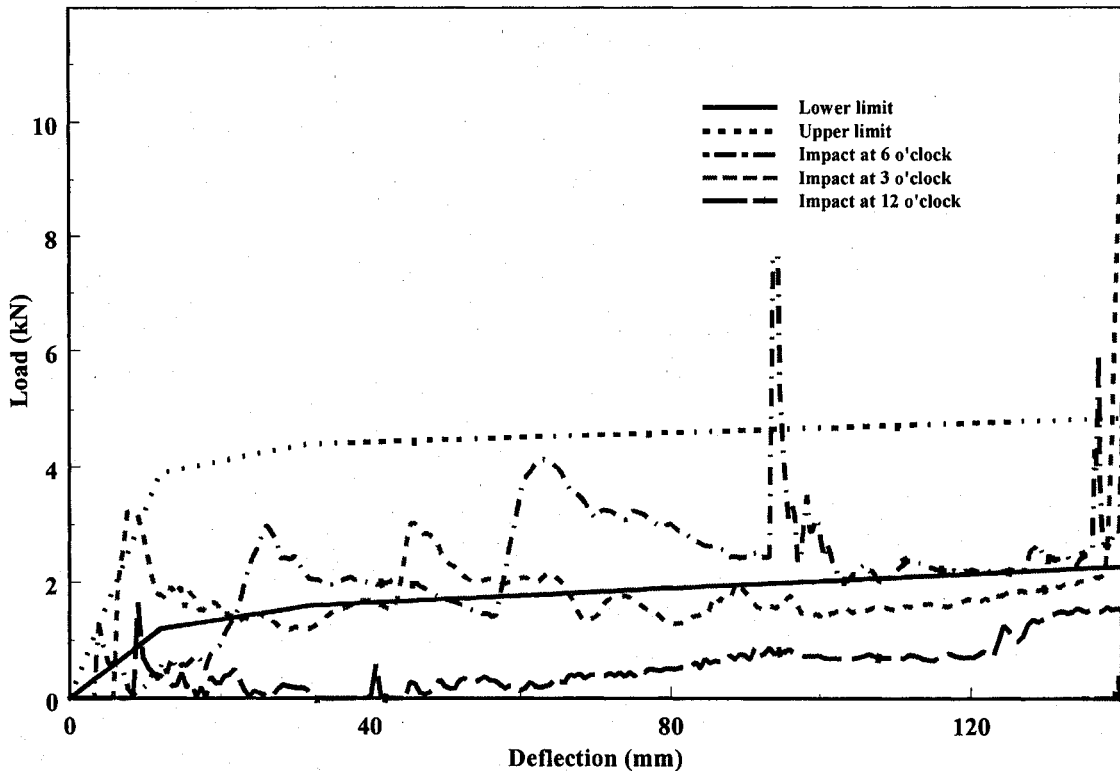
Figure 42. Load versus deflection response of test no. 35 for impact prior to bottoming out.

For the first 135 mm of deflection, the response for test no. 35 closely followed the load versus deflection specification curve with impact at the 6 o'clock position as illustrated in Figure 42. For impact at both the 3 o'clock and 12 o'clock position the response of this armature fell below the load versus deflection specification curve. Due to the shallow dish depth, the steering wheel armature bottomed out. The initial compliance with the load versus deflection specification curve for impact at the 6 o'clock position may be attributed to the location of the spokes along the rim of the armature. The spokes in this design at the 6 o'clock position are much closer together, making this rim position the strongest position for this particular design. However for impact at the 3 o'clock and 12 o'clock position, the low spoke angle left the upper region of the rim unsupported, consequently a small increase in load resulted in large

deflections because the rim was unable support the impact load. In addition, impact at the 12 o'clock position resulted in the largest peak load. Low spoke angles should be avoided in any design unless the dish depth is large enough to compensate for the unsupported portion of the rim. Alternatively increasing the spoke width, especially on spoke sections closer to the hub may result in lower peak loads and lower occurrences of bottoming out.

7.0 FINITE ELEMENT MODEL AND IMPACT INVESTIGATION BETWEEN THE HYBRID III AND STEERING WHEEL ARMATURES

Using a rigid plate as the impacting entity in all the simulations ensured that all the deformation occurred in the steering wheel armatures and provided a basis of comparison for all the steering wheel armatures tested. In addition, it was assumed that the response of the armatures, in terms of trends, when impacted with the rigid plate would follow the response of the armatures when impacted with a rigid Hybrid III dummy. Based on these assumptions, further investigations involving a Hybrid II dummy were conducted.

7.1. Finite element models used in this study

In order to simulate the passenger compartment in a frontal collision, finite element models were developed for the seat, seatbelt, and airbag and Hybrid III dummy.

7.1.1. Hybrid III finite element model

The dummy model used in the simulations is based on the 50th percentile Hybrid III model and is available in LS-DYNA. The motion of the dummy is governed by equations integrated in LS-DYNA and the default joint characteristics in LS-DYNA were utilized. Since the primary concern of this study was to investigate the performance of a steering wheel armature with the aim of optimizing the steering wheel's geometry, all segments of the dummy were modeled with rigid body characteristics. The positioning file for the Hybrid III may be found in Appendix C.

7.1.2. Development of the seat and seatbelt finite element model.

The seat belt was modeled using 480 fully integrated membrane elements while the seat was modeled using 4320 constant stress solid elements. All the nodes at the anchorage points of the seatbelt were constrained to simulate a three-point belt. The seatbelt model did not include the retractor or slack. Typically an airbag takes approximately 30 ms to inflate [56]. Contact between the airbag and occupant

during the deployment phase can result in considerable forces to the head and chest of the occupant. In an effort to correctly model the motion of the Hybrid III in an impact situation, a rigid back plate was introduced. The back plate was modeled using 976 fully integrated shell elements. The back plate was prescribed an acceleration pulse, illustrated in Figure 43, as detailed in FMVSS 208 using *BOUNDARY_PRESCRIBED_MOTION_NODE card in the input file, and the nodes at the back of the seat were constrained to move with the back plate resulting in a forward motion of the dummy similar to that observed in frontal barrier test.
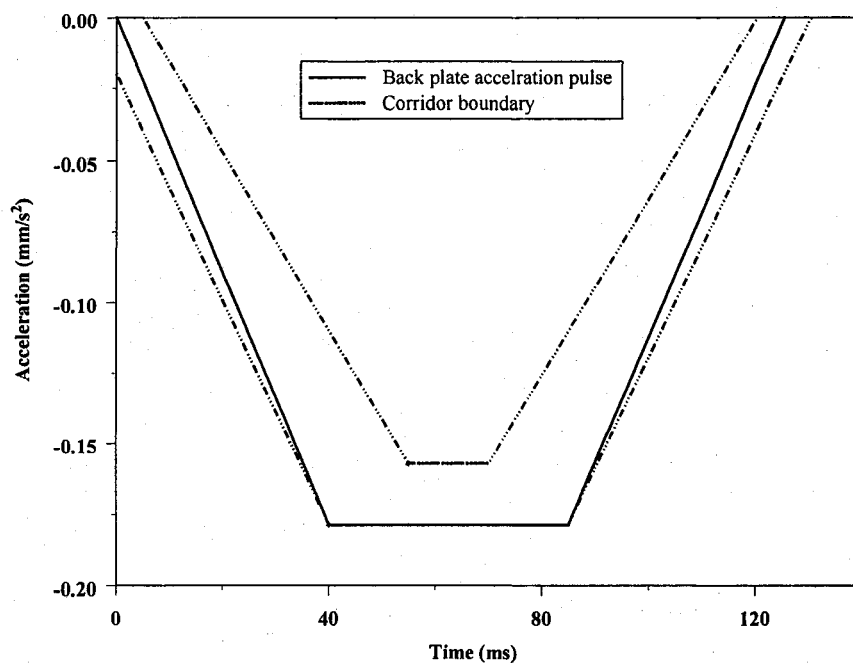
Figure 43.   Acceleration pulse with maximum and minimum corridors for 48 km/h sled test [2]

The seat material employed the low density foam model which is generally recommended to model seat cushions and padding. This material model requires input for density (0.154 g/cm^3), Young's Modulus (643 kPa) and a nominal stress versus strain curve for the material illustrated in Figure 44. The seatbelt was treated as an isotropic elastic material utilizing the fabric material model. Input for this material model includes density (0.841 g/cm^3), Young's Modulus (4 MPa), and Poisson's ratio (0.3).

70
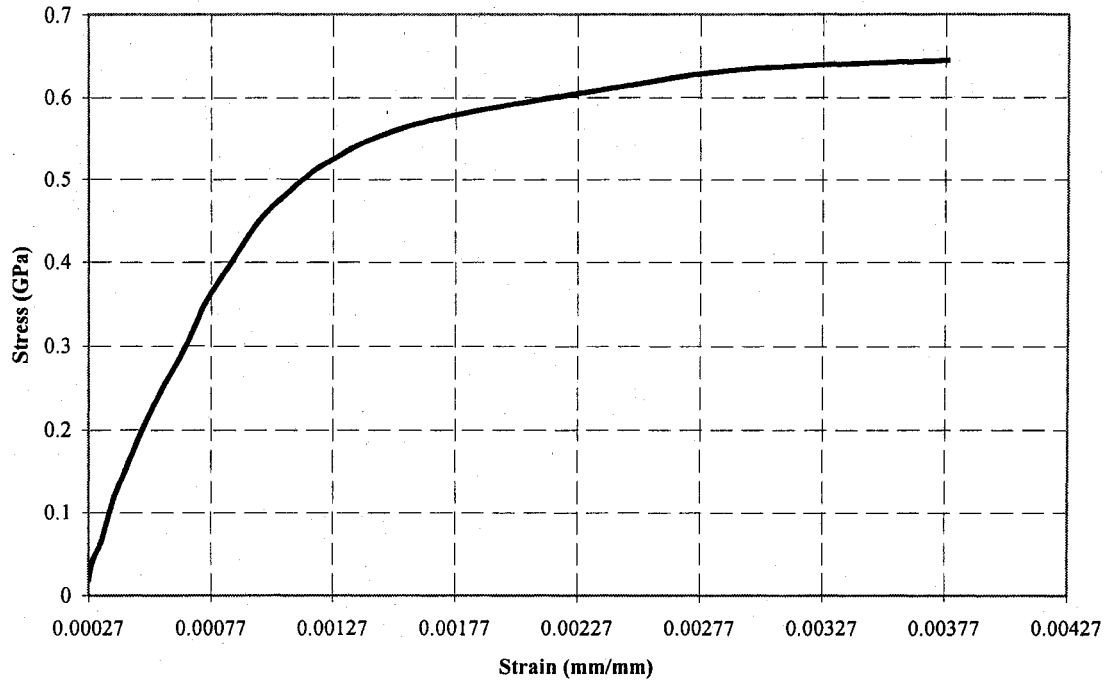
Figure 44. Stress Versus Strain used for the seat material model

7.1.3. Development of the finite element model of the airbag

The keyword *AIRBAG, in LS-DYNA, defines the thermodynamic behavior of gas flow in an airbag. The airbag is treated as a control volume with input including specific heats (specific heat at constant volume, 836 J/(Kg·K), specific heat at constant pressure 1710 J/(Kg·K)), input mass flow rate, and input gas temperature (800 K). The simple airbag model was obtained from the National Highway Traffic and Safety Association website. This airbag model assumes uniform thermodynamic properties, which is an accurate approximation when there is no interaction between the bag and occupant during the unfolding of the bag [30]. The airbag consisted of 2816 quadrilateral and 44 triangular membrane elements. The airbag was mounted onto a rigid plate attached to the spokes of the steering wheel armature using spot welds. The airbag material employed a similar material model as the seatbelt with density (0.825 g/cm^3), Young's Modulus (200 MPa), shear modulus (38 MPa) and Poisson's ratio (0.3).

The input file for all the material models used in this investigation may be found Appendix D.

7.2. Numerical simulation setup and procedure

The steering wheel armature model was combined with the Hybrid III, seat seatbelt and airbag models as illustrated in Figure 45. Nine contact algorithms were required to completely define all the contact interfaces in this model. All contact algorithms employed the *CONTACT_AUTOMTATIC_SURFACE_TO_SURFACE contact algorithm in which only the nodes of each element are checked for penetration against the impact body. In addition the *CONTACT_AIRBAG_SINGLE_SURFACE algorithm, specifically designed to treat the contact between airbag folds, was used to model the folded surfaces of airbag. The algorithms employed between all contacting surfaces may be found in Appendix E.
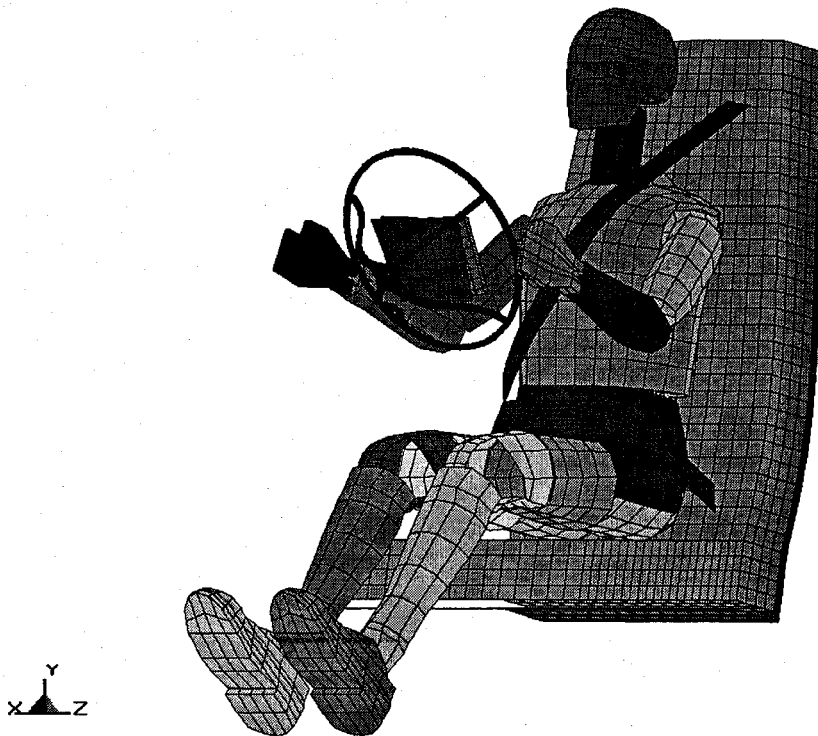
Figure 45. Illustration of the Hybrid III, seat, seatbelt, airbag and steering wheel armature finite element models

In frontal vehicle collisions, the crushing of the front of the vehicle displaces the steering column horizontally into the passenger compartment. Steering column displacement (into the passenger compartment) is regulated by FMVSS 204 [57]. In order to mimic this steering column intrusion, the nodes at the center of the steering wheel hub were prescribed a displacement in the z-direction ,not exceeding 127 mm, using *BOUNDARY_PRESCRIBED_MOTION_NODE.

A total of 4 simulations were run on a personal computer with two 1.6 GHz AMD-Athlon processors with 384 Megabytes of RAM. A summary of the test setups is provided in Table 11. Typical simulations run for 120 ms of the crash event, with processing times ranging from 20 to 24 hours.

Table 11. Summary of the numerical simulation setup

Test No	Impacting Entity	Dimensions	
		Dish depth mm	Spk3theta1 degrees
36	Unrestrained Hybrid III	129.33	30
37	Unrestrained Hybrid III	76.00	-10
38	Restrained Hybrid III with airbag deployment	129.33	30
39	Restrained Hybrid III with airbag deployment	76.00	-10

7.3. Results and discussion of impact between the steering wheel armatures and the unrestrained Hybrid III dummy

The simulated system kinematics illustrating impact between the Hybrid III and 76 mm dish depth and −10 degree armature (test no. 37) are shown in Figure 46. As illustrated, the Hybrid III dummy crushed into and rebounded from the steering wheel. In both cases the steering wheel bottomed out and the rim deformed past the hub resulting in little or no elastic response.
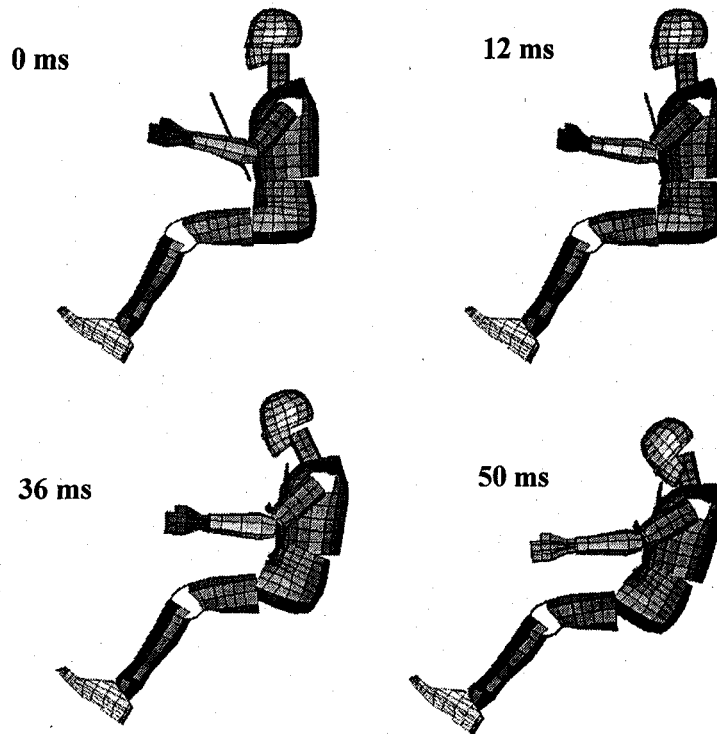
Figure 46. Simulated system kinematics for test no. 37

The peak load, C.F.E, elastic response, energy efficiency, and the EAF test no. 36 and test no. 37 are presented in Table 12 to give a clear comparison of the differences in response of the two armature designs. Figure 47 through Figure 49 compare results for the peak load and energy absorption of the two steering wheel armatures.

Table 12-Summary of the response for Test no. 36 and Test no. 37

Test no.	F_{peak} (kN)	C.F.E (%)	$E_{absorbed}$ (J)	e_e	E.A.F
36	258.82	4.14	934.28	0.44	0.65
37	393.5	3.77	629.66	0.11	0.56
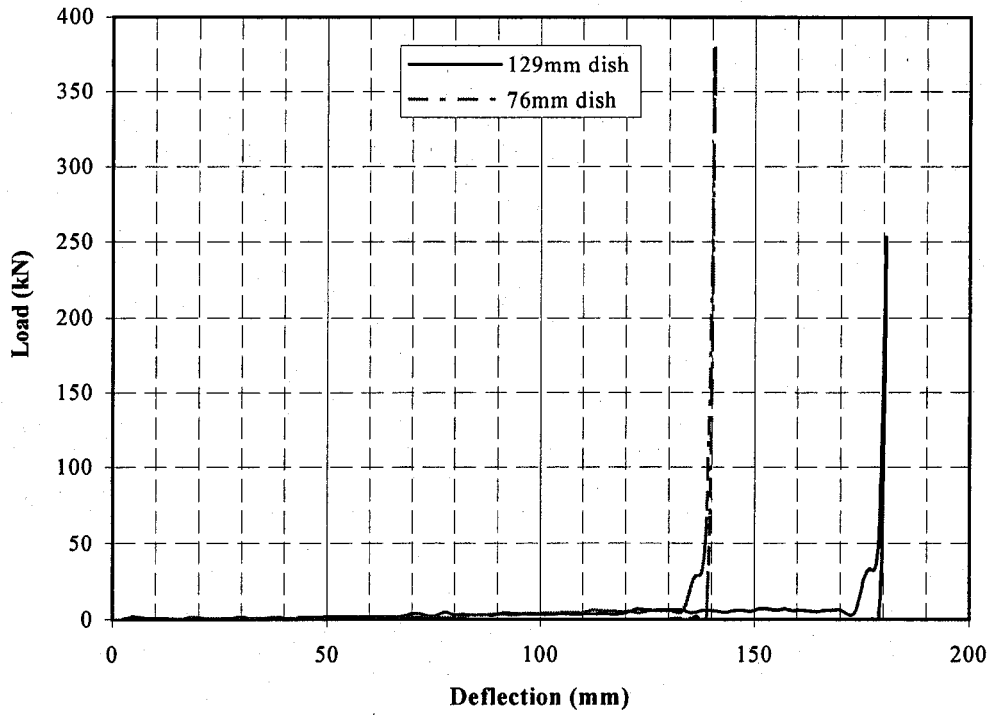
Figure 47. Load versus deflection response of test no. 36 (129 mm dish) and test no. 37 (76 mm dish).
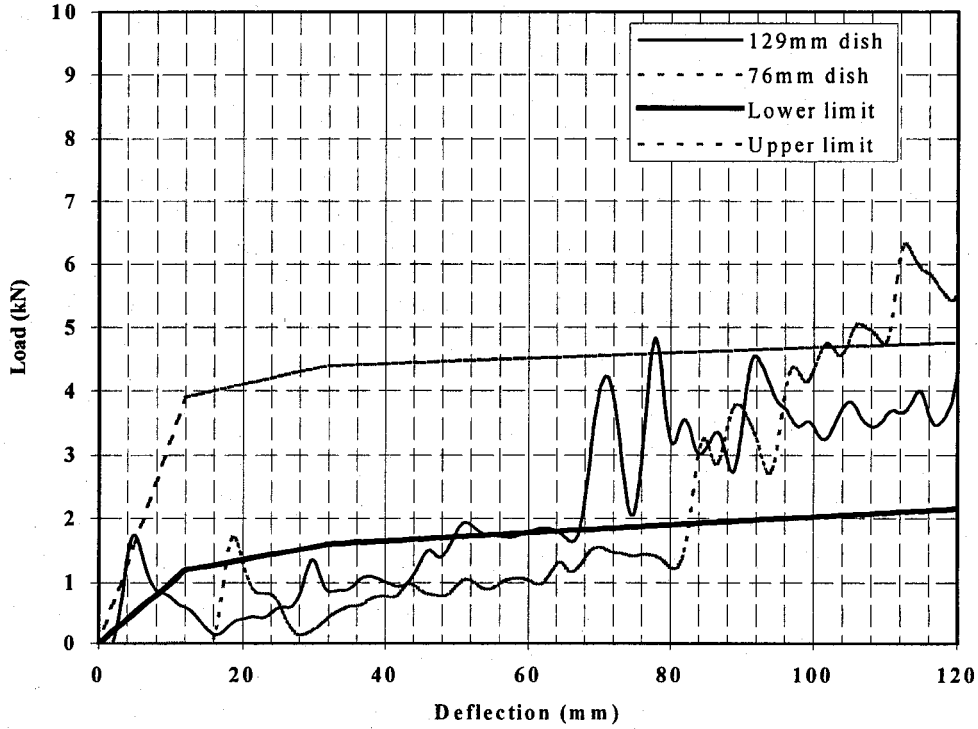
Figure 48. Load versus deflection response of test no. 36 (129 mm dish) and test no. 37 (76 mm dish)
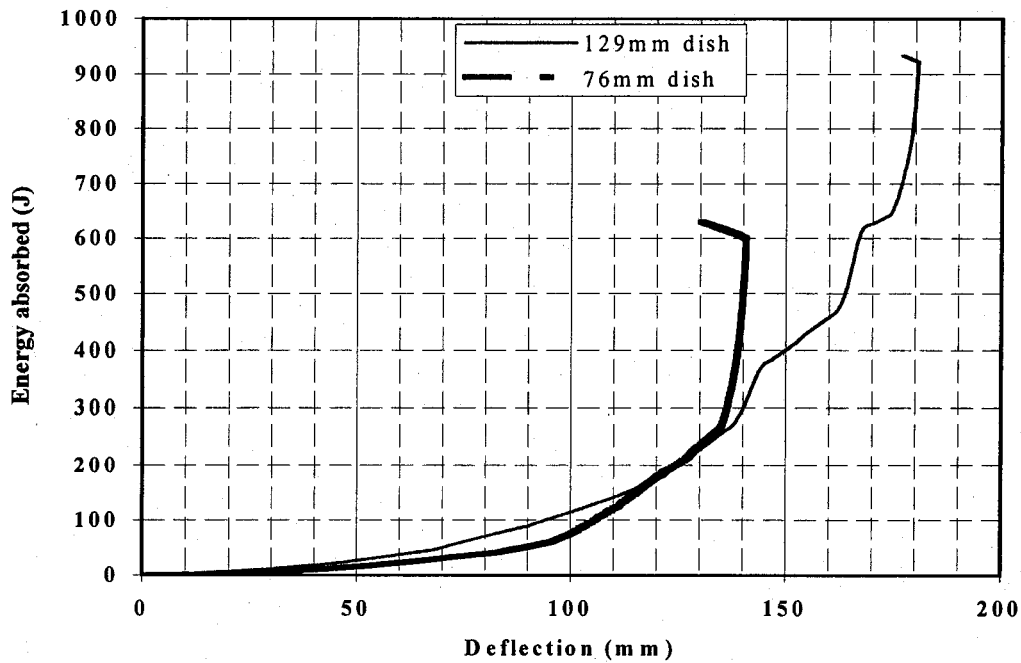
Figure 49. Energy absorbed versus deflection response of test no. 36 (129 mm dish) and test no. 37 (76 mm dish).

Predicted force levels from these analyses demonstrated an unrealistically large force when contact with the hub occurred as illustrated in Figure 47. Since the hub is a relatively stiff structure and all the nodes at the center of the hub are fully constrained, and the Hybrid III dummy segments are modeled with rigid body characteristics, contact between the hub and the dummy resulted in the large forces observed here. A more realistic model would require for the chest and abdomen of the dummy to be deformable to allow for some energy absorption through deformation of the dummy.

Nevertheless, as previously observed when impact occurred between the armature and the rigid plate, the more shallow dish depth resulted in a much higher peak load and lower energy absorption. While the larger dish depth resulted in a lower peak load and higher energy absorption. This is because, in addition to the larger crush space available in armature designs with a large dish depth, large dish depths allow for longer effective spoke lengths providing a more adequate load path to the steering column. They also result in better load distribution, with higher rim loads being

76

mostly distributed on the spokes near the hub. This would explain why an increase in dish depth is accompanied by a decrease in peak loads even when the armature bottoms out.

Figure 48 illustrates the response of the armatures prior to bottoming out. For the first 120 mm of deflection, the response of test no. 36 (129 mm dish), closely follows the load versus deflection specification curve while the response of test no 37. (76 mm dish) lies outside the load versus deflection specification curve limits. As was previously observed, the larger dish depth exhibits a more favorable response resulting in better armature loading characteristics.

7.4. Results and discussion of impact between the steering wheel armatures with airbag deployment and the restrained Hybrid III dummy

The simulated system kinematics illustrating impact between the restrained Hybrid III and 76 mm dish depth and –10 degree armature (test no. 39) with airbag deployment are shown in Figure 50. As illustrated, the airbag deployment load significantly deforms the steering wheel armature prior to impact with the Hybrid III dummy.
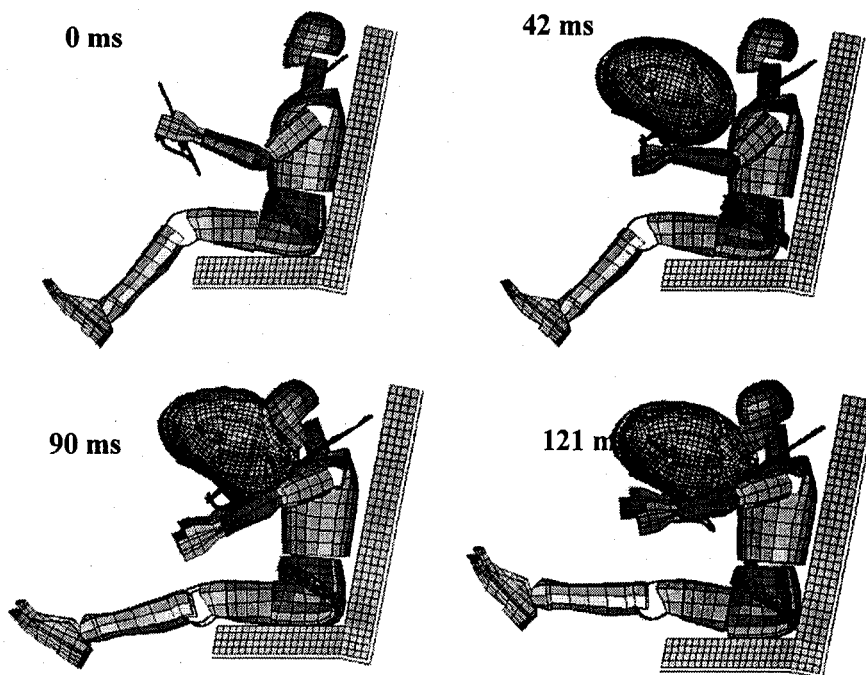
Figure 50. Simulated system kinematics for test no.39.

77

The peak load and energy absorbed for test no. 38 and test no. 39 are presented in Table 13 to provide a comparison of the differences in response of the two armature designs. Figure 51 and Figure 52 compare results for the peak load and energy absorption of the two steering wheel armatures. Due to the airbag deployment and the internal energy associated with the deployment of the airbag, it would be misleading to compare the performance of the steering wheel armatures in terms of $C.F.E$, energy efficiency and the $E.A.F$.

Table 13-Summary of the response for Test no. 38 and Test no. 39

Test no.	F_{peak} (kN)	$E_{absorbed}$ (J)
38	1.2	158.94
39	1.8	172.96
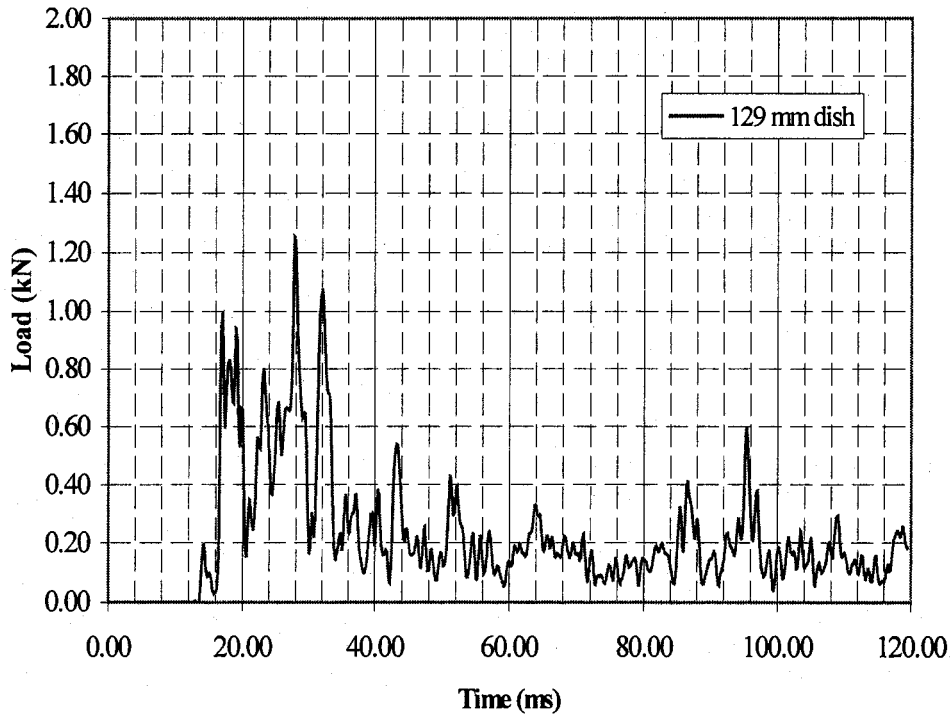
(a

Figure 51. Load versus time response for test no. 38 (129 mm dish).
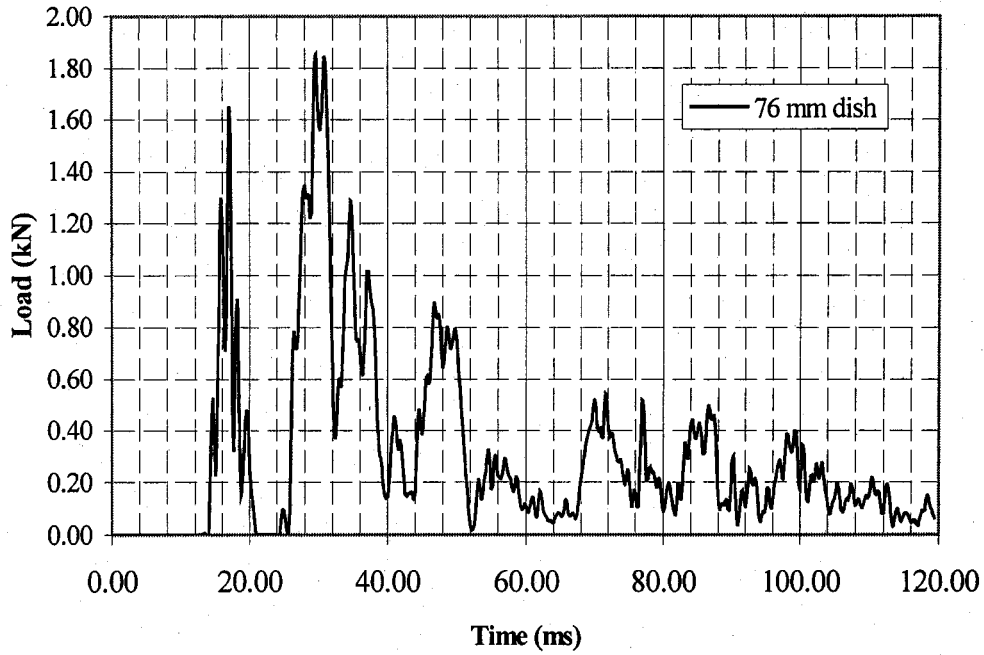
Figure 52. Load versus time response for test no. 39 (76 mm dish).
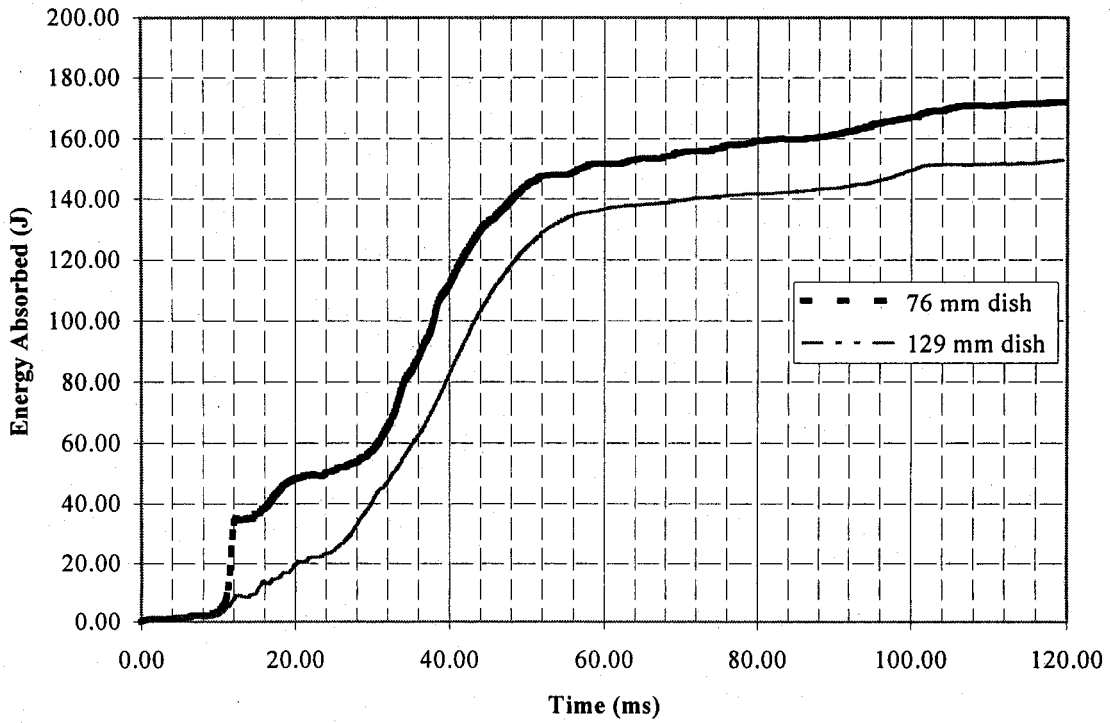
Figure 53. Energy absorbed versus time response of test no. 38 (129 mm dish)
and test no. 39 (76 mm dish).

As illustrated in Figure 51 the more shallow dish depth results in higher peak loads as was previously observed for impact with both the rigid plate and the unrestrained Hybrid III dummy. The difference is not as significant as that observed for impact with the rigid plate. This is because steering wheel loading observed in test no. 38 and test no. 39 is primarily due to airbag loading which is distributed along the rim of the armature.

Similarly the energy absorbed by the steering wheel armatures in test no. 38 and test no. 39, illustrated in Figure 52, represents the plastic deformation of the steering wheel armatures due to airbag loading. The more shallow dish depth results in larger energy absorption. These results differ from the results obtained from impact with the rigid plate. In the latter case, the more shallow dish depth resulted in less energy absorption. The reason for this difference may be due to difference in spoke length between the two armatures. For the given rim radius, the more shallow dish depth has a much shorter effective spoke length and may not be able to support the airbag deployment load as well as the armature with a longer effective spoke length. This resulted in larger deformations in the more shallow dish depth armature and consequently greater energy absorption as observed in Figure 52.

In addition, both armatures initially interacted with the airbag resulting in the airbag "rolling over" the upper portion of the rim and resulting in a sharp increase in energy absorption at approximately 10 ms as illustrated in Figure 52. This effect, which was more pronounced for the deep dished armature, is undesirable because it leaves the lower portion of the rim exposed without airbag coverage and may result in injury to the abdomen of the occupant during a crash event.

The results presented in Table 13 and Table 14 indicate that the trends observed on impact with the rigid plate are also observed when impact occurs with the unrestrained Hybrid III dummy when there is no airbag deployment. Airbag deployment significantly influences interaction between the Hybrid III dummy and

the steering wheel, thus in designing steering wheel armatures for energy absorption, engineers may use a rigid plate as an impacting entity but consideration must be given to the response of the steering wheel armature with airbag deployment.

8.0 CONCLUSIONS AND RECOMMENDATIONS FOR FUTURE WORK

8.1. Conclusions

This thesis focused on two primary objectives:

- Experimental testing of steering wheel armatures to examine how the variations in armature geometry affect the crashworthiness performance of steering wheels.

- Developing a highly detailed parametric model of a steering wheel armature in order to carry out simulations with variations in predetermined parameters.

Conclusions dealing with the experimental and numerical analyses will be presented in the following section,

8.1.1 Conclusions dealing with experimental testing

1. A comparison of the magnitudes of the loads observed in the experimental testing indicates that the parametric models are an adequate approximation of the system under simulation.

2. The load versus displacement profile of the steering wheel armatures during impact with the rigid plate is a function of the location of the spokes along the rim of the armature (spoke angle). Larger spoke angles are more favorable resulting in better approximation to the square load versus displacement profile required for maximum energy absorption.

3. Experiments have shown that the dish depth has a significant influence over the energy absorption and that the larger dish depth of 140 mm results in higher energy absorption although the energy efficiency may suffer somewhat if too large a dish depth is chosen.

4. In addition, the spoke cross section must be able to provide an adequate load path for the impact load to the hub in order to ensure that no failure occurs in the spokes causing additional potential injury to the occupant.

8.1.2 Conclusions dealing with finite element modeling and simulation

1. In a crash event involving steering wheel impact, the loads developed on the steering wheel armature are largely dependent on the spoke angle and impact location.

   - Since decreasing the spoke angle increases the support of the lower portion of the rim, the response of the armature when impacted at the 6 o'clock position stiffens as the spoke angle decreases.

   - For impact at the 3 o'clock position the response is influenced by the location of the spoke (spoke angle) along the rim, with spoke angles below 0° resulting in stiffer responses.

   - The response is weakest for impact at the 12 o'clock position for all spoke angles with frequent occurrences of bottoming out.

2. The energy absorption of the steering wheel armatures is influenced by the spoke angle, dish depth and location of impact.

   - For impact at the 6 o'clock position the energy absorption is generally higher for armatures with a dish depth above 108mm for all spoke angles investigated.

   - For impact at the 3 o'clock position, large dish depth armatures absorbed more energy, similar to impact at the 6 o'clock position. With peak energy absorption at 140 mm dish depth and −10 degrees of spoke angle.

   - Lower spoke angles and dish depths absorb more energy for impact at the 12 o'clock position although this mode of energy absorption is undesirable because the armature bottoms and gives rise to the excessive peak loads which pose a significant threat to the ribs and soft tissue of the torso.

3. Similar to the experimental findings the peak loads developed on the steering wheel depend mainly on the spoke angle and location of impact.

   - For impact at the 6 o'clock position, the peak load is significantly lower for dish depths above 97 mm, for all spoke angles investigated.

- Similarly for impact at the 3 o'clock position, peak loads are lower for dish depths above 97 mm for all spoke angles investigated.

- For impact at the 12 o'clock position, the peak load increases with both dish depth and spoke angle with the highest peak load occurring at a dish depth of 76mm and a spoke angle of -10°.

4. The *C.F.E* and energy efficiency of the steering wheel armatures also depend on the dish depth.

- For impact at the 6 o'clock and 3 o'clock position, larger dish depths above 97 mm are more favorable demonstrating higher efficiencies.

- For impact at the 12 o'clock position, the spoke angle significantly influences the efficiencies of the armatures. Armatures with dish depths above 108 mm and spoke angles above 10° possess the highest efficiencies.

5. The *E.A.F.* of the steering wheel armatures is also greatly influenced by the dish depth.

- For impact at the 6 o'clock position, the armatures with the larger dish depths, above 108 mm, exhibit the highest *E.A.F.*

- For impact at the 3 o'clock position, larger dish depth above 97 mm and lower spoke angles below 20° result in higher *E.A.F.*

- For impact at the 12 o'clock position, lower spoke angles and dish depths result in higher *E.A.F.* due to bottoming out of the armature.

6. The performance of the steering armature when impacted with a rigid plate is an adequate approximation of the performance the armature when impacted with a Hybrid III dummy.

7. The presence of the airbag greatly influences the response of the steering wheel armature and should not be neglected when designing for crashworthiness. Deep

dish armatures may have the potential of airbag roll over and potentially give rise to contact between the rim portion of the armature and the occupant.

8.2. Recommendations for future work

- Although the results observed in this investigation compare well with results observed in previous investigations involving occupant simulation, a number of details need to be included in these models to better represent the passenger compartment and interaction with dummy during a crash event. These include vehicle interior (seat, knee bolster, steering column) and dummy joint characteristics.

- The airbag model should incorporate the airbag cover because the resistance of the cover may have an effect on the pressure history of the airbag and deployment.

- For more severe crash events results may show a different trend, a wider range of impact velocities should be investigated.

- While this study sought to investigate the effect of two parameters on the response of a steering wheel armature, altering the dish depth inadvertently altered the spoke profile. Since the spokes of the steering wheel armature provide the primary load path, an investigation of the spoke profile for a given dish depth and its influence on the performance of the steering wheel armature would be very beneficial.

- A steering wheel armature consisting of a continuous spoke would provide uniform stiffness along the rim the armature, regardless of the impact location. Investigations into the crashworthiness performance of such an armature would be beneficial in determining further performance characteristics.

REFERENCES

[1] Motor Vehicle Safety act, Statues of Canada, 1993, Website: http://laws.justice.gc.ca/en/M-10.01/, Accessed February 2003.

[2] Motor Vehicle Safety Act, Motor Vehicle Safety Regulations Standard 203, "Driver Impact Protection"., Statues of Canada., 1997.

[3] Motor Vehicle Safety Act, Motor Vehicle Safety Regulations Standard 208, "Occupant Restraint Systems in Frontal Impact", Statues of Canada., 1997.

[4] NHTSA, "Federal Motor Vehicle Safety Standards: Impact protection for the driver from the steering control system"., Code of Federal Regulations, 49 CFR571.203, Washington D. C., 1997.

[5] NHTSA, "Federal Motor Vehicle Safety Standards: Occupant crash protection"., Code of Federal Regulations, 49 CFR571.208, Washington D. C., 1997.

[6] Economic Commission For Europe Inland Transport Committee (ECE) Reg. No.12, "Protection of Drivers Against the Steering Mechanism in the Event of Impact", Agreement Concerning the Adoption of Uniform Conditions of Approval and Reciprocal Recognition of Approval for Motor Vehicle Equipment and Parts, done at Geneva on 20 March 1958.

[7] National Automotive Sampling System Crashworthiness Data System, U. S. Department Of Transportation, National Highway Traffic Safety Administration, 1994-1996, Washington D. C., October 1999.

[8] J. B. Morris, L. Stucki, R. M. Morgan and N. Bondy, "Occupant Protection from Impact with the Steering Assembly", National Highway Traffic Safety Administration, SAE Technical Paper No. 826025, 1982.

[9] K. Tanno, M. Kohno, K. ono, N. Ohashi, M. Doy, K. Yamazaki, S. M., A. Takada, K. Saito, "Fatal Cardiovascular Injuries to the Unbelted Occupant Associated with Airbag Deployment: Two Case-reports", Journal of Legal Medicine, Volume 4, 2000.

[10] W. J. Reed, MD, S. E. Doyle, MD, and C. Aprahamian, MD, "Tracheoesophageal Fistula after Blunt Chest Trauma", Society of Thoracic Surgens, Paper No. 59, 1995.

[11] P. Thomas and M. Bradford, "The Natures and Source of Head Injuries Sustained by Restrained Front-Seat Car Occupants in Frontal Collisions", Accident Analysis and Prevention, Volume 27, Paper No. 4, 1995

[12] S. P. F. Petty and M. A. Fenn, "A Modified Steering Wheel to Reduce Facial Injuries and Associated Test Procedure", 10th International Technical Conference on Experimental Safety Vehicles, Section 4, pp. 342-347, Oxford, U. K., 1-4 July, 1985.

[13] J. D. Horsch, D. C. Viano and J. Decou, "History and Safety Research and Development on the General Motors Energy-Absorbing Steering System", SAE Paper No. 912890, pp. 1818-1863, 1991.

[14] Society of Automotive Engineers, Steering Control System –Passenger Car- Laboratory Test Procedure- SAE J944, 1992, SAE Handbook, Volume 4, Warrendale, PA., U. S. A., (1992), pp 34.230 – 34.232

[15] J.T. Wang and K. Lin, "A CAL3D Steering System Impact Model", Paper No. 880650, Society of Automotive Engineers, 1988.

[16] J M Lim, D H Wuh and G J Park, "Analysis and Design Consideration of an Energy Absorbing Steering System Using Orthogonal Arrays", International Journal of Crashworthiness, Volume. 5 No. 3, 2000.

[17] Y. Park, J. Lee, J. M. Lim and G. Parks, "Optimum Design of a Steering Column to Minimize the Injury of a Passenger", International Journal of Vehicle Design, Volume. 17 No. 4. 1996.

[18] K. N. Naab, S. L. Stucki, "Development and Testing of Steering Assembly Countermeasures for Driver Impacts", SAE Techincal Paper 900546, 1990.

[19] S. Shyu, A. Mani, P. Krishnaswamy, R. Conroy, M. Shermetaro, G. Exner, "Designing Energy Absorbing Steering Wheels through Finite Element Impact Simulation", SAE Future Transportation Technology Conference, Paper No. 931844, 1993.

[20] W. Altenhof, S. Paonessa, and N. Zamani, "Observations on the Energy Absorption Characteristics of a Three-Spoke Steering Wheel Armature During Impact", Journal of Automobile Engineering, Volume. 215, 2001.

[21] W. Altenhof, Z. Li, and N. Zamani, "An Investigation into the Energy Absorption Characteristics of a Four-Spoke Steering Wheel Armature Subjected to Impact Loading", International Journal of Crashworthiness, Volume 7, No. 1, 2002.

[22] M. R. Maltese, R. R. Samaha, R. H. Eppinger and G. Strassbury, "Response of the Eurosid-1 Thorax to Lateral Impact", Paper No. 1999-01-0709, Society of Automotive Engineers, 1999.

[23] Y. Deng, W. Kong and H. Ho, "Development of A Finite Element Human Thorax Model for Impact Injury Studies", Paper No. 1999-01-0715, Society of Automotive Engineers, 1999.

[24] K. H. Yang, F. Zhu, F. Luan, L. Zhao, and P. C. Begeman, "Development of a Finite Element Model of the Human Neck", Paper No. 983157, Society of Automotive Engineers, 1998.

[25] J. S. Ruan, T. Khalil and A. I. King, "Finite Elements Analysis of the Human Head to Impact", Bioengineering Division, Winter Annual Meeting of ASME BED-Volume. 22, pp. 249-252, 1992.

[26] G. S. Nusholtz and Y. Shi, "Physical Reality in FE Head Models: Rotation and Strain" Paper No. 980355, Society of Automotive Engineers, 1998.

[27] B. Besnault, H. Guilemot, S. Robin, F. Lavaste, J. Le Coz, "A parametric Model of the Human Pelvis", Society of Automotive engineers Paper No. 983147, 1998.

[28] J. K. Foster, J. O. Kortge, and M. J. Wolanin, "Hybrid III- A Biomechanically-Based Crash Test Dummy", Proceedings of the 21st Stapp Car Crash Conference, Paper No. 770938, 1977.

[29] US Department of transportation, Part 572 subpart E, "Anthropomorphic Test Dummy", 38fr 20449, August 1973.

[30] J. D. Horsch, D. Schneider, "Biofidelity of the Hybrid III Thorax in High-Velocity Frontal Impact", SAE Paper No. 880718, 1988.

[31] R. Happee, M. Hoofman, A.J.van den Kroonenbery, P. Morsink, and J. Wismans, "A Mathematical Human Body Model for Frontal and Rearward Seated Automotive Impact Loading", Paper No. 983150, Society of Automotive Engineers, 1998.

[32] A. Noureddine, K. H Diggs and N. E bedewi, "An Evaluation of Deformation Based Chest Injury Criteria using a Hybrid III Finite Element Model", International Journal of Crashworthiness, Volume.1 No.2, 1996.

[33] Em. Lizee, S. Robin, E. Song, N. Bertholon, J.Le Coz, B. Besnault, and F. Lavaste, "Development of a 3D Finite Element Model of the Human Body", Proceedings of the 42nd Stapp Car Crash Conferencee, Paper No. 983152, 1998.

[34] C. K. Demetropouls, K. H. Yang, M. J. Grimm, K. K. Arthan, and A. I. King, "High Rate Mechanical Properties of the Hybrid III and Cardeveric Lumbar Spines in Flexion and Extension", Proceedings of the 43rd Stapp Car Crash Conferencee, Paper No. 99SC18, 1999.

[35] J. S. Ruan and P. Prasad, "Head Injury Potential Assessment in Frontal Impacts by Mathematical Modeling", Paper no. 942212, Society of Automotive Engineers, 1994.

[36] D. Marzougui, C. Kan, N. E. Bedewi, "Development and Validation of an NCAP Simulation", Fourth International LS-DYNA3D Conference, Cray Research, pp. 319-322, 1996.

[37] Livermore Software Technology Company, LS-DYNA Keyword User's Manual Version 950, Appendix k, 1999.

[38] N. Jones, "Structural Impact", Cambridge University Press, Cambridge United Kingdom, pp 423-428, 1997.

[39] R. F. Neathery, "Analysis of Chest Impact Response Data and Scaled Performance Recommendations", 18th Stapp Car Cash Conference, SAE Paper 741188, Decemeber 1974.

[40] A. Dayal, J. L. Sahni, K. S. Dave, S. Kumar, S. Singh, "Physiological and Anatomical Index in Reference to Management of Thoracic Trauma.", International Journal of Thoracic and Cardiovascular Surgery, Vol 11, 1995.

[41] Society of Automotive Engineers, Human Tolerance to Impact Conditions as Related to Motor Vehicle Design- SAE J885, 1986, SAE Handbook, (1986)

[42] W. Altenhof., "A Prototype Testing Machine and Methodology for Impact Loading of Steering Wheels", Masters Thesis, Department of Mechanical, Automotive and Materials Engineering, University of Windsor, 1997.

[43] J. Baumeister, J. Banhart and M.Weber., "Aluminum Foams for Transport Industry", Materials and Design Volume 18, Nos. 4/6, p217-220, 1997.

[44] C. A. Krauss and D. H. Laananen., "A Parametric Study of Crush Initiators for a Thin Walled Tube", International Journal of Vehicle Design, Volume 15, Nos. 3/4/5, 1994.

[45] C. L. Magee and P. H. Thorton., "Design Considerations in Energy Absorption by Structural Collapse", Society of Automotive Engineers, Paper No. 880894, 1988.

[46] S. K. Maiti, L. J. Gibson, M. F. Ashby., "Deformation and Energy Absorption Diagrams for Cellular Solids", Acta Metallurgica, Volume 32, No. 11, November 1984.

[47] Society of Automotive Engineers, Instrumentation for Impact Tests- SAE J211, 1992, SAE Handbook, Volume 4, Warrendale, PA., U. S. A., (1992)

[48]   S. E. Benzley, E. Perry, K. Merkley, B. Clark, and G. Sjaardema, "A Comparison of All Hexagonal and All Tetrahedral Finite Element Meshes for Elastic and Elasto-Plastic Analysis", Proceedings 4th International Meshing Roundtable, Sandia National Laboratories, Oct. 16-17, 1995.

[49]   XYZ Scientific Applications, Inc., TrueGrid Manual Version 2.1.0, 2001.

[50]   Y. Kawase and T. Yoshida, "Development of Magnesium Steering Wheel." Society of Automotive Engineers, Paper No. 910549, 1991

[51]   Personal communication with K. Nuschlat, U. S. Department Of Transportation, National Highway Traffic Safety Administration, June 2002.

[52]   W. Altenhof and W. Ames., "Observations of the Relative Performance of Magnesium and Aluminum Steering Wheel Skeletons with Identical Geometry.", SAE Technical Paper No. 2000-01-0784, SAE world congress 2000.

[53]   W. L. fink, F. Keller, W. E. Sicha, J. A. Nock, E. H. Dix, "Physical Metallurgy of Aluminum Alloys", Published by the American Society for Metals, Cleveland, Ohio, 1949.

[54]   K. Sadayappan, Natural Resources Canada, Minerals and Metals Sector, Material Technology Laboratory-CANMET, Ottawa, Ontario, 2002.

[55]   ASTM B557M "Standard Test Methods of Tension Testing Wrought and Cast Aluminum and Magnesium Alloy Products"., ASTM International, 2003.

[56]   C. Chan, "Fundamentals of Crash Sensing in Automotive Air Bag Systems.", Society of Automotive Engineers Inc. Warrendale P.A., U. S. A., 2000.

[57]   NHTSA, "Federal Motor Vehicle Safety Standards: Steering Column Rearward Displacement"., Code of Federal Regulations, 49 CFR571.204, Washington D. C., 1997.

[58]   Ward's Communication Inc. "Motor Vehicle Facts and Figures", Southfield, Michigan, 2002.

[59]   Personal communication with J. Ferrari, Grant Steering Wheels, August 2002.

APPENDIX A

Top 6 selling passenger cars [58].

TOP PASSENGER CARS

1999	2000	2001
1 Honda Civic	Honda Civic	Honda Civic
2 **Chevrolet Cavalier**	**Ford Focus**	**Ford Focus**
3 Oldsmobile Alero	**Chevrolet Cavalier**	**Chevrolet Cavalier**
4 **Chrysler Neon**	Oldsmobile Alero	Nissan Sentra
5 Nissan Sentra	**Chrysler Neon**	Oldsmobile Alero
6 **Ford Focus**	Nissan Sentra	**Chrysler Neon**

NUMBER OF VEHICLES SOLD

	1999	2000	2001
Honda Civic	318,308	324,528	331,780
Ford Focus	55,846	286,166	264,414
Chevrolet Cavalier	272,122	236,803	233,298
Nissan Sentra	63,134	98,083	111,082
Oldsmobile Alero	118,941	122,722	109,302
Chrysler Neon	112,236	113,381	107,299

APPENDIX B

Measurements taken on steering wheels from different passenger cars.

After market wheels have dish depth ranging from 2.25 to 4.25 inches. Although they are not required to pass government issues safety standards, steering wheel manufacturers perform in house impact and fatigue test equivalent to those required by government regulations [59]. However, the dish depths observed in after market steering wheels were not considered in deriving the range and baseline dimensions for the dish of the steering wheel armature investigated here.

Model	Year	Dish depth mm
Dodge Truck	1990	5.50
Pontiac Grand prix	1991	4.50
Ford truck Ranger	1993	4.00
Ford windstar	1995	4.00
Chevrolet Tracker	1990	4.00
Mustang	1997	3.00
Daytona	1990	4.00
GMC Yukon	1999	4.00
Taurus	2001	4.50
Intrepid	1999	4.50
Durango	2001	3.50
Lincoln navigator	2002	3.25
Mercury sable	2001	3.25
Mazda	2000	3.00
Crossfire	2001	3.75
Saab	1999	3.50
Saturn	1999	3.25
Camry	1999	4.00
Corolla	1998	3.25
Echo	2000	3.75
Sunfire	1999	4.00
Blazer	2000	4.50
Hyundai elantra	1997	4.00
Acura	1997	3.25
Audi	2001	3.00

APPENDIX C

The Hybrid III dummy positioning file.

The base set of units used are kg, mm, ms all other units are derived from this base set.

Sample input data from the LS-DYNA input file:

```
*COMPONENT_HYBRIDIII
$        DID       SIZE       UNITS       DEFRM          VX          VY          VZ
          10          2           5           1
$         HX         HY          HZ          RX          RY          RZ
         0.0     -350.0       477.0                    79.3        90.0
*COMPONENT_HYBRIDIII_JOINT_LEFT_SHOULDER
$        DID         Q1          Q2          Q3        FRIC
          10      -40.0        10.0
$         C1       ALO1        VLO1        AHI1        BHI1        QLO1        QHI1

$         C2       ALO2        VLO2        AHI2        BHI2        QLO2        QHI2

$         C3       ALO3        VLO3        AHI3        BHI3        QLO3        QHI3


*COMPONENT_HYBRIDIII_JOINT_RIGHT_SHOULDER
$        DID         Q1          Q2          Q3        FRIC
          10      -40.0       -10.0
$         C1       ALO1        VLO1        AHI1        BHI1        QLO1        QHI1

$         C2       ALO2        VLO2        AHI2        BHI2        QLO2        QHI2

$         C3       ALO3        VLO3        AHI3        BHI3        QLO3        QHI3


*COMPONENT_HYBRIDIII_JOINT_LEFT_ELBOW
$        DID         Q1          Q2          Q3        FRIC
          10      -60.0
$         C1       ALO1        VLO1        AHI1        BHI1        QLO1        QHI1

$         C2       ALO2        VLO2        AHI2        BHI2        QLO2        QHI2

$         C3       ALO3        VLO3        AHI3        BHI3        QLO3        QHI3


*COMPONENT_HYBRIDIII_JOINT_RIGHT_ELBOW
$        DID         Q1          Q2          Q3        FRIC
          10      -60.0
$         C1       ALO1        VLO1        AHI1        BHI1        QLO1        QHI1

$         C2       ALO2        VLO2        AHI2        BHI2        QLO2        QHI2

$         C3       ALO3        VLO3        AHI3        BHI3        QLO3        QHI3


*COMPONENT_HYBRIDIII_JOINT_LEFT_HIP
$        DID         Q1          Q2          Q3        FRIC
          10                             -80.0
$         C1       ALO1        VLO1        AHI1        BHI1        QLO1        QHI1

$         C2       ALO2        VLO2        AHI2        BHI2        QLO2        QHI2

$         C3       ALO3        VLO3        AHI3        BHI3        QLO3        QHI3


*COMPONENT_HYBRIDIII_JOINT_RIGHT_HIP
$        DID         Q1          Q2          Q3        FRIC
          10                             -80.0
$         C1       ALO1        VLO1        AHI1        BHI1        QLO1        QHI1

$         C2       ALO2        VLO2        AHI2        BHI2        QLO2        QHI2

$         C3       ALO3        VLO3        AHI3        BHI3        QLO3        QHI3


*COMPONENT_HYBRIDIII_JOINT_LEFT_KNEE
$        DID         Q1          Q2          Q3        FRIC
          10       50.0
$         C1       ALO1        VLO1        AHI1        BHI1        QLO1        QHI1

$         C2       ALO2        VLO2        AHI2        BHI2        QLO2        QHI2

$         C3       ALO3        VLO3        AHI3        BHI3        QLO3        QHI3
```

```
*COMPONENT_HYBRIDIII_JOINT_RIGHT_KNEE
$       DID        Q1        Q2        Q3       FRIC
         10       50.0
$        C1      ALO1      VLO1      AHI1      BHI1      QLO1      QHI1

$        C2      ALO2      VLO2      AHI2      BHI2      QLO2      QHI2

$        C3      ALO3      VLO3      AHI3      BHI3      QLO3      QHI3
```

APPENDIX D

Material properties.

The base set of units used are kg, mm, ms all other units are derived from this base set.

Material properties for the seat

Material property	Corresponding value
Density	0.154 g/cm^3
Young's modulus	643 KPa

Sample input data from the LS-DYNA input file:

```
*MAT_LOW_DENSITY_FOAM
$       MID        RO         E      LCID        TC        HU      BETA      DAMP
       61.538E-007 0.0006436        7.     1E+020      0.39        0.    0.4047
$     SHAPE      FAIL    BVFLAG        ED     BETA1      KCON       REF
          5.        0.        0.        0.        0.        0.        0.
*DEFINE_CURVE
$ STRESS VERSUS STRAIN CURVE FOR THE LOW DENSITY FOAM
$      LCID      SIDR      SCLA      SCLO      OFFA      OFFO    DATTYP
          7         0        0.        0.        0.        0.         0
$            STRAIN              STRESS
                0.                  0.
                0.02        0.0002701905
             0.04075        0.0002865025
               0.065        0.0003200287
             0.10697        0.0003614603
              0.1225        0.0003776757
             0.15043        0.0004180826
             0.19979        0.0004891528
             0.24976        0.0005716659
             0.29928        0.0006661435
              0.3515        0.0007465157
             0.40107        0.0008553347
             0.45635        0.0009840518
             0.50587         0.001169221
             0.52231         0.001256099
             0.54912          0.00142821
             0.57681         0.001736736
             0.61083         0.002402282
             0.63334         0.002951007
             0.64439         0.003776543
```

Material properties for the seatbelt

Material property	Corresponding value
Density	0.841 g/cm^3
Young's modulus	4 MPa
Poisson's ratio	0.3

Sample input data from the LS-DYNA input file:

```
*MAT_FABRIC
$      MID        RO        EA        EB        EC      PRBA      PRCA      PRCB
         7 8.41e-07       4.0        0.        0.      0.30        0.        0.
$      GAB       GBC       GCA       CSE        EL       PRL    LRATIO      DAMP
         0.        0.        0.        0.        0.        0.        0.        0.
$     AOPT       FLC       FAC       ELA      LNRC      FORM
         0.        0.        0.        0.        0.        0.
$                                     A1        A2        A3

$       V1        V2        V3        D1        D2        D3      BETA
```

Material properties for the steering wheel armature

Material property	Corresponding value
Density	2.7 g/cm^3
Young's modulus	72 GPa
Poisson's ratio	0.35
Yield stress	67 MPa

Sample input data from the LS-DYNA input file:

```
*MAT_PIECEWISE_LINEAR_PLASTICITY
$       MID        RO         E        PR      SIGY      ETAN      EPPF      TDEL
          3 2.700E-06 7.200E+01 3.500E-01 6.660E-02 0.000E+00 0.000E+00 0.000E+00
$         C         P      LCSS      LCSR
       6500         4         4  .000E+00
$      EPS1      EPS2      EPS3      EPS4      EPS5      EPS6      EPS7      EPS8

$       ES1       ES2       ES3       ES4       ES5       ES6       ES7       ES8

*DEFINE_CURVE
$ STESS VERSUS EFFECTIVE PLASTIC STRAIN CURVE FOR THE ALUMINUM MATERIAL
$      LCID      SIDR      SCLA      SCLO      OFFA      OFFO
          4         0              1.0E-06
$               STRAIN              STRESS
       0.000000000000          66604.15182
       0.000031760436          67496.16260
       0.000561576355          72111.73621
       0.001566696915          77156.17361
       0.003024371273          82613.01251
       0.004911848587          88372.72645
       0.007206378014          94358.31649
       0.009885208711          100513.4947
       0.012925589840          106794.9208
       0.016304770550          113167.7952
       0.020000000000          119603.2415
       0.023988527350          126076.6609
       0.028247601760          132566.6462
       0.032754472390          139054.2347
       0.037486388380          145522.3750
       0.042420598910          151955.5358
       0.047534353120          158339.4107
       0.052804900180          164660.6910
       0.058209489240          170906.8859
       0.063725369460          177066.1793
       0.069329789990          183127.3126
       0.075000000000          189079.4870
       0.080713248640          194912.2813
       0.086446785070          200615.5823
       0.092177858440          206179.5229
       0.097883717920          211594.4280
       0.103541612700          216850.7663
       0.109128791800          221939.1053
       0.114622504500          226850.0701
       0.120000000000          231574.3045
```

Material properties for the airbag

Material property	Corresponding value
Density	0.825 g/cm^3
Young's modulus	200 MPa
Poisson's ratio	0.3
Shear modulus	38 MPa

Sample input data from the LS-DYNA input file:

```
*MAT_FABRIC
$       MID          RO         EA         EB         EC       PRBA       PRCA       PRCB
          4  8.250E-07       0.20       0.20       0.20       0.30       0.30       0.30
$       GAB         GBC        GCA        GSE         EL        PRL     LRATIO       DAMP
        0.038       0.038      0.038        0.0        0.0        0.0        0.0      0.050
$      AOPT         FLC        FAC        ELA       LNRC       FORM
        0.0         0.0        0.0        0.0        0.0        0.0
$        XP          YP         ZP         A1         A2         A3
        0.0         0.0        0.0        0.0        0.0        0.0
$        V1          V2         V3         D1         D2         D3
        0.0         0.0        0.0        0.0        0.0        0.0
```

APPENDIX E

Contact algorithms employed between all contact surfaces

Sample input data from the LS-DYNA input file:

```
$ THIS CONTACT IS BETWEEN THE HYBRID III DUMMY AND THE SEAT. THE SLAVE NODES ARE
$ DEINED BY PART SET #5, THE DUMMY BODY SEGMENTS, WHILE THE MASTER SURFACES ARE
$ DEFINED BY PART #12482, THE SEAT.
*CONTACT_AUTOMATIC_SURFACE_TO_SURFACE
$      SSID      MSID     SSTYP     MSTYP    SBOXID    MBOXID       SPR       MPR
          5     12482         2         3         0         0         0         0
$        FS        FD        DC        VC       VDC    PENCHK        BT        DT
        0.3       0.2        0.        0.       20.         0        0.    20E+20
$       SFS       SFM       SST       MST      SFST      SFMT       FSF       VSF
        0.6       1.5        0.        0.        0.        0.        1.        1.
$      SOFT    SOFSCL    LCIDAB    MAXPAR      EDGE     DEPTH     BSORT    FRCFRQ
          2      0.05        0.        0.        0.        2.        0.        1.
$    PENMAX    THKOPT               SNLOG      ISYM     I2D3D    SLDTHK    SLDSTF
        0.         0                   0         0         0        0.        0.
$---+----1----+----2----+----3----+----4----+----5----+----6----+----7----+----8


$ THIS CONTACT IS BETWEEN THE HYBRID III DUMMY AND THE SEATBELT. THE SLAVE NODES
$ ARE DEINED BY PART SET #5, THE DUMMY BODY SEGMENTS, WHILE THE MASTER SURFACES
$ ARE DEFINED BY PART #12485, THE SEATBELT.
*CONTACT_AUTOMATIC_SURFACE_TO_SURFACE
$      SSID      MSID     SSTYP     MSTYP    SBOXID    MBOXID       SPR       MPR
          5     12485         2         3         0         0         0         0
$        FS        FD        DC        VC       VDC    PENCHK        BT        DT
        0.3       0.2        0.        0.        0.         0        0.    20E+20
$       SFS       SFM       SST       MST      SFST      SFMT       FSF       VSF
        0.0       0.0        0.        0.        0.        0.        1.        1.
$      SOFT    SOFSCL    LCIDAB    MAXPAR      EDGE     DEPTH     BSORT    FRCFRQ
          2      0.05        0.        0.        0.        2.        0.        1.
$---+----1----+----2----+----3----+----4----+----5----+----6----+----7----+----8


$ THIS CONTACT IS BETWEEN THE HYBRID III DUMMY AND THE AIRBAG. THE SLAVE NODES
$ ARE DEINED BY PART SET #5, THE DUMMY BODY SEGMENTS, WHILE THE MASTER SURFACES
$ ARE DEFINED BY PARTSET #4, THE AIRBAG.
*CONTACT_AUTOMATIC_SURFACE_TO_SURFACE
$      SSID      MSID     SSTYP     MSTYP    SBOXID    MBOXID       SPR       MPR
          5         4         2         2         0         0         0         0
$        FS        FD        DC        VC       VDC    PENCHK        BT        DT
        0.0       0.0        0.        0.        0.         0        0.    20E+20
$       SFS       SFM       SST       MST      SFST      SFMT       FSF       VSF
        0.0       0.0        0.        0.        0.        0.        1.        1.
$      SOFT    SOFSCL    LCIDAB    MAXPAR      EDGE     DEPTH     BSORT    FRCFRQ
          2      0.05        0.        0.        0.        2.        0.        1.
$---+----1----+----2----+----3----+----4----+----5----+----6----+----7----+----8


$ THIS CONTACT IS BETWEEN THE SEATBELT AND THE AIRBAG. THE SLAVE NODES ARE DEINED
$ BY PART #12485, THE SEATBELT, WHILE THE MASTER SURFACES ARE DEFINED BY PARTSET #4,
$ THE AIRBAG.
*CONTACT_AUTOMATIC_SURFACE_TO_SURFACE
$      SSID      MSID     SSTYP     MSTYP    SBOXID    MBOXID       SPR       MPR
      12485         4         3         2         0         0         0         0
$        FS        FD        DC        VC       VDC    PENCHK        BT        DT
        0.0       0.0        0.        0.        0.         0        0.    20E+20
$       SFS       SFM       SST       MST      SFST      SFMT       FSF       VSF
        1.0       1.0        0.        0.        0.        0.        1.        1.
$      SOFT    SOFSCL    LCIDAB    MAXPAR      EDGE     DEPTH     BSORT    FRCFRQ
          2
$---+----1----+----2----+----3----+----4----+----5----+----6----+----7----+----8
```

```
$ THIS CONTACT IS BETWEEN THE AIRBAG AND THE STEERING WHEEL. THE SLAVE NODES ARE
$ DEINED BY PART #12485, THE SEATBELT, WHILE THE MASTER SURFACES ARE DEFINED BY
$ PARTSET #4, THE AIRBAG.
*CONTACT_AUTOMATIC_SURFACE_TO_SURFACE
$      SSID      MSID     SSTYP     MSTYP     SBOXID    MBOXID       SPR       MPR
          4         3         2         2                             0         0
$        FS        FD        DC        VC       VDC    PENCHK        BT        DT
       0.00      0.00       0.0       0.0       0.0         0       0.0 1.000E+20
$       SFS       SFM       SST       MST      SFST      SFMT       FSF       VSF
    1.0E-02       4.0       0.0       0.0       1.0       1.0       1.0       1.0
$      SOFT    SOFSCL    LCIDAB    MAXPAR    PENTOL     DEPTH     BSORT    FRCFRQ
          2
$    PENMAX    THKOPT    SHLTHK     SNLOG      ISYM     I2D3D
        0.0         0         0         0         0         0
$---+----1----+----2----+----3----+----4----+----5----+----6----+----7----+----8
```

106

APPENDIX F

Rating score for all steering wheel armatures investigated

Test	θ	L_{dish}	Impact	F_{Peak}	C.F.E.	$E_{absorbed}$	e_e	E.A.F.	Rating
26A	30	140.00	6 o'clock	1	1	1	1	2	6
24A	30	129.33	6 o'clock	1	1	1	1	2	6
9A	10	118.67	6 o'clock	1	1	1	0	2	5
8B	10	108.00	3 o'clock	1	1	1	1	1	5
6B	0	86.67	3 o'clock	1	1	1	1	1	5
5B	0	97.33	3 o'clock	1	1	1	1	1	5
4B	0	140.00	3 o'clock	1	1	1	0	2	5
4A	0	140.00	6 o'clock	1	1	1	0	2	5
3B	0	129.33	3 o'clock	1	1	1	0	2	5
3A	0	129.33	6 o'clock	1	1	1	0	2	5
34B	-10	86.67	3 o'clock	1	1	1	1	1	5
33B	-10	97.33	3 o'clock	1	1	1	1	1	5
32B	-10	140.00	3 o'clock	1	1	1	0	2	5
32A	-10	140.00	6 o'clock	1	1	1	0	2	5
31B	-10	129.33	3 o'clock	1	1	1	0	2	5
31A	-10	129.33	6 o'clock	1	1	1	0	2	5
30B	-10	118.67	3 o'clock	1	1	1	0	2	5
2A	0	118.67	6 o'clock	1	1	1	0	2	5
29B	-10	108.00	3 o'clock	1	1	1	1	1	5
27B	30	86.67	3 o'clock	1	1	1	1	1	5
26B	30	97.33	3 o'clock	1	1	1	1	1	5
26B	30	140.00	3 o'clock	1	1	1	1	1	5
24B	30	129.33	3 o'clock	1	1	1	1	1	5
23C	30	118.67	12 o'clock	2	1	1	1	0	5
23B	30	118.67	3 o'clock	1	1	1	1	1	5
23A	30	118.67	6 o'clock	1	1	1	1	1	5
22B	30	108.00	3 o'clock	1	1	1	1	1	5
20B	20	86.67	3 o'clock	1	1	1	1	1	5
1B	0	108.00	3 o'clock	1	1	1	1	1	5
1B	10	97.33	3 o'clock	1	1	1	1	1	5
19B	20	97.33	3 o'clock	1	1	1	1	1	5
18B	20	140.00	3 o'clock	1	1	1	0	2	5
18A	20	140.00	6 o'clock	1	1	1	0	2	5
17A	20	129.33	6 o'clock	1	1	1	0	2	5
16B	20	118.67	3 o'clock	1	1	1	1	1	5

Test	θ	L_{dish}	Impact	F_{Peak}	C.F.E.	$E_{absorbed}$	e_e	E.A.F.	Rating
16A	20	118.67	6 o'clock	1	1	1	0	2	5
15B	20	108.00	3 o'clock	1	1	1	1	1	5
13B	10	86.67	3 o'clock	1	1	1	1	1	5
11B	10	140.00	3 o'clock	1	1	1	0	2	5
11A	10	140.00	6 o'clock	1	1	1	0	2	5
10A	10	129.33	6 o'clock	1	1	1	0	2	5
9B	10	118.67	3 o'clock	1	1	1	0	1	4
8A	10	108.00	6 o'clock	1	1	1	0	1	4
30A	-10	118.67	6 o'clock	1	1	1	0	1	4
2B	0	118.67	3 o'clock	1	1	1	0	1	4
29A	-10	108.00	6 o'clock	1	1	1	0	1	4
27A	30	86.67	6 o'clock	1	1	1	1	0	4
22A	30	108.00	6 o'clock	1	1	1	0	1	4
20A	20	86.67	6 o'clock	1	1	1	1	0	4
1A	0	108.00	6 o'clock	1	1	1	0	1	4
17B	20	129.33	3 o'clock	1	1	1	0	1	4
15A	20	108.00	6 o'clock	1	1	1	0	1	4
13A	10	86.67	6 o'clock	1	1	1	1	0	4
10B	10	129.33	3 o'clock	1	1	1	0	1	4
6A	0	86.67	6 o'clock	1	1	1	0	0	3
5A	0	97.33	6 o'clock	1	1	1	0	0	3
35C	-10	76.00	12 o'clock	0	0	1	0	2	3
34C	-10	86.67	12 o'clock	0	0	1	0	2	3
34A	-10	86.67	6 o'clock	1	1	1	0	0	3
33A	-10	97.33	6 o'clock	1	1	1	0	0	3
26C	30	140.00	12 o'clock	1	1	1	0	0	3
26A	30	97.33	6 o'clock	1	1	1	0	0	3
24C	30	129.33	12 o'clock	1	1	1	0	0	3
1A	10	97.33	6 o'clock	1	1	1	0	0	3
19A	20	97.33	6 o'clock	1	1	1	0	0	3
9C	10	118.67	12 o'clock	0	0	1	0	1	2
8C	10	108.00	12 o'clock	0	0	1	0	1	2
7C	0	76.00	12 o'clock	0	0	1	0	1	2
6C	0	86.67	12 o'clock	0	0	1	0	1	2
5C	0	97.33	12 o'clock	0	0	1	0	1	2
4C	0	140.00	12 o'clock	0	0	1	0	1	2

Test	θ	L_{dish}	Impact	F_{Peak}	C.F.E.	$E_{absorbed}$	e_e	E.A.F.	Rating
3C	0	129.33	12 o'clock	0	0	1	0	1	2
33C	-10	97.33	12 o'clock	0	0	1	0	1	2
32C	-10	140.00	12 o'clock	0	0	1	0	1	2
31C	-10	129.33	12 o'clock	0	0	1	0	1	2
30C	-10	118.67	12 o'clock	0	0	1	0	1	2
2C	0	118.67	12 o'clock	0	0	1	0	1	2
29C	-10	108.00	12 o'clock	0	0	1	0	1	2
28C	30	76.00	12 o'clock	0	0	1	0	1	2
27C	30	86.67	12 o'clock	0	0	1	0	1	2
26C	30	97.33	12 o'clock	0	0	1	0	1	2
21C	20	76.00	12 o'clock	0	0	1	0	1	2
20C	20	86.67	12 o'clock	0	0	1	0	1	2
1C	0	108.00	12 o'clock	0	0	1	0	1	2
1C	10	97.33	12 o'clock	0	0	1	0	1	2
19C	20	97.33	12 o'clock	0	0	1	0	1	2
16C	20	118.67	12 o'clock	0	0	1	0	1	2
15C	20	108.00	12 o'clock	0	0	1	0	1	2
14C	10	76.00	12 o'clock	0	0	1	0	1	2
14A	10	76.00	6 o'clock	0	0	1	0	1	2
13C	10	86.67	12 o'clock	0	0	1	0	1	2
11C	10	140.00	12 o'clock	0	0	1	0	1	2
10C	10	129.33	12 o'clock	0	0	1	0	1	2
7B	0	76.00	3 o'clock	0	0	1	0	0	1
7A	0	76.00	6 o'clock	0	0	1	0	0	1
35B	-10	76.00	3 o'clock	0	0	1	0	0	1
35A	-10	76.00	6 o'clock	0	0	1	0	0	1
28B	30	76.00	3 o'clock	0	0	1	0	0	1
28A	30	76.00	6 o'clock	0	0	1	0	0	1
22C	30	108.00	12 o'clock	0	0	1	0	0	1
21B	20	76.00	3 o'clock	0	0	1	0	0	1
21A	20	76.00	6 o'clock	0	0	1	0	0	1
18C	20	140.00	12 o'clock	0	0	1	0	0	1
17C	20	129.33	12 o'clock	0	0	1	0	0	1
14B	10	76.00	3 o'clock	0	0	1	0	0	1

VITA AUCTORIS

Name: Ophelia Nabeta

Place of Birth: Kampala, Uganda

Date of Birth: February 14th, 1977

Education: *Makerere University, Kampala, Uganda*

          Degree: Mechanical Engineering, Graduated

          B..Sc., June 2000, 1996- 2000.

VITA AUCTORIS

Name: Ophelia Nabeta

Place of Birth: Kampala, Uganda

Date of Birth: February 14th, 1977

Education: *Makerere University, Kampala, Uganda*

                        Degree: Mechanical Engineering, Graduated

                                              B..Sc., June 2000, 1996- 2000.